공학석사 학위논문

Hysteresis Modeling Framework Using Bouc-Wen Model Considering Cracking Effects

균열 효과를 고려한 Bouc-Wen 모델 기반
이력 거동 모델링 프레임워크

2022 년 2 월

서울대학교 대학원
건설환경공학부
오 세 빈

Hysteresis Modeling Framework Using Bouc-Wen Model Considering Cracking Effects

지도교수 송 준 호

이 논문을 공학석사 학위논문으로 제출함
2022 년 2 월

서울대학교 대학원
건설환경공학부
오 세 빈

오세빈의 공학석사 학위논문을 인준함
2022 년 2 월

위 원 장 ____________________ (인)

부위원장 ____________________ (인)

위 원 ____________________ (인)

Abstract

Bouc-Wen class models, i.e., hysteretic models developed based on the original Bouc-Wen model, have been extensively used to describe hysteretic behaviors in various fields of engineering. Nonetheless, it has been consistently pointed out that Bouc-Wen class models may not provide accurate predictions of the force-deformation relationships if the loads are different from those actually used to fit the model. Accordingly, in seismic performance evaluation, the application range of the equivalent-single-degree-of-freedom system employing a Bouc-Wen class model is limited to a nonlinear static seismic analysis. Applications to nonlinear time history analysis requiring a highly accurate model are considered challenging.

In this thesis, a hysteresis modeling framework based on Bouc-Wen class models is developed to improve the predictive performance for general loads including seismic excitations. To this end, first, a novel Bouc-Wen model that broadens the coverage of Bouc-Wen class models to the structural elements susceptible to cracks, such as reinforced concrete, is developed. Two additional parameters are introduced to consider the effects of cracking on hysteresis.

Next, a new strategy is proposed to identify the parameters of the developed Bouc-Wen model. The proposed strategy is represented by a cyclic loading history with which one can obtain simulation or experiment data for effective parameter identification. A quasi-static cyclic loading history is developed to investigate the full modes of hysteretic behaviors of the specimen.

The proposed hysteresis modeling framework is demonstrated by nonlinear finite element analyses and 50 actual experimental datasets of reinforced concrete columns. The proposed model exhibits more accurate and reliable predictive performance than existing Bouc-Wen class models under various types of quasi-static loads. Comparison with finite element analysis results for El Centro and Loma Prieta earthquakes confirms that the nonlinear time history analyses employing the proposed model predict the peak displacement more accurately than existing models. Furthermore, for an RC column, the equivalent SDOF system with the proposed Bouc-Wen model shows notable matching with the finite element analysis results for six earthquakes. The proposed framework is expected to facilitate efficient nonlinear time history analyses that would provide results similar to those by time-consuming finite element analyses.

Keyword : Hysteretic behaviors, Bouc-Wen model, Loading protocol, Nonlinear finite element method, Nonlinear time history analysis, Cracking effects

Student Number : 2020-27136

Table of Contents

List of Figures

List of Tables

Chapter 1. Introduction

1.1. Research background

The hysteretic nonlinear behavior is often encountered in a wide variety of processes in which the input-output relations between variables involve memory effect, e.g., biology, optics, electronics, ferroelectricity, mechanics, structures, and so forth (Ismail et al., 2009; Pelliciari et al., 2018). Among other areas, in mechanical and structural systems, hysteresis refers to a memory-dependent and multivalued relation between restoring force and deformation (Song and Der Kiureghian, 2006), which arise from a natural mechanism of materials to supply restoring forces against movements and dissipate energy (Ismail et al., 2009). Due to the intricate nature of the hysteretic mechanism, many mathematical models that imitate the appearance of hysteretic relations in a mathematical way have been developed, instead of involving the detailed physics immanent in hysteretic systems. The most popular mathematical models that simulate the hysteretic behavior are the Bouc-Wen class models, i.e., the mathematical models for hysteresis based on the original Bouc-Wen model proposed by Bouc (1967) and subsequently generalized by Wen (1976).

The Bouc-Wen class models have been used to simulate a variety of hysteretic behaviors of structural materials and elements. Among them, the Bouc-Wen-Baber-Noori (BWBN) model (Baber and Noori, 1985), one of the most widely used Bouc-Wen class models, has proved its versatility in describing various characteristics of hysteretic behavior in previous literature, such as the degrading of stiffness and strength and the pinching effect (Ma et al., 2006; Hossain et al., 2013; Sengupta and Li, 2013; Yu et al., 2016; Ning et al., 2021). Moreover, the Bouc-Wen class models including the BWBN model are mathematically tractable since they incorporate only one auxiliary nonlinear differential equation to describe hysteretic behavior. Owing to the broad coverage and the convenient mathematical tractability, Bouc-Wen class models have been widely used in structural engineering, especially to represent complex structural systems by an equivalent SDOF system. This simplification has been adopted in many design codes and guidelines, e.g., the capacity spectrum method presented in ATC-40 (1996), and the coefficient method of displacement modification specified in FEMA 356 (2000).

However, the accuracy and reliability issues in predicting the responses under a new load using the Bouc-Wen class models have been consistently reported in the literature (Ikhouane et al., 2007; Hamburger et al., 2016; Kim, 2021). The prediction accuracy for a new load cannot be guaranteed even if a Bouc-Wen class model presents a good matching with the experimental data for a specific input load. The issue on the response prediction of the Bouc-Wen class models may stem from the following two reasons: First, the coverage of existing Bouc-Wen class models may be insufficient to incorporate the hysteretic behaviors that appear in a wide variety of structural elements. Especially for composite materials such as reinforced concrete (RC), it is still challenging to accurately simulate the highly nonlinear and heterogeneous characteristics of hysteresis. Next, the accuracy of Bouc-Wen class models is largely dependent on the experimental data with which parameters of the models are identified. Thus, if the data used for identifying the parameters do not sufficiently incorporate the overall hysteresis of the structure, the parameters of the Bouc-Wen class model cannot be accurately estimated, which leads to inaccurate response prediction for new loads.

Therefore, this study proposes a hysteretic modeling framework to broaden the coverage of the existing models and improve the performance in response prediction for arbitrary loads including quasi-static loads and dynamic loads. To this end, this study develops a novel Bouc-Wen class model that can describe hysteretic behaviors of structural elements affected by cracks. Furthermore, this study also suggests a series of procedures for parameter identification, namely, a loading protocol that incorporates a loading history for experiments and a strategy for parameter identification. The applicability and effectiveness of the proposed hysteresis modeling framework is demonstrated by performing a nonlinear finite element analysis using the actual experimental data of RC columns.

1.2. Research objectives and scope

The three main objectives of this study are as follows. First, this study aims to develop a novel Bouc-Wen class model that can simulate hysteretic behaviors depending on cracks. To this end, the cracking effects on hysteresis are first identified from the actual experimental data for structural elements that are susceptible to cracks. Based on the experimental data, a novel Bouc-Wen model is developed by modifying the existing Bouc-Wen model to involve the cracking effects.

Second, this study focuses on the development of a systematic loading protocol for accurate and consistent parameter identification of the proposed Bouc-Wen model. Even if the proposed Bouc-Wen model shows considerable versatility in describing various hysteretic behaviors, the model cannot be used to predict responses of the structure unless parameters of the model are accurately estimated. Accordingly, this thesis suggests several requirements for loading histories to induce the overall hysteresis in structural elements susceptible to cracks. Based on the characteristics required for the loading history, an appropriate loading history is developed. Furthermore, an efficient strategy to identify many parameters in the proposed model is proposed.

Last, this study demonstrates the performance of the proposed hysteresis modeling framework through numerical examinations. The demonstration incorporates not only quasi-static loads but also seismic excitations. Numerical experiments using the nonlinear finite element method are used as an alternative for actual experiments.

The three main objectives of this study are summarized in Figure 1.1, and the overall scopes within each objective are described in Figure 1.2.

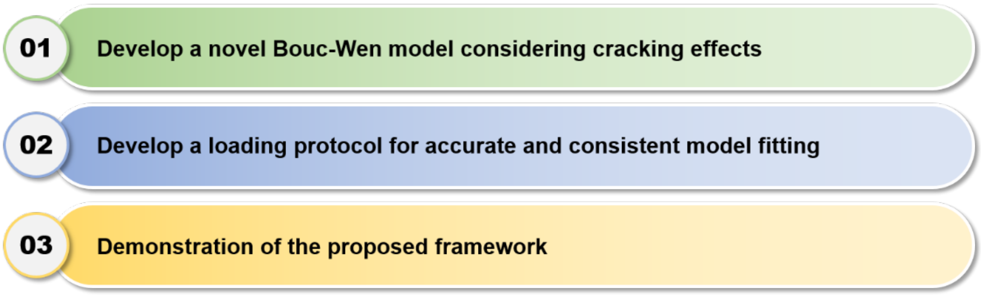

Figure 1.1 Three main research objectives

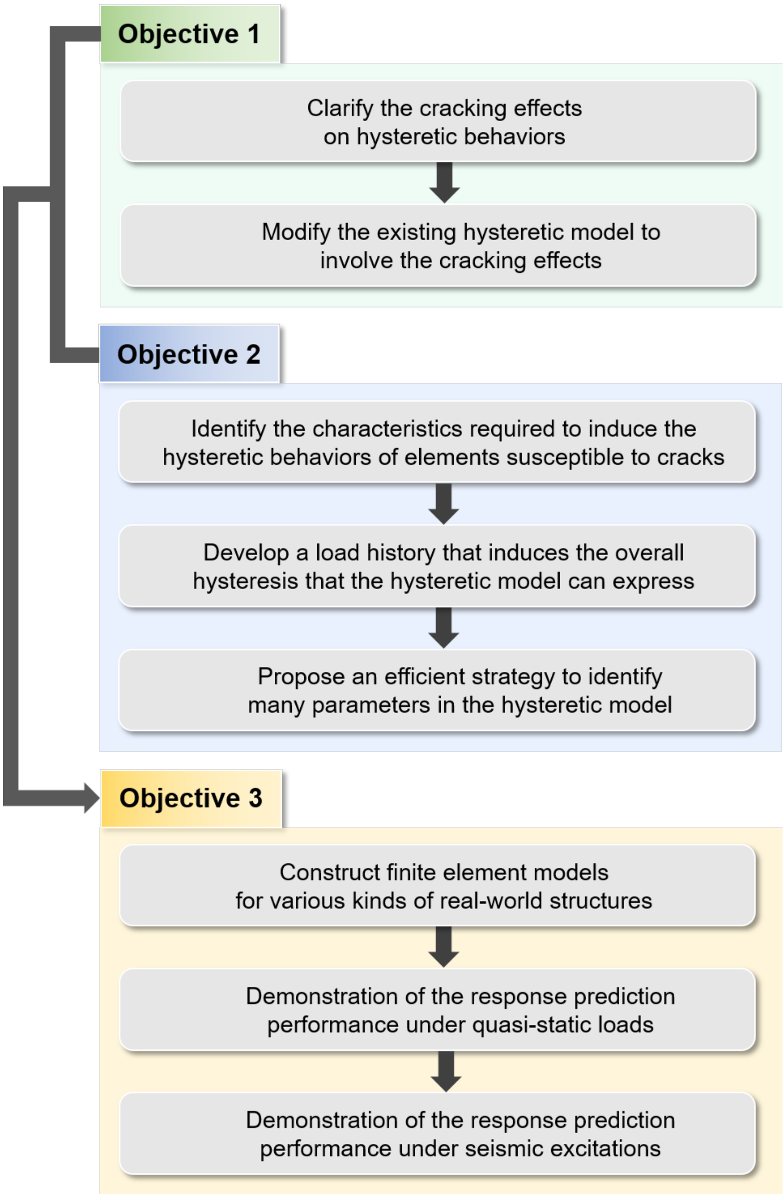

Figure 1.2 Research scopes for each research objective

1.3. Organization

This thesis consists of 6 chapters. Chapter 2 provides the generic framework for developing an equivalent SDOF system using a hysteretic model. The necessity and the importance of an equivalent SDOF system are presented, and how the equivalent SDOF can be constructed using the hysteretic model is explained. Furthermore, the representative Bouc-Wen class models that are widely used in previous studies are described. The typical loading protocols specified in various design codes and standards are also illustrated. Lastly, the limitations on the existing Bouc-Wen class models and the loading protocols are provided, which are addressed in the following chapters.

Chapter 3 elucidates the development of a novel Bouc-Wen model that can simulate the hysteretic behaviors of structural components susceptible to cracks. The effects of cracking on hysteretic behaviors are first presented, and a new Bouc-Wen model is proposed by modifying the existing model to consider the cracking effects.

Chapter 4 proposes a loading protocol for accurate and consistent model fitting. To this end, various modes of hysteretic behaviors are identified, and a loading history is proposed based on the identified modes of hysteresis. Along with a loading history with which the experimental data are obtained, a parameter identification strategy is also presented.

Chapter 5 demonstrates the proposed hysteresis modeling framework using nonlinear finite element analysis and the experimental data for RC columns provided by the PEER Center. The finite element models for various kinds of RC columns are first constructed. Using the finite element models, the prediction accuracy of the proposed hysteresis modeling framework is presented. The loads used for demonstration consist of three quasi-static loads and two seismic excitations.

Finally, Chapter 6 summarizes the results and the conclusions of this study. Possible future studies are also presented with the limitations of this study.

Chapter 2. Existing hysteresis modeling framework for equivalent single degree of freedom system

To estimate nonlinear seismic response of structural systems, many research efforts have been made on development of single degree of freedom (SDOF) system (Veletsos and Newmark, 1960; ATC 40, 1997; FEMA 440, 2005, ASCE 41-13, 2013). The idealized system employs hysteretic models to consider the inelastic and hysteretic behaviors of the structural system, which requires a well-structured hysteresis modeling framework. However, the methods with an idealized system have several limitations. For example, the methods have often shown the limited applicability for various structural systems due to the insufficient coverage of the existing hysteretic models. Moreover, they are hard to be used to estimate nonlinear time history of a structure due to the limited prediction performance.

In this regard, the generic framework for developing an equivalent SDOF system using a hysteretic model is first described in this chapter. Next, several hysteretic models are explained to introduce existing models which are designed to capture the hysteretic behaviors of structural systems. Following that, the existing loading protocols from which one can identify the parameters of the hysteretic models are described. Last, the limitations of the existing hysteresis modeling framework, i.e., the existing hysteretic models and the existing loading protocols, are presented.

2.1. Generic framework for equivalent SDOF systems using a hysteretic model

To estimate seismic responses of a hysteretic system, i.e., a structural system showing hysteretic behaviors, nonlinear time history analysis (NTHA) is the most accurate way to evaluate the responses of the system (Kim et al., 2019). To carry out NTHA, a sophisticated numerical model, such as a three-dimensional (3D) structural finite-element (FE) model with detailed structural, is often used. Considering that NTHA requires solving the dynamic equilibrium equation at every time step by a numerical integration scheme, however, estimating the nonlinear seismic responses using the refined numerical models is far from practical due to the significant computational costs (Kang et al., 2017; Kim et al., 2019). Thereby, to evaluate the seismic demands in a practical and efficient way, methodologies using an equivalent SDOF system are often used as an alternative.

To idealize structural systems as an equivalent SDOF system, the corresponding governing equation is established following the traditional structural dynamics as

$$m\ddot{u} + c\dot{u} + f_s = -m\ddot{u}_g \tag{2.1}$$

where m is the concentrated mass of a system, c is the viscous damping coefficient, u is the translational displacement, $\ddot{u}_g$ is the ground motion acceleration, and f_s is the restoring force which consists of the elastic force and the inelastic hysteretic force. Herein, the hysteresis of a structural system takes place in the restoring force of a system. In other words, the restoring force in terms of displacement depends on the load history that the system has been experienced. Figure 2.1 illustrates the equivalent SDOF system. Hence, for the idealized system, a hysteretic model that can represent the overall inelastic behaviors of a structural system is required. In most cases, hysteretic models are displacement-driven, i.e., they return restoring force given displacement. For more details, three representative hysteretic models are suggested in Section 2.2.

When the appropriate hysteretic model which can describe the nonlinear hysteretic behaviors of a structural system is selected, the values of model parameters should be identified. Even though various research efforts have been made to employ the equivalent SDOF system for evaluating seismic performance, the values of model parameters involved in the equivalent SDOF system are often prescribed empirically without any experimental calibration (Ning et al., 2021). However, the hysteretic parameters need to be identified based on experimental data, not on the researchers' experience, for practical application.

Consequently, to accurately describe the hysteretic behaviors of a system, the hysteretic parameters need to be identified from load-deformation experimental data that represent the hysteresis of a system. The load-deformation data can be obtained from a numerical experiment using the detailed FE model or from the actual experiment on the structure. Furthermore, load-deformation data from quasi-cyclic testing is commonly used to identify the values of hysteretic parameters because it can constitute a consistent basis for the cooperative research on the development of design models, compared to the shake table testing (Ning et al., 2021). In a quasi-static cyclic test, the specimen is tested in sufficiently slow rate so that the inertia force and the viscous damping force of the equivalent SDOF system become insignificant.

Various guidelines and design codes provide a loading protocol that specifies a cyclic loading history for quasi-static cyclic loading tests (ATC-24, 1992; CUREE, 2001; FEMA 461, 2007; ACI 374, 2013). Such protocols have often been used to identify the hysteretic parameters. However, it is found from this study that the loading protocols specified in several design codes are not suitable to induce hysteretic behaviors from the specimen. The details will be presented in Chapter 4.

In addition, representative existing loading protocols are presented in Section 2.3.

In summary, a generic procedure for the development of the equivalent SDOF system using a hysteresis model is illustrated in Figure 2.2. If the scale of a structural system is component-level, such as a reinforced concrete column, an actual experiment with a cyclic loading history can be conducted. Numerical analyses using FE analysis are also possible for an alternative. On the other hand, if the scale of a structural system is a system-level consisting of components, an experiment in laboratory environment is nearly impossible, which requires the refined structural model for the structural system. Using the test specimen or the detailed structural model, load-deformation data is obtained under cyclic load history. Once the data is obtained, an appropriate hysteretic model is required to capture the overall hysteresis shown in the load-deformation data. By identifying parameters in the hysteretic model, an equivalent SDOF system for the structural system is constructed. The idealized system can be used to estimate the responses for the structural system under various excitations, including quasi-static and dynamic loading such as earthquakes.

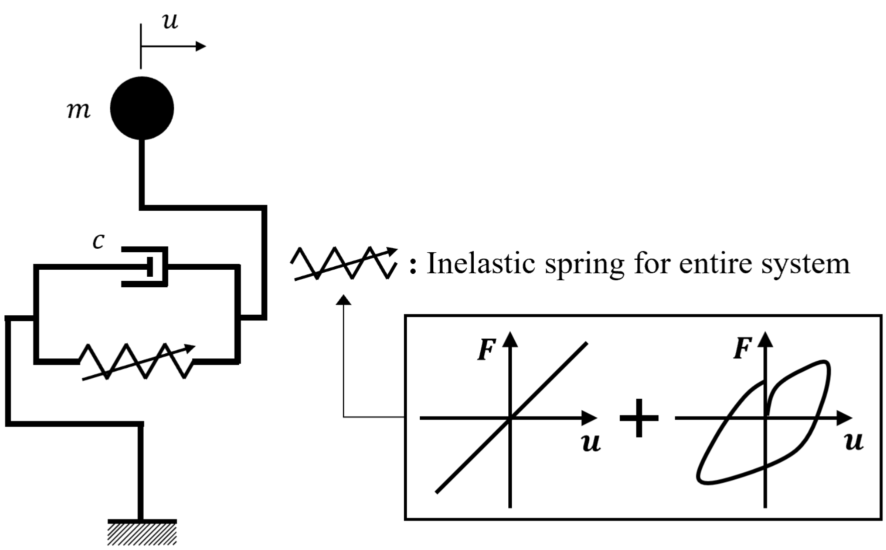

Figure 2.1 Illustration of the equivalent SDOF system

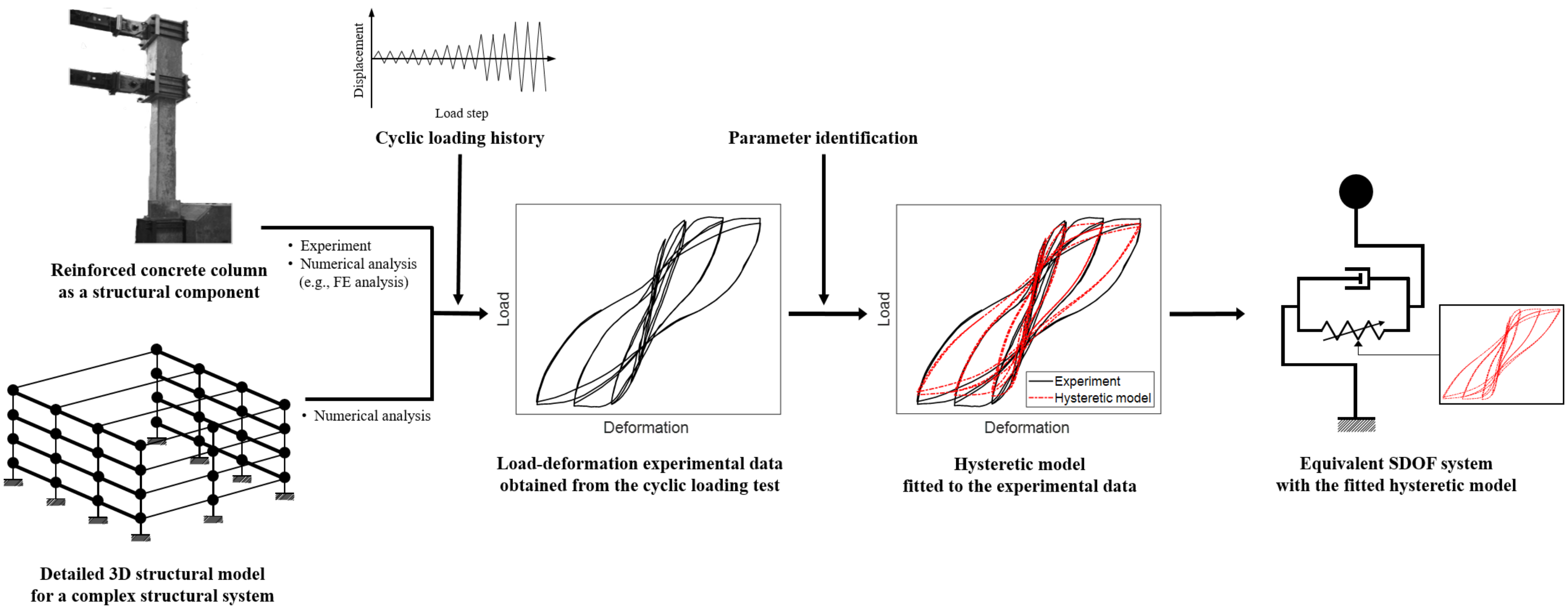

Figure 2.2 Illustration of the development of an equivalent SDOF system

2.2. Existing Bouc-Wen class models

The hysteretic models can be broadly classified into polygonal hysteresis models (PHMs) and smooth hysteresis models (SHMs) (Sengupta, 2017). In PHMs, e.g., the Ibarra-Medina-Kranwinkler model proposed in Ibarra et al. (2005), a hysteresis loop is described by several featured points, i.e., peak-oriented approach, and simulate the hysteresis loop by connecting the points. In contrast, in the SHMs, represented by the Bouc-Wen model, the hysteresis loop is represented in a smooth curve using a first-order non-linear differential equation involving a hysteretic displacement, also known as an auxiliary variable.

A differential equation-based model of hysteresis has many advantages in analysis. The versatility to generate a wide variety of realistic hysteresis loops is of utmost significance. Besides, the ability to form an overall system into a differential system is also one of the considerable advantages (Ma et al., 2004). Because of the versatility that stems from the mathematical tractability, Bouc-wen class models, the hysteretic models using the basic framework in the original Bouc-Wen model, has been extended and applied to a wide variety of engineering problems, particularly within the areas of civil and mechanical engineering (Ismail et al., 2009). Moreover, it has been validated that Bouc-Wen class models are suitable to simulate the hysteretic behaviors of various structures, e.g., RC columns (Yu et al., 2016; Sengupta and Li, 2017; Pelliciari et al., 2018; Lee and Han 2021; Ning et al., 2021), RC beam-column joints (Sengupta and Li, 2013), ferrocement shear walls (Ortiz et al., 2013), yielding shear panel devices (Hossain et al., 2013), wood members (Ma et al., 2006), and flexible strap connectors in electrical substation equipment (Song and Der Kiureghian, 2006). The hysteretic model used in this study also belongs to the Bouc-Wen class models, and three representative Bouc-Wen class models are reviewed in the following sections.

2.2.1. Bouc-Wen model

The original Bouc-Wen (BW) model was proposed by Bouc (1967) and later generalized by Wen (1976). This model describes the hysteresis of a wide variety of structural systems using the first-order nonlinear differential equation that relates the displacement of an equivalent SDOF system, u, and the hysteretic displacement z, also known as an auxiliary variable. The BW model denotes the restoring force f_s in Eq. (2.1) as a combination of an elastic and a hysteretic part, i.e.,

$$f_s = f(u, z) = \alpha k_0 u + (1 - \alpha) k_0 z \tag{2.2}$$

where k_0 is the initial stiffness, and α is the post-yield stiffness ratio, the ratio of final asymptote tangent stiffness to initial stiffness which is 1 for a linear system and 0 for a nonlinear system. The differential equation that relates the hysteretic displacement z to the displacement u is

$$\dot{z} = \dot{u} \cdot [A - |z|^n (\gamma + \beta \mathrm{sgn}(\dot{u} z))] \tag{2.3}$$

where $\mathrm{sgn}(\cdot)$ is the signum function, A is a scale parameter, n indicates the sharpness of yield, and β and γ control the basic shape of hysteresis loops especially hardening and softening, respectively. All A, n, β, and γ are dimensionless quantities.

2.2.2. Bouc-Wen-Baber-Noori model

The Bouc-Wen-Baber-Noori (BWBN) model proposed by Baber and Noori (1985) has been one of the most widely used Bouc-Wen class models as the model can describe a variety of hysteretic shapes which include degradation and pinching. The BWBN model shares the same basic expression for the restoring force in Eq. (2.2), but the differential equation for the hysteretic displacement z is slightly different as

$$\dot{z} = \frac{h}{\eta}\dot{u}[A - |z|^n(\gamma + \beta sgn(\dot{u}z))\nu] \tag{2.4}$$

In the above expressions, h is the pinching function, and ν and η are the degradation shape functions for strength and stiffness, respectively. In the BWBN model, the degradation and pinching are assumed to depend on the response duration and severity, and a convenient measure of the combined effect of duration and severity is the energy whose time rate is given by

$$\dot{\varepsilon} = (1 - \alpha)k_0 z\dot{u} \tag{2.5}$$

Note that the term $(1 - \alpha)k_0 z$ is the hysteretic part of the total restoring force as shown in Eq. (2.2). Thus, the term ε is called a cumulative hysteretic energy. The pinching function h and the degradation functions ν and η are assumed to depend linearly on the cumulative hysteretic energy as the system evolves:

$$\nu(\varepsilon) = 1 + \delta_\nu \varepsilon \tag{2.6}$$

$$\eta(\varepsilon) = 1 + \delta_\eta \varepsilon \tag{2.7}$$

Two unspecified degradation parameters δ_ν and δ_η indicate the rates of strength and stiffness degradation, respectively.

The pinching function h in Eq. (2.4) takes the form

$$h(z, \varepsilon) = 1 - \zeta_1 \exp\left(-\frac{(z \cdot sgn(\dot{u}) - qZ_u)^2}{\zeta_2^2}\right) \tag{2.8}$$

where q is a constant value that controls the pinching initiation, ζ_1 and ζ_2 are the function that control the progress of pinching, and Z_u is the ultimate value of z given by

$$Z_u = \left(\frac{A}{\nu(\beta+\gamma)}\right)^{\frac{1}{n}} \tag{2.9}$$

In addition, the two functions ζ_1 and ζ_2 are written as

$$\zeta_1(\varepsilon) = \zeta_0(1 - \exp(-p\varepsilon)) \tag{2.10}$$

$$\zeta_2(\varepsilon) = (\psi + \delta_\psi \varepsilon)(\lambda + \zeta_1) \tag{2.11}$$

where ζ_0 controls the total slip, p is the rate of the initial drop in the slope, ψ affects to the magnitude of pinching, δ_ψ controls the dispersion rate of pinching, and λ contributes to the pinching severity.

Altogether there are 14 hysteretic parameters α, k_0, A, β, γ, n, δ_ν, δ_η, q, p, ζ_0, ψ, δ_ψ, and λ. However, it has been reported that the parameters of the BWBN model are functionally redundant; there exist multiple sets of parameters that produce an identical hysteresis loop (Ma et al., 2004; Charalampakis and Koumousis, 2009; Ismail et al., 2009). To tackle this issue, Ma et al. (2004) suggested that the redundancy can be removed by fixing the scale parameter A to unity. Thus, this constraint is assumed to hold in this study. The constraint reduces the number of parameters in the BWBN model to 13.

This generalized model of hysteresis with 13 hysteretic parameters possesses all the important features observed in real structures, which include strength degradation, stiffness degradation, and the pinching effect of the successive hysteresis loops (Ma et al., 2004).

2.2.3. Modified Bouc-Wen-Baber-Noori model

Among a wide variety of Bouc-Wen class models have been developed to describe hysteretic behaviors, this study adopts the modified Bouc-Wen-Baber-Noori (m-BWBN) model proposed by Kim (2021) as the reference hysteretic model. It is because the model not only can describe degradation and pinching but also further control the yield force which is a critical feature for dynamic responses of a structural system. In the m-BWBN model, some modifications are made to explicitly control the yield force, the initial stiffness, and the post-yield stiffness ratio.

The m-BWBN model denotes the restoring force f_s as follows:

$$f_s = f(u, z) = \alpha k_0 u + (1 - \alpha) F_y z \tag{2.12}$$

where F_y is the yield force of a structural system. In the m-BWBN model, unlike the BWBN model, the yield force F_y serves as a hysteretic parameter. Note that the difference between Eq. (2.2) and (2.12) lies in the dimension of the hysteretic displacement z. While z has the same dimension as the displacement u in Eq. (2.2), the hysteretic displacement z is dimensionless in the m-BWBN model. Consequently, the differential equation for z is given by

$$\dot{z} = \frac{h}{\eta} \dot{u} [1 - |z|^n (\gamma + \beta sgn(\dot{u} z)) \nu] \frac{k_0}{F_y} \tag{2.13}$$

where all the parameters and functions in Eq. (2.13) are defined the same as in the BWBN model, except the cumulative hysteretic energy that is expressed in normalized by the yield force F_y and the yield displacement d_y as follows:

$$\dot{\varepsilon} = \frac{(1-\alpha) F_y z \dot{u}}{F_y d_y} = (1 - \alpha) \frac{1}{d_y} z \dot{u} = (1 - \alpha) \frac{k_0}{F_y} z \dot{u} \tag{2.14}$$

It is noted that the term k_0/F_y makes the hysteretic displacement z dimensionless in Eq. (2.13), and the constraint for the scale parameter A is adopted. Moreover, an additional constraint for the shape control parameters β and γ is assumed in this model: $\beta + \gamma = 1$. Considering Eq. (2.9), it is justifiable in that the ultimate value of z, denoted by Z_u, needs to be bounded within $(-1, 1)$ when the strength degradation does not occur, $\delta_\nu = 0$. The value for Z_u as -1 or 1 implies the yield force at the ultimate, the yield force, is identical to the specified yield force $-F_y$ or F_y, respectively. Eventually, there exist 13 independent parameters α, k_0, F_y, β(or γ), n, δ_ν, δ_η, q, p, ζ_0, ψ, δ_ψ, and λ in the m-BWBN model.

2.3. Existing loading protocols

A performance-based design has gained popularity as a widely accepted alternative to routine code design (Krawinkler, 2009). Since a performance-based design requires quantification of performance, the need for proper loading histories for seismic performance testing is also becoming more significant. Thereby, various codes, standards, and guidelines have provided loading protocols. In such guidelines, a loading protocol refers to the reference for seismic performance assessment through testing, including configurations of the cyclic loading history. In this section, several loading protocols in the guidelines are presented, and the main features that the protocols are developed.

2.3.1. Loading protocols in guidelines

Many loading protocols that have been proposed in the literature are summarized in Kranwinkler (2009). According to the paper, several loading protocols have been used in multi-institutional testing programs (e.g., ATC-24, 1992; CUREE, 2001), or are proposed for standards (e.g., FEMA 461, 2007; ACI 374, 2013). It is noted that most of the presented protocols are material-specific, primarily steel and wood, and have not found application for materials other than those mentioned (Krawinkler, 2009). Hence, among the loading protocols that have been proposed in the literature, four representative loading protocols developed for steel, wood, reinforced concrete, and general structural components, respectively, are presented as follows:

- *Steel: ATC-24 protocol (ATC-24, 1992)*. Figure 2.3(a) represents the ATC-24 protocol. The ATC-24 protocol, one of the first formal loading protocols developed for seismic performance evaluation of components using a cyclic loading history (Krawinkler, 2009), was developed specifically for components of steel structures. This protocol requires the yield deformation Δ_{yield} to make a reference for increasing the amplitude of cycles. As shown in Figure 2.3(a), the loading history specified in the ATC-24 protocol contains at least 6 elastic cycles, the cycles with the amplitude smaller than the yield deformation Δ_{yield}, followed by three cycles each of amplitude Δ_{yield}, $2\Delta_{yield}$, and $3\Delta_{yield}$, followed by two cycles with the monotonically increasing amplitude until severe cyclic deterioration occurs. The magnitudes of the amplitudes were derived from statistical studies of time history responses of SDOF systems.

- *Wood: CUREE protocol (CUREE, 2001).* The outcome of the cyclic loading history specified in the CUREE protocol is shown in Figure 2.3(b). This protocol intends to evaluate the seismic performance of components of wood-frame structures. As shown in Figure 2.3(b), the CUREE protocol seems to be similar to the ATC-24 protocol but has two clearly different features: the reference parameter for amplitude variation, and the presence of trailing cycles.

For the reference value for increasing the amplitude of cycles, the CUREE protocol uses the maximum displacement Δ, not the yield displacement as in the ATC-24 protocol, for which the test specimen is expected to exhibit acceptable performance when subjected to this loading history. In other words, the maximum displacement is a measure of the deformation capacity of the specimen. Thus, it is required to estimate the deformation capacity prior to the cyclic loading test. The estimation can be made based on the execution of a monotonic loading test, or a consensus value.

Furthermore, as shown in Figure 2.3(b), there exist smaller cycles following the preceding primary cycle at each step in the CUREE protocol. All trailing cycles have an amplitude equal to 75% of that of the preceding primary cycle. Since an excessive number of cycles results in migration of dominant mode of failure, the presence of trailing cycles is statistically justifiable, which leads to a more realistic loading history compared to the other loading protocols.

- *Reinforce concrete: ACI 374 protocol (ACI 374, 2013)*. For components of reinforced concrete structures, the American Concrete Institute (ACI) suggested a cyclic loading history as shown in Figure 2.3(c). Two parameters are introduced in defining the loading history: the increment of deformation to specify each amplitude of cycles, and the number of cycles at each amplitude.

  First, for the increment of deformation, the ACI 374 protocol uses a drift ratio associated with yielding, ϕ_y, which can be computed analytically using measured material properties, or experimentally by performing monotonic tests using companion specimens or during the actual test under reversed cyclic loading. The drift ratio associated with yielding, ϕ_y, is recommended as a value for an increase in subsequent deformation level, and the test continues until severe strength degradation is observed. Besides, for the elastic range of deformations, approximately one-half of the yield drift ratio ϕ_y is used.

  Next, a minimum of two cycles at each deformation level is suggested for the number of cycles, while three cycles can also be used when appropriate. Specifically, the ACI 374 protocol suggests that the selection of number of cycles at each amplitude of cycles can be chosen by the judgment of the researcher and the particular degradation characteristics of the system being tested. If degradation with each cycle tends to be gradual, three cycles for each deformation level may be appropriate. On the other hand, if degradation intensifies rapidly, two cycles at each deformation level may be appropriate to inspect a wider range of deformation levels before most strength of the specimen is lost.

- *General: FEMA 461 protocol (FEMA 461, 2007)*. Figure 2.3(d) illustrates the cyclic loading history suggested by FEMA 461 (2007). This protocol was developed for testing general structural and nonstructural elements in buildings aiming at the development of component fragility curves. It uses a targeted maximum deformation amplitude Δ_m and a targeted smallest deformation amplitude Δ_0 as reference values. The targeted smallest deformation amplitude Δ_0 should be smaller than the amplitude at which the lowest damage state is first observed. The amplitude of each cycle, a_i, monotonically increases as the step progresses with the specified ratio between adjacent amplitudes given by $a_{i+1}/a_i = 1.4$. The amplitude of the first cycle, a_1, is equal to Δ_0, and the amplitude of the last cycle is suggested as Δ_m. However, if the last damage state has not yet occurred at the target maximum deformation level Δ_m, the cyclic loading test shall be continued by using further increments of amplitude of $0.3\Delta_m$. Two cycles are adopted for the number of each cycle.

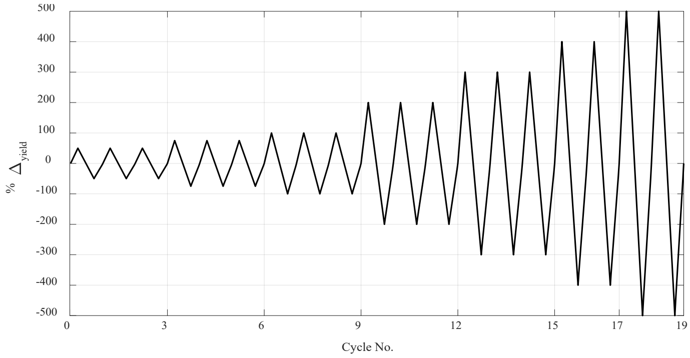

(a)

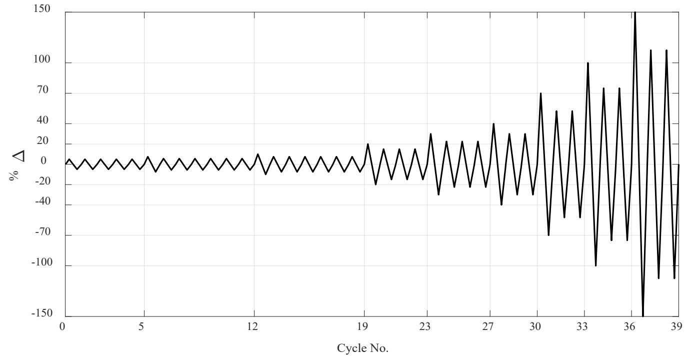

(b)

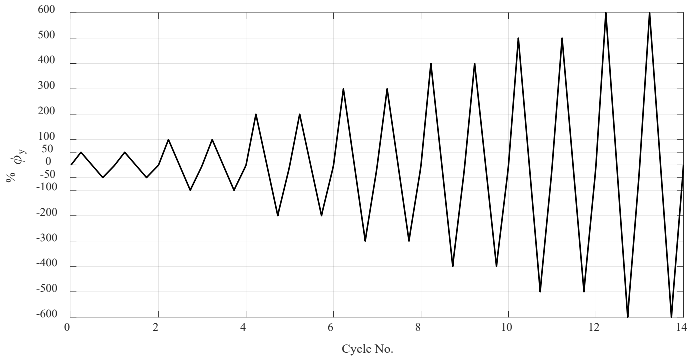

(c)

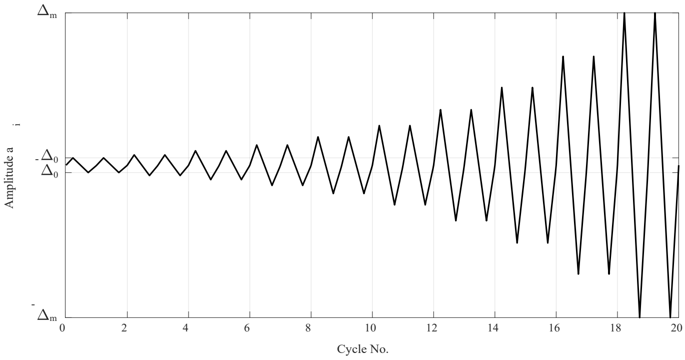

(d)

Figure 2.3 Loading histories specified in (a) ATC-24, (b) CUREE, (c) ACI 374, and (d) FEMA 461

2.3.2. Common properties of existing loading protocols

Various loading protocols have been developed in addition to the four representatives illustrated in Section 2.3.1 (e.g., Marder et al., 2018). These protocols appear to recommend somewhat different loading histories, but in most cases, they differ more in detail than in concept (Krawinkler, 2009). In this section, the commonalities of the existing loading protocols are presented in two perspectives: objectives and the overall configurations.

The primary objective of the existing loading protocols is to evaluate the seismic performance of structural components. Specifically, previous research efforts have been made to develop a cyclic loading history that replicates the load and deformation histories a component will undergo in an earthquake (Krawinkler, 1996). Accordingly, since the seismic capacities depend on the history of previously applied damage, the overriding issue for the development of a realistic and practical loading protocol is to simulate cumulative damage effects through quasi-static cyclic loading test. To account for the damage effects from earthquakes, several analytic models for low-cycle fatigue are used. Low-cycle fatigue is one type of cumulative damage, which is usually associated with cracking or fracture in metals (FEMA 461, 2007). The simplest low-cycle fatigue model is the one that based on the two hypotheses of a Manson-Coffin relationship and Miner's rule. The first hypothesis postulates that a logarithm of the number of excursions to failure has a linear relationship with a logarithm of the plastic deformation range. The second hypothesis postulates that the damage per excursion and the damage from excursions with different plastic deformation ranges can be combined linearly. The details for the low-cycle fatigue model can be found in FEMA 461 (2007). Several loading protocols in guidelines are developed based on the low-cycle fatigue model to replicate the damage effects from actual earthquakes through quasi-static cyclic loading test.

Furthermore, when it comes to the overall configurations, the existing loading protocols share several features. First, most loading protocols developed in the literature show monotonically increasing trends. Although the trailing cycles of the CUREE protocol may be a counterexample, one cannot deny the overall trends of monotonically increase of the loading. Second, the cyclic loading test continues until the test specimen fails or shows a severe damage state. The first and the second characteristic are necessary for the existing loading protocols with which the seismic performance of components should be directly evaluated. To assess the capacities for seismic excitations, it is reasonable to inspect the ultimate state of the specimen when it is subjected to the load that replicates earthquakes. Third, in terms of the amplitude of cycles, most loading protocols show incrementally increasing trends without a considerable difference from a preceding cycle. This is to inspect the whole damage states that the specimen can show. Last, regarding the number of cycles, the existing loading protocols commonly suggest 2 or 3 cycles for the amplitudes larger than the yield deformation and sufficient number, up to 6, of cycles for the elastic region to ensure the reliable estimation for stiffness of the components.

Besides, it should be noted that there is no complete loading history because any two earthquakes cannot be identical and because the specimen may be part of many different structural configurations (Krawinkler, 2009). Most guidelines for a cyclic loading test add a comment at the end of their specification that a different loading history may have to be employed for tests with different objectives (ATC-24, 1992; CUREE, 2001; FEMA 461, 2007; ACI 374, 2013).

2.4. Limitations of existing hysteresis modeling framework

As presented in Sections 2.2 and 2.3, many Bouc-Wen class models and several loading protocols have been proposed in numerous literatures. However, questions have been raised as to whether the existing hysteresis modeling framework can be used to perform reliable nonlinear dynamic analysis (Hamburger et al. 2016). Indeed, the existing hysteretic modeling framework has been mainly applied to nonlinear static seismic analyses such as capacity spectrum analysis (ATC-40, 1996) and the coefficient method of displacement modification (FEMA 356, 2000). Moreover, in such nonlinear static seismic analyses, polygonal hysteretic models (PHMs), not Bouc-Wen class models, are mainly used to account for various kinds of hysteresis. Considering that the computational tractability of Bouc-Wen class models is superior to the PHMs, and further, nonlinear time history analysis generally provides more reliable assessment of seismic performance than nonlinear static analysis (NIST, 2010), it shall be highly beneficial to perform nonlinear time history analysis using a Bouc-Wen class model. Therefore, in this section, to investigate the applicability on a nonlinear time history analysis, several limitations of the existing hysteretic modeling framework, especially for components susceptible to cracks, are suggested.

2.4.1. Limitations of existing Bouc-Wen models

The accuracy of the results of nonlinear dynamic analysis depends on the hysteretic model and how faithfully it captures the significant behavioral effects (NIST, 2010). Furthermore, in contrast to a nonlinear static analysis, a dynamic analysis requires more explicit modeling of cyclic response including strength and stiffness degradation (Haselton et al., 2016). However, a Bouc-Wen class model may present a good matching with the experimental data for a specific input while the model fails to keep significant physical properties inherent to the real data, independently of the exiting input (Ikhouane et al., 2007). Specifically, the existing Bouc-Wen class models have often shown limitations in predicting the hysteretic behaviors of components susceptible to cracks such as reinforced concrete columns.

For example, Figure 2.4 shows the comparison of the data obtained from the FE analysis on a reinforced concrete column and the m-BWBN model fitted to the load-deformation data. The black solid line indicates the FE analysis result, and the blue dotted line indicates the m-BWBN model fitted to the data. In addition, the loading history shown in Figure 2.5 is the applied load to obtain the hysteresis loop shown in Figure 2.4. It is seen that the m-BWBN fails to describe the elastic region after large deformation, and also shows notable and asymmetric error in the first excursion. The implications of the two parts in which the m-BWBN shows gap from the FE analysis results are suggested in detail in Chapter 3. Note that detailed properties of an actual reinforced concrete column provided by the Pacific Earthquake Engineering Research (PEER) Center are used for constructing a FE model in order to guarantee that the hysteresis loop obtained from the FE analysis is a realization of the behavior of actual reinforced concrete columns. Details for the structural database provided by the PEER center are presented in Chapter 5.

Furthermore, even if the estimated hysteretic model enables a proper illustration of the experimental hysteresis, it is difficult to guarantee that the estimated parameters produce the equivalent restoring force when the history of the input displacement is changed (Kim, 2021). For instance, Figure 2.6 presents the comparison between the FE analysis result and the m-BWBN prediction result for another cyclic loading history other than the cyclic loading history used for fitting the m-BWBN model. The black solid line and the blue dotted line in the figures denote the FE analysis result and the m-BWBN model, respectively, while the loading history in the upper left of each figure represents the applied cyclic loading history for each numerical experiment. In Figure 2.6(a), the m-BWBN seems well fitted so that the model simulates the result of FE analysis well. On the other hand, in Figure 2.6(b), the m-BWBN model shows poor prediction performance for another cyclic loading history that is different from the loading history used for fitting the model. This issue on the prediction accuracy has been consistently pointed out (Ikhouane et al., 2007; Hamburger et al., 2016; Kim 2021). In specific, the lack of consistency in prediction accuracy is not only attributed to the existing hysteretic model, but also to the applied loading history, which is presented in the following section.

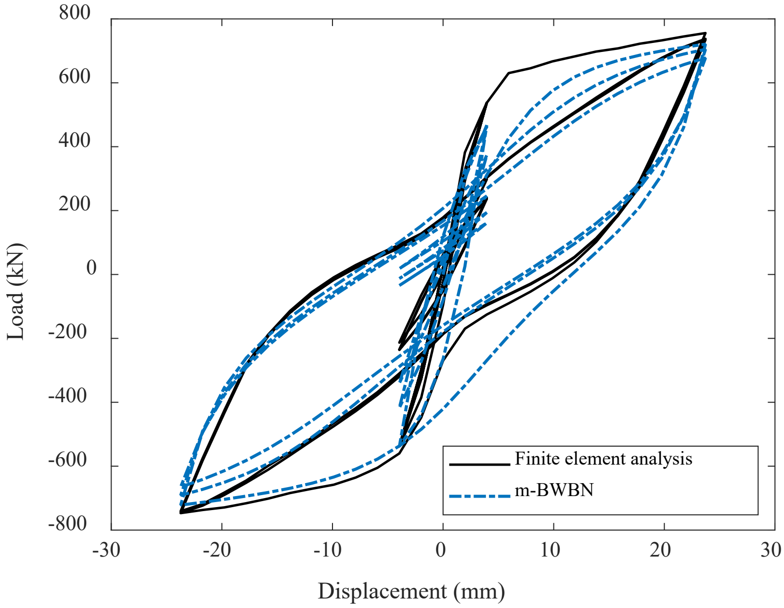

Figure 2.4 Comparison between the FE analysis result for a reinforced concrete column and the m-BWBN model fitted to the load-deformation data obtained from the FE analysis

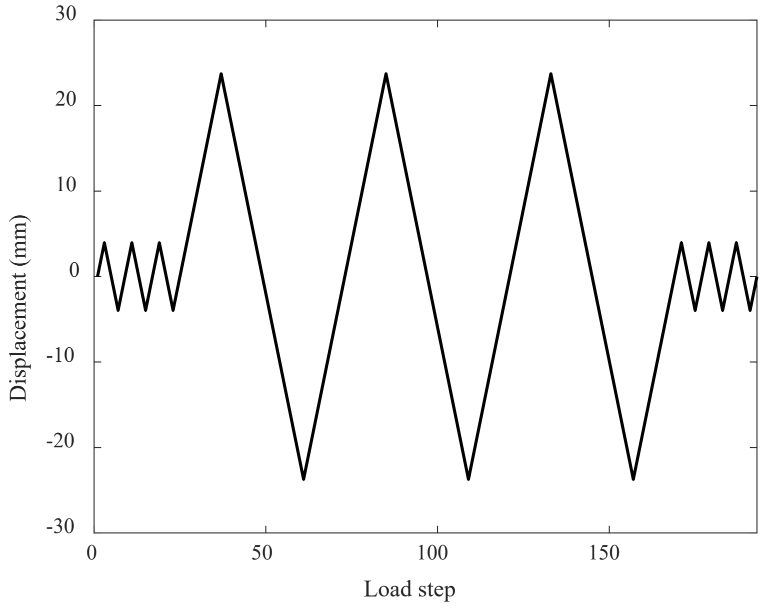

Figure 2.5 The cyclic loading history applied for the numerical experiment conducted for Figure 2.4

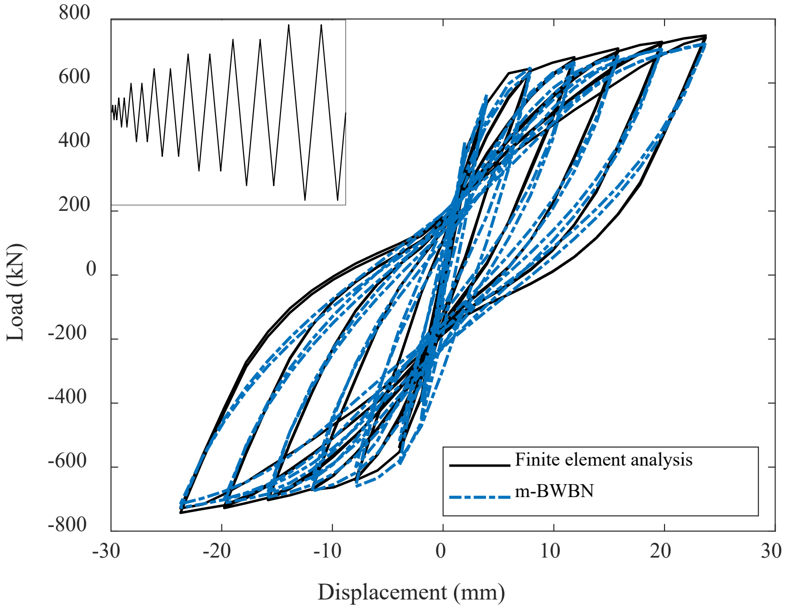

(a)

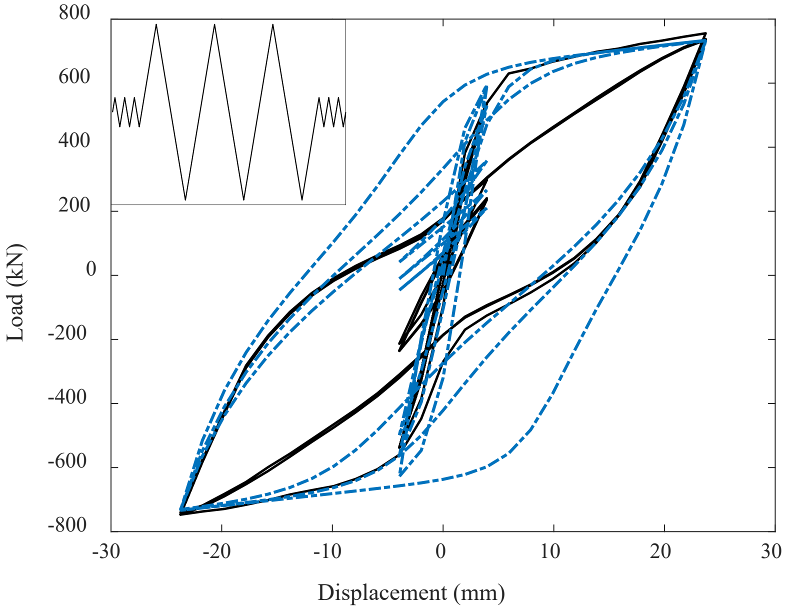

(b)

Figure 2.6 Comparison between the FE analysis result and the m-BWBN model for (a) the cyclic loading history used for model fitting and (b) the new loading history

2.4.2. Limitations of existing loading protocols

To identify the hysteretic parameters with the load-deformation data obtained using loading protocols, the load-deformation data should reflect the hysteretic behaviors of the test specimen. As stated in Section 2.3, however, the existing loading protocols have shortcomings in inducing the overall hysteresis of structures as they mainly focus on replicating a realistic load comparable to earthquakes for seismic performance evaluation. The hysteretic behaviors of structural components cannot be achieved simply by the loading with progressively increasing level of deformation. The loading history should contain the appropriate mode for each hysteretic behavior, i.e., the way of how hysteresis appears. In fact, Lee and Han (2021) stated that cyclic envelope, which is an envelope of the cycles on a hysteresis loop, varies according to loading protocols. Marder et al. (2018) also pointed out the lack of consistency in the loading protocols being used for large-scale laboratory testing, although protocols typically consist of quasi-static, reversed cyclic loading with multiple cycles at each level of progressively increasing peak displacement demands.

Comparing the figures shown in Figures 2.4 and 2.6, the performance of the existing loading history for fitting the hysteretic model can be recognized. Note that the applied loading history shown in the upper left par of Figure 2.6(a) is the loading history proposed by ACI 374 shown in Figure 2.3(c). The ACI 374 loading protocol is the representative loading protocol developed for reinforced concrete components. However, the m-BWBN fitted with the ACI 374 protocol fails to predict the response of the reinforced concrete column subjected to the loading history with large amplitude changes as shown in the upper left part of Figure 2.6(b). This is because the ACI 374 protocol consists of only small increments in amplitudes while not involving the large amplitude changes. One might say that the poor prediction performance shown in Figure 2.6(b) arose from the limited coverage of the m-BWBN model. That is also true, however, the coverage of the m-BWBN model for large amplitude changes shows somehow acceptable performance in Figure 2.4, although it is not good enough. This indicates that the poor performance shown in Figure 2.6(b) is not only a problem with the m-BWBN model but also a considerable issue with the loading history used to fit the model.

Chapter 3. Development of Bouc-Wen class model considering cracking effects

Bouc-Wen class models in this thesis refer to the hysteretic models based on the basic formation used in the original Bouc-Wen model. The existing Bouc-Wen class models can describe various hysteretic behaviors, such as the stiffness and strength degradation and pinching effect (Ismail et al., 2009). The BWBN model, which constitutes a basis for the Bouc-Wen class models for degrading and pinching systems, postulates that the stiffness and strength degradation and pinching effect are functions of the cumulative hysteretic energy (Baber and Noori, 1985). However, as presented in Section 2.2.4, the postulation was shown to have limitations in describing the behavior of composite structures, especially to mimic the hysteresis of reinforced concrete columns.

Therefore, this chapter first identifies two cracking effects affecting the behavior of composite material, which sheds light on the root of the existing models' limitations. Next, a novel Bouc-Wen class model is proposed considering the specified cracking effects.

3.1. Cracking effects affecting hysteresis

Structural components susceptible to cracks, such as reinforced concrete columns, show a distinct trend in hysteresis for the systems in which cracks do not have a dominant influence on the behaviors. This section suggests two effects of cracks affecting the hysteresis of structural components, stepwise deterioration, and the crack closure effect. The changes that appear on the hysteresis loop due to the cracking are illustrated in Section 4.1.

3.1.1. Stepwise deterioration

There exist various sources of cracks in a structural member. For example, thermal cracking, shrinkage cracking, freeze-thaw might cause cracks. In addition, external forces damage structural members in terms of cracks in tension, flexure, and shear (Shaikh, 2018). In this study, only the cracks formed from the external forces are considered, excluding the environmental factors.

Cracks are the realization of damage for structures, and composite materials are usually susceptible to cracks. Cracks degrade the stiffness of composite material, which is usually observed in reinforced concrete (Zhong et al., 2010) and laminates (Kashtalyan and Soutis, 2016). For reinforced concrete structures, specifically, the deterioration in stiffness is due to the loss of reinforcing steel and the cracks in the cover concrete (Zhong et al., 2010). Furthermore, the pinching effect is a phenomenon related to the stiffness while the strength of a structure highly depends on the total damage of the structure. In other words, the formulation of cracks not only degrades the stiffness of a structural component but also affects the strength and the pinching effect. Moreover, the deterioration of composite material occurs dramatically and stepwise as cracks are formed.

The cracking effects of stepwise deterioration can be found in the actual experimental data. The Pacific Earthquake Engineering Research (PEER) Center provides 416 experimental datasets for reinforced concrete columns under quasi-static cyclic test, and Figure 3.1 shows brief configurations of the quasi-static cyclic test. The load-deformation data shown in Figure 3.2 are obtained when the cyclic loading history shown in Figure 3.3 is applied to the reinforced concrete column of Figure 3.1. The red lines in Figure 3.3 represent the range in which the column experiences a larger deformation than the previous maximum deformation, which implies cracks are formed. In other words, the red lines in Figure 3.3 refer to the cracking zones. In Figure 3.2, the strength and stiffness of the column degraded dramatically between the two cycles with the same amplitudes. Since the second cycle of each amplitude is the cycle after the cracking zones, the stepwise deterioration can be considered as the results of the cracks that are formed after the cracking zones.

Figure 3.1 A reinforced concrete column used for the quasi-static cyclic test (Figure from Pacific Earthquake Engineering Research Center, 2021)

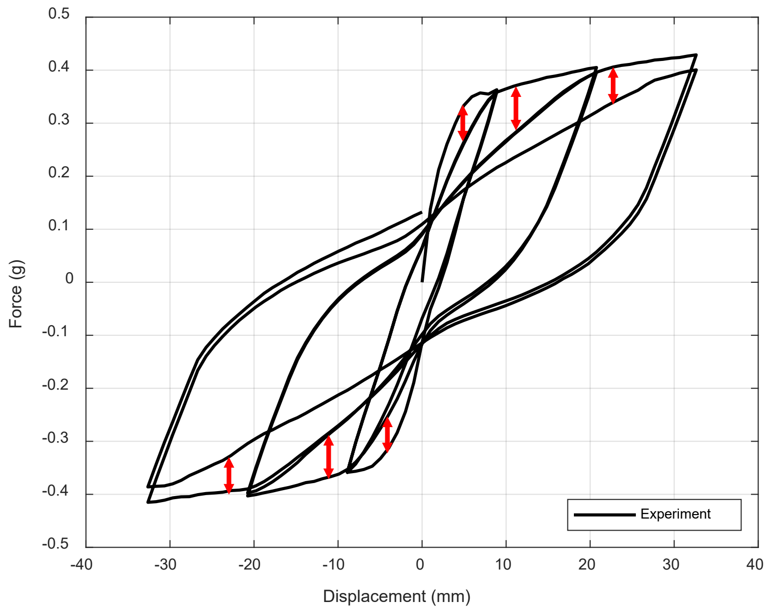

Figure 3.2 The load-deformation data obtained from a quasi-static cyclic test (The red arrows indicate the stepwise degradation in strength and stiffness)

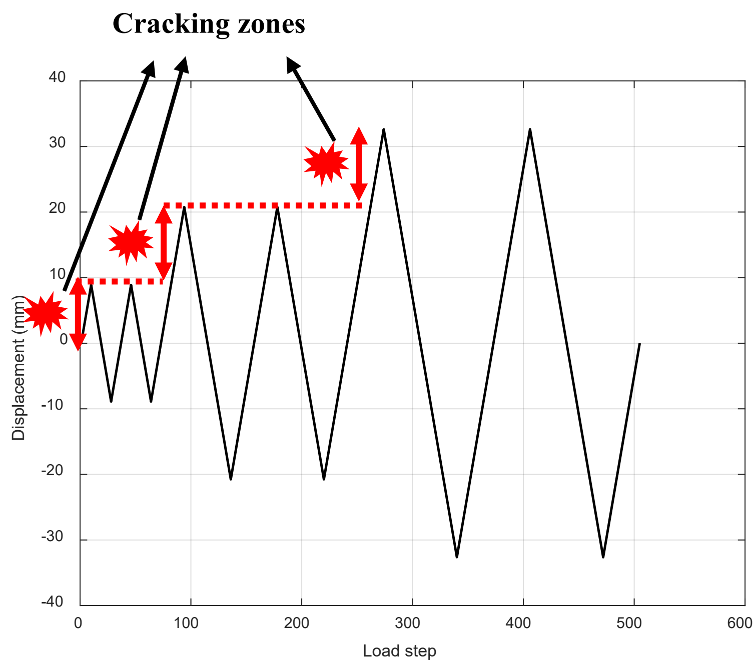

Figure 3.3 The cyclic loading history used for a quasi-static cyclic test from which the load-deformation data in Figure 3.2 is obtained (The red indications denote the cracking zones)

3.1.2. Crack closure effect

Wolf (1970) discovered that contact between the fracture surfaces could occur even during cyclic tensile loading. In the research, the fracture surface contact is attributed to the plastic deformation in the wake of a growing crack, which is nowadays usually called plasticity-induced crack closure (Pippan and Hohenwarter, 2017). Several other mechanisms, e.g., roughness-induced crack closure (Minakawa et al., 1983), oxide-induced crack closure (Suresh et al., 1981), and phase transformation induced crack closure (Ritchie, 1999), responsible for premature contact of the cracks also have been proposed during the decades.

The pinching effect in reinforced concrete is caused by shear lock, slippage of longitudinal reinforcement, and crack closure (Yu et al., 2016). Moreover, the pinching effect is caused by cyclic closure/opening of cracks, leading to a significant reduction of the stiffness in the load-inversion phase due to the closure of the cracks (Blasi et al., 2018). The mechanism of how the crack closure relates to the pinching effect is as follows. Even in the cracked material, crack closure causes a load transfer only during a certain part near the minimum load of the load amplitude and therefore only affects the cyclic deformation of the crack tip (Pippan and Hohenwarter, 2017). In other words, cracks in a structural component may transfer the load when the load is too small to open the cracks. However, the cracks become unable to transfer the load when the load is larger than the threshold value. There is abrupt degradation in stiffness near the threshold load for crack closure, which means the crack closure is related to the pinching effect, i.e., a sudden deterioration in stiffness near the origin under cyclic loading.

However, most mechanical models available in finite element software packages cannot simulate the responses under cyclic loads, particularly in the case of sizeable tensile strain/displacement. It is because the crack closure cannot be accurately reproduced in the numerical model (Blasi et al., 2018).

The crack closure effect on the pinching is illustrated in Figures 3.4 and 3.5. The load-deformation data shown in Figure 3.5 is obtained under the cyclic loading shown in Figure 3.4 using nonlinear finite element analysis. The finite element model used for the numerical test is constructed based on the details of the reinforced concrete column shown in Figure 3.1 so that the finite element analysis result may represent the behavior of the actual structure. During the second range shown in Figure 3.4, it is expected that the cracks are opened as the last peak displacement, about 24 mm, is large enough to open the cracks. Consequently, there exists a relatively strong pinching effect in the second range. In contrast, only a little pinching effect appeared during the first range since the last peak displacement, about 7 mm, is not large enough to open all the cracks. It can also be found that the intensity of the pinching effect is weakened as the last peak displacement decreases; that is, the shape of the slope becomes linear.

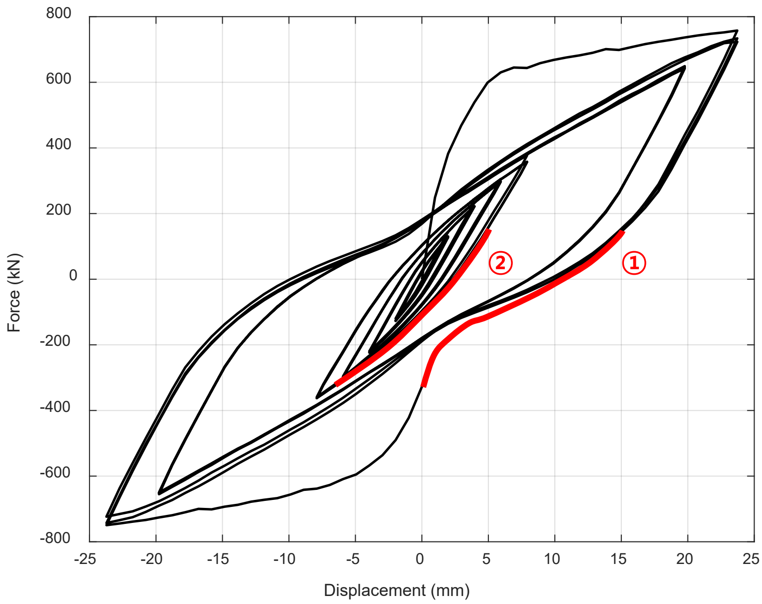

Figure 3.4 The load-deformation data under quasi-static cyclic loading using nonlinear finite element analysis (The stiffness change between ranges 1 and 2 shows the crack closure effect)

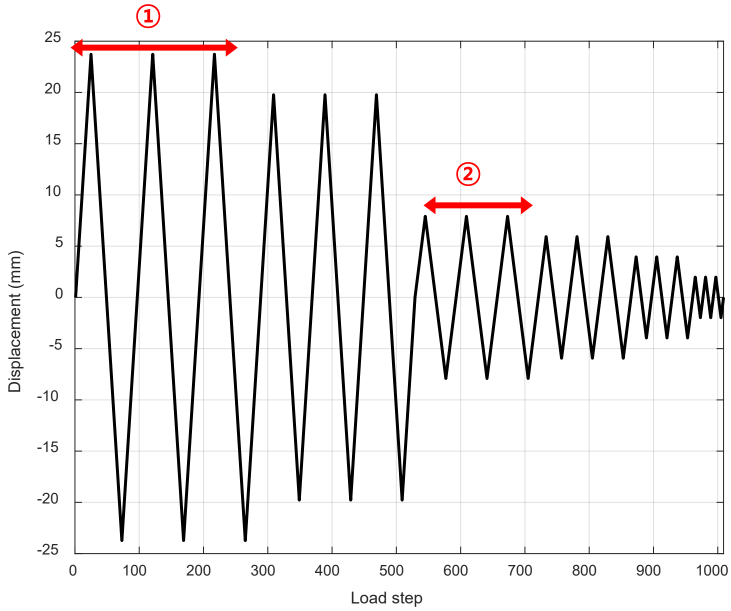

Figure 3.5 The cyclic loading history used for the quasi-static cyclic test by which the load-deformation data in Figure 3.4 is obtained (The two red ranges correspond to the ranges denoted in Figure 3.4, respectively)

3.2. Proposed Bouc-Wen model considering cracking effects

Among the various existing Bouc-Wen models capable of describing the stiffness and strength degradation and pinching effect, the m-BWBN model by Kim (2021) is considered as a reference model. Based on the m-BWBN model, modifications are made in two ways to incorporate the two cracking effects presented in Section 3.1, respectively. The following sections illustrate the two details of the proposed Bouc-Wen model considering cracking effects.

3.2.1. Modification of the cumulative hysteretic energy

The basic assumption of the Bouc-Wen class models considering degradation and pinching is that the intensity of degradation in stiffness and strength and the pinching effect is proportioned to the cumulative hysteretic energy, which is expressed in Eq. (2.5) However, the cumulative hysteretic function defined by Eq. (3.1) cannot capture the stepwise deterioration in composite materials. To account for the cracking effect, this thesis proposes to amplify the rate of cumulating hysteretic energy when cracks occur. To define a criterion for the occurrence of cracks, an assumption is made such that cracks are formed when a structure experiences a displacement larger than the previous maximum displacement. In composite structures such as reinforced concrete columns, cracks occur on the tensile side when a new magnitude of tensile strain is applied because the tensile strength of concrete is small. Thereby, based on the assumption, the modified cumulative hysteretic energy is proposed as follows:

$$\varepsilon = \left(\varepsilon_+ \cdot H(u) + \varepsilon_- \cdot \left(1 - H(u)\right)\right) \tag{3.1}$$

where ε is the cumulative hysteretic energy used for the current state, ε_+ and ε_- are the cumulated hysteretic energy for each side, i.e., two sides corresponding to the positive and negative direction under uniaxial loading, respectively. Note that when a deformation is made in a positive direction, i.e., the sign of u is positive, ε_+ becomes the cumulated hysteretic energy of a system, ε, and vice versa. The cumulated hysteretic energy is defined in each side separately to reflect that cracks, specifically flexural cracks, in reinforced concrete occur in the tensile side, not in the compression side. In addition, $H(\cdot)$ is the Heaviside step function, or the unit step function, in which the value is zero for negative arguments and one for positive arguments, which is defined herein as

$$H(x) = \begin{cases} 1, & x > 0 \\ 0, & x \leq 0 \end{cases} \tag{3.2}$$

In addition, the cumulative hysteretic energy for each side, ε_+ and ε_-, is defined by the following rate equations, respectively:

$$\dot{\varepsilon}_+ = \{1 + c_\varepsilon \cdot H(u - u^{max})\}(1-\alpha)\frac{k_0}{F_y} z\dot{u} \tag{3.3}$$

$$\dot{\varepsilon}_- = \{1 + c_\varepsilon \cdot H(u^{min} - u)\}(1-\alpha)\frac{k_0}{F_y} z\dot{u} \tag{3.4}$$

where c_ε is the hysteretic energy amplification factor, which is newly introduced in this study, u_{max} is the previous maximum displacement applied, and u_{min} is the previous minimum displacement applied, which are defined in mathematical expression as

$$u_i^{max/min} = \max/\min\{u_j\} \text{ for } j \in \{1,2,\ldots,i-1\} \tag{3.5}$$

where i indicates the current load step, and $u_i^{max/min}$ is the maximum/minimum displacement until the i-th load step.

In Eq. (3.3) to (3.5), a sign of displacement is considered. That is, a sign of u becomes positive when the displacement is in a positive direction, and vice versa. Similarly, u_{min} is the displacement that is maximum in magnitude in a negative direction. The signs of u_{max} and u_{min} are positive and negative, respectively. Note that $c_\varepsilon = 0$, which implies that no amplification effect exists, results in the original formulation of the cumulative hysteretic energy.

3.2.2. Modification of the pinching function

This study proposes the modified pinching function to describe the crack closure effect on pinching based on the existing pinching function. In the m-BWBN model, the pinching effect of a system is determined by Eq. (2.8). However, the pinching function defined by Eq. (2.8) cannot describe the pinching effect that depends on the closure/opening of cracks. Therefore, this study proposes the modified pinching function to consider the crack closure effect on pinching as follows:

$$h(z,\varepsilon) = 1 - \zeta_1(\varepsilon)\exp\left(-\left(\frac{z\cdot sgn(\dot{u}) - qZ_u}{\zeta_2(\varepsilon)}\right)^2\right)\left(1 - \exp\left(-c_h\frac{|\tilde{u}|}{d_y}\right)\right) \tag{3.6}$$

where c_h is the crack closure coefficient, which is newly introduced in this study, d_y is the yield displacement of a system, and $\tilde{u}$ is the last peak displacement which is defined as:

$$\tilde{u}_i = \max_j\left\{u_j \middle| |u_j| > |u_{j-1}| \cap |u_j| > |u_{j+1}|,\ j \in \{1,2,\dots,i-1\}\right\} \tag{3.7}$$

where i indicates the current load step, and $\tilde{u}_i$ is the last peak displacement at the i-th load step.

By comparing two equations of Eq. (2.8) and (3.6), it is noted that a new exponential term, termed crack closure function f, is added in Eq. (3.6) from Eq. (2.8). Figure 3.6 shows three realizations of the crack closure function in terms of three different values for the crack closure coefficient c_h. As shown in Figure 3.6, the smaller last previous peak displacement $\tilde{u}_i$, the closer the value of a crack closure function to zero. The crack closure function with a value of zero leads the modified pinching function to 1, which implies that there is no pinching effect. It is justifiable because a small value of the last previous peak displacement cannot open cracks that are the main sources of the pinching effect. Note that the conventional pinching function in Eq. (2.8) cannot capture this relaxed pinching effect from the crack closure effect. On the other hand, as the value for $\tilde{u}_i$ increases, the crack closure function approaches 1, which makes the modified pinching function identical to the conventional pinching function in Eq. (2.8). It can also be justified in that the crack closure effect does not need to be considered when the last peak previous displacement is so large that there are no closed cracks. Likewise, in terms of the crack closure coefficient c_h, a small value of c_h implies the intense crack closure effect and vice versa.

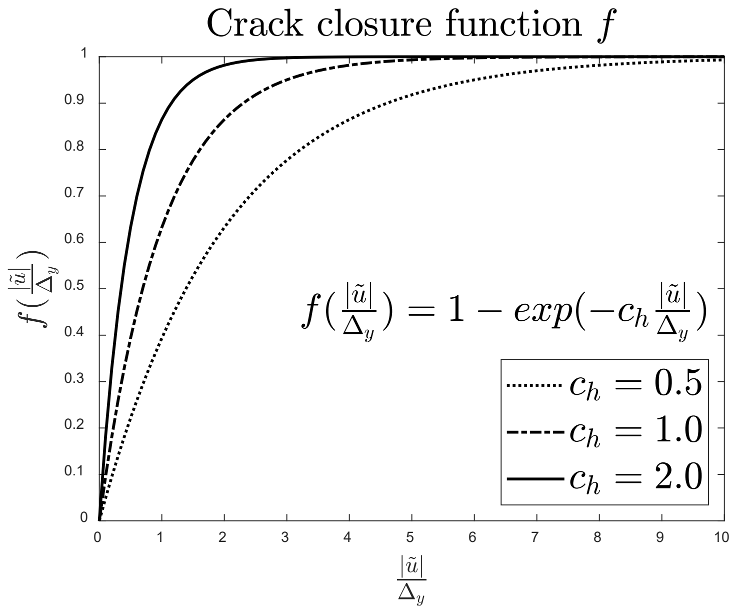

Figure 3.6 Three realizations of the crack closure function with three crack closure coefficients

3.2.3. Integrated mathematical formulation of the proposed model

An integrated mathematical formulation of the proposed Bouc-Wen class model that incorporates the two modifications explained in the sections above are as follows:

$$f_s = f(u,z) = \alpha k_0 u + (1-\alpha)F_y z \tag{3.8}$$

$$\dot{z} = \frac{h(z,\varepsilon)}{\eta(\varepsilon)}\dot{u}[1 - |z|^n\{\gamma + \beta \cdot sgn(\dot{u}z)\}\nu(\varepsilon)]\frac{k_0}{F_y} \tag{3.9}$$

$$\eta(\varepsilon) = 1 + \delta_\eta \varepsilon \tag{3.10}$$

$$\nu(\varepsilon) = 1 + \delta_\nu \varepsilon \tag{3.11}$$

$$h(z,\varepsilon) = 1 - \zeta_1(\varepsilon)\exp\left(-\left(\frac{z \cdot sgn(\dot{u}) - qZ_u}{\zeta_2(\varepsilon)}\right)^2\right)\left(1 - \exp\left(-c_h\frac{|\tilde{u}|}{d_y}\right)\right) \tag{3.12}$$

$$\zeta_1(\varepsilon) = \zeta_0(1 - \exp(-p\varepsilon)) \tag{3.13}$$

$$\zeta_2(\varepsilon) = (\psi + \delta_\psi \varepsilon)(\lambda + \zeta_1(\varepsilon)) \tag{3.14}$$

$$Z_u = \left(\frac{1}{\nu(\varepsilon)(\beta+\gamma)}\right)^{\frac{1}{n}} \tag{3.15}$$

$$\varepsilon = \left(\varepsilon_+ \cdot H(u) + \varepsilon_- \cdot \left(1 - H(u)\right)\right) \tag{3.16}$$

$$\dot{\varepsilon}_+ = \{1 + c_\varepsilon \cdot H(u - u^{max})\}(1-\alpha)\frac{k_0}{F_y}z\dot{u} \tag{3.17}$$

$$\dot{\varepsilon}_- = \{1 + c_\varepsilon \cdot H(u^{min} - u)\}(1-\alpha)\frac{k_0}{F_y}z\dot{u} \tag{3.18}$$

$$u_i^{max/min} = \max/\min u_j \;\; \text{for } j \in \{1,2,\dots,i-1\} \tag{3.19}$$

$$\tilde{u}_i = \max_j\left\{u_j \middle| |u_j| > |u_{j-1}| \cap |u_j| > |u_{j+1}|,\; j \in \{1,2,\dots,i-1\}\right\} \tag{3.20}$$

where the total of 16 parameters exists. However, to reduce the number of parameters in Bouc-Wen class models for simplicity, the constraint for β and γ is adopted: $\beta + \gamma = 1$. Consequently, the number of parameters used in the proposed Bouc-Wen class model becomes 15 as listed in Table 3.1. The proposed Bouc-Wen class model is different from the reference model mainly in two parts: the pinching function h and the cumulative hysteretic energy ε. An incremental algorithm for estimating the restoring forces given load step in terms of displacement is presented in Appendix A based on previous studies (Hossain et al., 2013; Yu et al., 2016; Ning et al., 2021; Kim, 2021).

Table 3.1 A total of 15 parameters used in the proposed Bouc-Wen class model

Parameter	Description
α	Post-yield stiffness ratio
k_0	Initial stiffness
F_y	Yield force
β	Basic hysteretic shape control
n	Sharpness of yield
δ_ν	Strength degradation rate
δ_η	Stiffness degradation rate
ζ_0	Measure of total slip
p	Pinching slope
q	Pinching initiation
ψ	Pinching magnitude
δ_ψ	Pinching rate
λ	Pinching severity
c_ε	Hysteretic energy amplification factor
c_h	Crack closure coefficient

Chapter 4. Loading protocol for model fitting

As stated in Section 2.3, various existing loading protocols have shown limitations in estimating the parameters of hysteretic models. It is mainly because the main objective of the existing loading protocols is to simulate a realistic loading history and reproduce the cumulative damage effect that a structure might experience during an earthquake (Krawinkler 2009; FEMA 356), leaving weaknesses in producing nonlinearities of the structure. A single loading protocol for laboratory testing cannot capture the variability in the earthquake demands as earthquakes produce unique ground motions (Marder, 2018).

Thereby, to evaluate the seismic performance, it is necessary to capture the nonlinearity including hysteresis in a structural member of interest, instead of simulating a loading akin to ground motions. With the cyclic loading history inducing sufficient hysteretic behaviors, one can obtain a load-deformation relationship that embodies enough nonlinearities of a structure. It is evident that the parameters cannot be estimated accurately if the load-deformation relationship contains little hysteretic behaviors. Consequently, a loading history inducing hysteretic behaviors is required to fit hysteretic models.

This chapter first categorizes various significant modes of hysteretic behaviors shown in structural components. Four widely studied modes are provided, and two additional modes for components susceptible to cracks are suggested. Next, a loading protocol as a series of procedures for model fitting is proposed. The loading protocol includes a quasi-static cyclic loading history that produces the specified hysteretic behaviors in Section 4.1 and the parameter estimation strategies for efficient and accurate model fitting.

4.1. Modes of hysteretic behaviors

A mode of hysteretic behaviors in this section refers to the distinct ways of how hysteresis, e.g., degrading of stiffness and strength and the pinching effect, manifest in the load-deformation relationship. Total six modes including four typical modes and two additional modes are provided in the following sections.

4.1.1. Typical modes specified in previous studies

A load-deformation relationship, from which one can specify structural components' strength and deformation capacities, depends on cumulative damage (Krawinkler 2009). The fact that the seismic performance of structures depends on the past damaging events implies that structures have a permanent memory of past loading histories, and the past loading histories affect behaviors of the current structures, which is called hysteresis. As a realistic evaluation of seismic performance cannot be achieved without understanding the hysteresis of structural members, numerous research has been conducted to consider the three most typical hysteretic behaviors, i.e., degrading of stiffness and strength and pinching effect (Sengupta 2017).

Stiffness and strength degradations and pinching effect occur in various modes. The four most typical modes of hysteretic behaviors under cyclic loadings are suggested by the Applied Technology Council and the Pacific Earthquake Engineering Research Center as follows (ATC 72-1, 2010):

① *Basic strength deterioration.* Strength deteriorates with the number and amplitude of cycles, even if the displacement associated with the strength cap has not been reached (denoted as mode 1 in Figure 4.1).

② *Post-capping strength deterioration*. Strength deteriorates further when a negative tangent stiffness is attained (denoted as mode 2 in Figure 4.1).

③ *Unloading stiffness deterioration*. Unloading stiffness deteriorates with the number and amplitude of cycles (denoted as mode 3 in Figure 4.1).

④ *Accelerated reloading stiffness deterioration*. For a given deformation amplitude, the second cycle indicates a smaller peak strength than the first cycle; however, the resistance increases, and the strength envelope is attained if the amplitude of the second cycle is increased (not denoted in Figure 4.1).

The first three modes of hysteretic behaviors are observed in the cyclic response of all structural components. In contrast, the fourth mode, i.e., accelerated reloading stiffness deterioration, is not discernible in components whose behaviors are controlled mainly by flexure (ATC 72-1, 2010). Although the characteristics of structural components in which the fourth mode is likely to occur are different, the existing loading protocols have been used by researchers to induce the accelerated reloading stiffness deterioration mode from a structural member as for the other modes (Ibarra 2005).

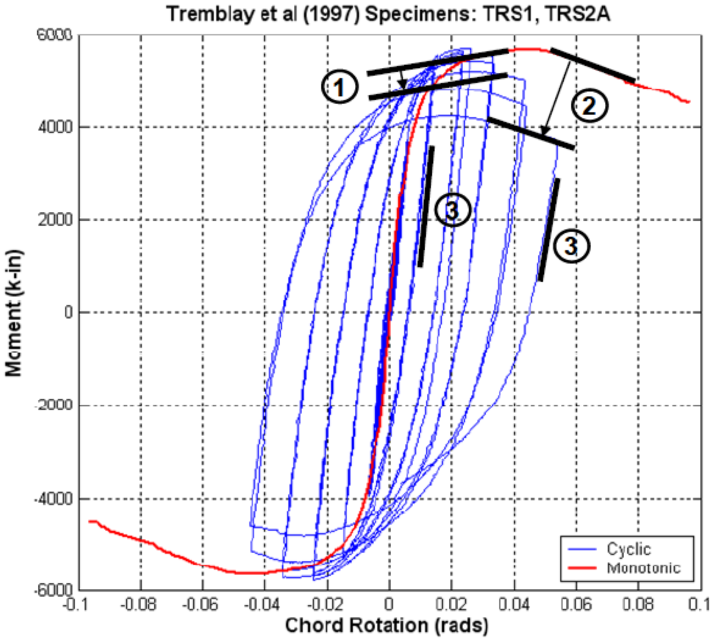

Figure 4.1 Monotonic and cyclic experimental response of a steel beam with the corresponding modes (Figure from ATC 72-1, 2010)

4.1.2. Additional modes for reinforced concrete

Besides the four typical modes of hysteretic behaviors stated above, this section suggests two additional modes that are discernible in composite material that is susceptible to cracks, such as reinforced concrete columns. The two additional modes of hysteretic behaviors are as follows:

⑤ *Stepwise degradation.* Stiffness, strength degradation, and pinching effect intensify stepwise as cracks propagate (denoted as mode 5 in Figure 4.2). Such stepwise degradation appears when a structural member experiences a larger deformation than the maximum deformation.

⑥ *Pinching relaxation*. The pinching effect is mitigated when cracks are closed as the applied amplitude decreases (denoted as mode 6 in Figure 4.2). The pinching relaxation appears when a cracked component experiences a deformation small enough to remain cracks closed.

Note that the additional two modes presented above stem from the cracking effects described in Section 3.1. Unlike the four typical modes, the existing protocols are insufficient to capture the two additional modes. As the 5th mode of hysteretic behaviors occurs when a structural component encounters a larger deformation than the previous maximum deformation, a cyclic loading with a large gap in deformation amplitudes is required to induce the stepwise deterioration. Likewise, to induce the hysteretic behavior of pinching relaxation by crack closure, small deformation near the yield deformation of a structure after large deformation is required to embody the crack closure effect. Therefore, to capture the full modes of hysteretic behaviors that appeared in a structural component susceptible to cracks, the existing loading protocols are not relevant.

Figure 4.2 provides an illustrative description of the two additional modes, and Figure 4.3 represents the cyclic loading applied for the numerical experiment performed using finite element analysis shown in Figure 4.2. Note that the cyclic loading history shown in Figure 4.2 clearly shows different configurations with the existing loading protocols.

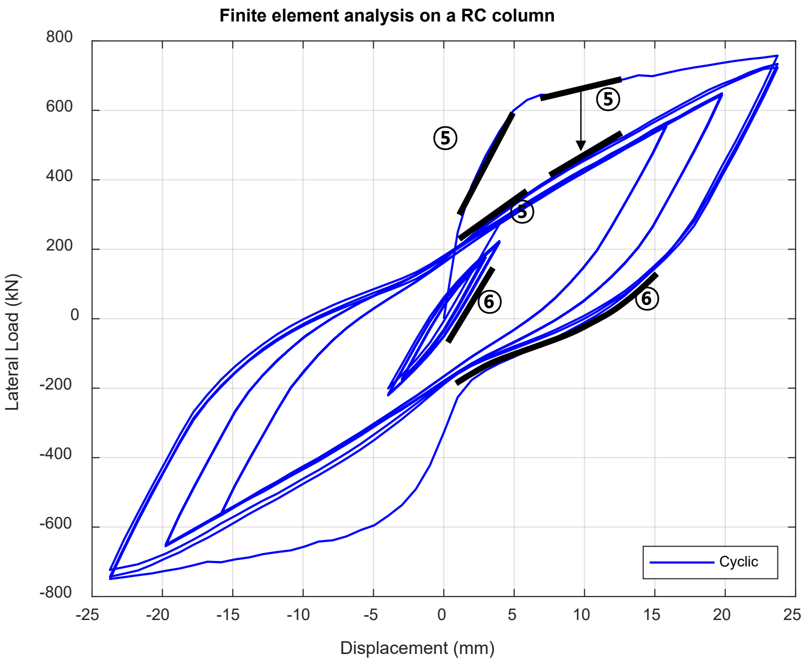

Figure 4.2 Cyclic response of a RC column obtained by FE analysis and the corresponding modes of hysteretic behaviors

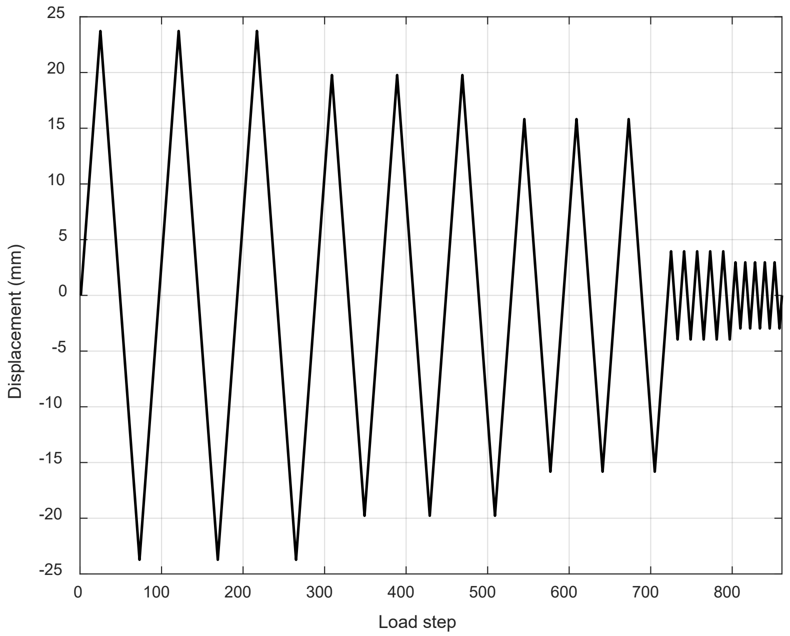

Figure 4.3 The cyclic loading history applied to obtain the load-deformation relationship shown in Figure 4.2

4.2. Proposed loading protocol

The loading protocol proposed in this section refers to an integrated procedure for fitting the Bouc-Wen model proposed in Section 3.2, not only a quasi-static cyclic loading history. The proposed loading protocol is composed of a two-step procedure with a pushover analysis followed by a quasi-static cyclic loading capable of inducing the full modes of hysteretic behaviors prescribed in Section 4.1. The details of each step and estimation strategies for efficient model fitting are provided in the following sections.

4.2.1. Step 1: Pushover analysis using a quasi-static monotonic load

In the existing approaches of nonlinear static analysis for seismic design, such as capacity spectrum method, coefficient method, and R-μ-T method, a nonlinear equivalent single degree of freedom (SDOF) system is used (FEMA 440, 2005; ASCE 41-13, 2013; Veletsos and Newmark, 1960). The parameters required to construct an equivalent SDOF system for a structure of interest are initial stiffness, yield force, and post-yield stiffness, which implies that the three parameters are the most critical to the dynamic characteristics. Therefore, the three parameters are first determined by applying quasi-static monotonic loading on a structural component, i.e., pushover analysis, as the first step for the proposed loading protocol.

For determining initial stiffness, yield force, and post-yield stiffness ratio, various methods have been developed to idealize a load-deformation curve under monotonic loading, i.e., a pushover curve. FEMA 356 (2000) and ASCE 41-13 (2014) suggest that the effective initial stiffness shall be taken as the secant stiffness calculated at a load equal to 60% of the effective yield strength of the structure, and the post-yield stiffness ratio shall be determined from the line segment with which the areas above and below the actual force-displacement curve are approximately balanced. Figure 4.4(a) illustrates the idealized force-displacement curves of FEMA 356 (2000) and ASCE 41-13 (2014).

Eurocode 8 (2004) provides the idealized force-displacement curves for the elasto-perfectly plastic force-displacement relationship. In the code, the yield force is taken as the ultimate strength, and the initial stiffness is determined such that the areas under the actual and the idealized force-deformation curves are equal, as illustrated in Figure 4.4(b).

However, current code-based idealization methods are found to be highly biased wherever widespread significant stiffness changes occur, generally leading to very conservative estimates of performance (De Luca et al., 2013). Hence, the idealization approach developed by De Luca et al. (2013) is used in this study. The "near-optimal" piecewise linear fits of static pushover capacity curves suggested in De Luca et al. (2013) showed much more stable and accurate estimates of seismic performance when it comes to the equivalent SDOF analysis. De Luca et al. (2013) proposed the initial stiffness as the secant stiffness corresponding to 10% of the effective yield force, instead of 60% suggested by FEMA 356 (2000) and ASCE 41-13 (2014). In addition, to balance the area enclosed by the fitted with the area enclosed by the exact curve, the absolute value that minimizes the area discrepancy between the curves is used instead of minimizing the total sum of area discrepancy itself. Figure 4.5 shows the difference between the idealized curves using the criteria of FEMA 356 (2000) and De Luca et al. (2013).

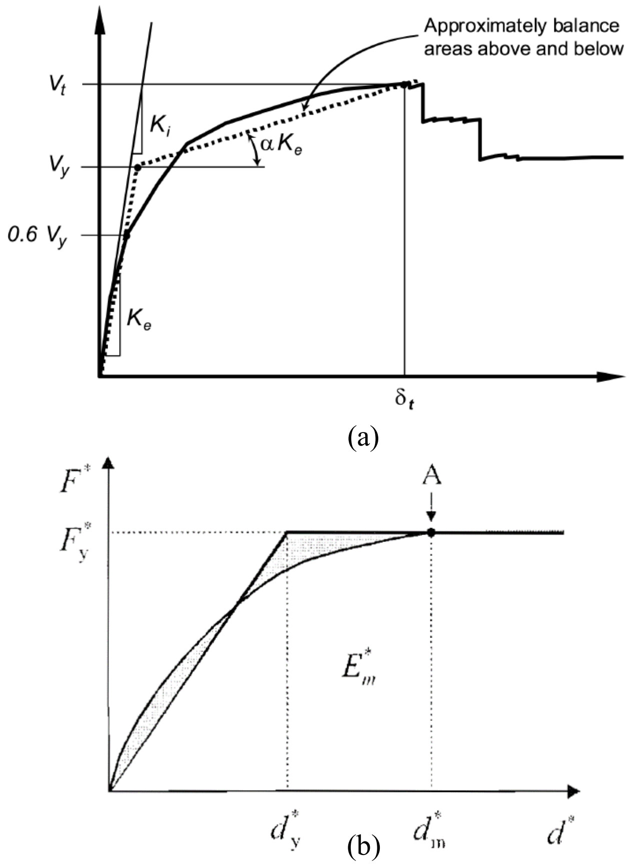

Figure 4.4 Idealized load-deformation curves presented in (a) FEMA 356 and in (b) Eurocode 8 (Figures from FEMA 356, 2000 and Eurocode 8, 2004)

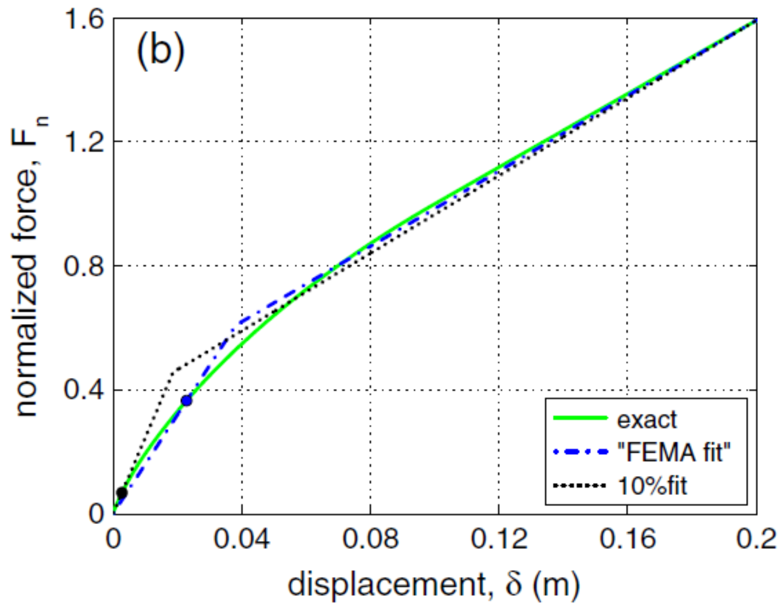

Figure 4.5 Comparison of idealized load-deformation curves using the criteria of FEMA 356 and De Luca et al. (2013) (Figure from De Luca et al., 2013)

4.2.2. Step 2: Quasi-static cyclic loading test

4.2.2.1. Features required for the cyclic loading history

To accurately estimate the parameters of hysteretic models, it is evident that the load-deformation relationship must contain the hysteresis that the structural component may show. Furthermore, to contain the hysteretic behaviors of structural components sufficiently, a cyclic loading history from which the load-deformation relationship is obtained should induce the full modes of hysteretic behaviors of the component. However, the full modes of hysteretic behaviors cannot be achieved with the existing loading histories suggested by the various guidelines.

In this regard, a cyclic loading history that can induce the full modes of hysteretic behaviors of a structural component susceptible to cracks is proposed. The three main features of the proposed cyclic loading history are as follows:

① *Three repetitions at various amplitudes.* The proposed cyclic loading history reflects the characteristics of the existing loading histories that repeat at least two or three times at various amplitudes (denoted by number 1 in Figure 4.6). It is required to ensure sufficient stiffness and strength degradation intensity and the pinching effect.

② *A section with a sharp increase in amplitude*. This feature is for the stepwise intensification on deterioration by generating cracks (denoted by number 2 in Figure 4.6).

③ *A re-elastic region after having inelastic behaviors*. This feature is for the pinching relaxation effect that appears when a cracked component experiences deformation so small that cracks remain closed (denoted by number 3 in Figure 4.6).

Note that the second and the third features of the proposed cyclic loading history are a new concept that are not shown in the existing loading histories. In the existing loading histories, it is recommended that tests should be terminated until the test specimen has degraded so severely that no relevant additional information about the performance can be acquired. It is because that the main objectives of the protocols are to determine the seismic capacities directly from the tests (CUREE, 2001; FEMA 461, 2007; ACI 374, 2013). However, to implement a re-elastic region after the inelastic region with large amplitudes, i.e., the third feature presented above, it is required for the test specimen not to be collapsed or failed before the beginning of the re-elastic region. In other words, the amplitudes of each step of the proposed cyclic loading history should be calibrated so that the test specimen can withstand the loading to the end.

The amplitudes $a_i's$ of the step i (not of each cycle since each step has one to four cycles) are given in Table 4.1. In Table 4.1, d_y indicates the yield deformation based on the definition provided by ASCE 41-13 (2013) and Δ_a represents the amplitude increment parameter defining the gaps between each amplitude. Note that the gap between the amplitude of the third and the fourth steps, i.e., a_3 and a_4, is two to four times larger than the gaps between the amplitudes of the other steps, reflecting the second feature of the proposed loading history.

4.2.2.2. Criterion for the ductile and brittle specimen

The value of the amplitude increment parameter Δ_a should be differently specified in ductile and brittle components so that the proposed cyclic loading history can be completed regardless of whether the test specimen is ductile or brittle. In this thesis, ductile and brittle components refer to the test specimen that can and cannot complete the proposed loading history having the maximum amplitude a_6 as $6d_y$ without severe damage, respectively. To determine whether the test specimen is ductile or brittle, i.e., the specimen can withstand the cyclic loading to the end, before the cyclic loading test, the results of pushover analysis performed in advance are used.

Using the simplest low-cycle fatigue model based on the hypothesis of Miner's rule (Krawinkler and Zonhrei, 1983), one can roughly forecast whether the specimen would fail or not during the cyclic loading test. Miner's rule of linear damage accumulation postulates that the damage per excursion is $1/N_f$, where N_f is the number of excursions to failure, and that the damage from excursions with different plastic deformation ranges, $\Delta\delta_{pi}$, can be combined linearly. Thus, the total damage D is given by the equation

$$D = C \sum_{i=1}^{N} \left(\Delta\delta_{pi}\right)^{c} \tag{4.1}$$

where C and c are structural performance parameters that are determined experimentally. In the simplest case, the value of c with 2.0 is an often-used value (FEMA 461, 2007), and the total damage of $D = 1.0$ constitutes failure. Using Eq. (4.1) and the value for c as 2.0, the result from the pushover curve can be related to the cyclic loading test as follows:

$$d_u^2 = \sum_{i=1}^{N} n_i \, a_{(i)}^2 \tag{4.2}$$

where n_i is the number of cycles of the amplitude $a_{(i)}$, $a_{(i)}$ is the magnitude of amplitude at step i, N is the number of steps, i.e., the number of groups with the same amplitude, and d_u is the ultimate displacement determined from the pushover curve. Note that the number of cycles for the ultimate displacement d_u is taken as

1 to constitute Eq. (4.2) from Eq. (4.1). The ultimate displacement d_u is defined as the displacement corresponding to 80% of the ultimate strength (FEMA P695, 2009; ATC 72-1, 2010). Figure 4.7 provides an illustrative description of the ultimate displacement d_u. Moreover, using Eq. (4.2), the discriminant constant is suggested as follows:

$$\widetilde{D} = \frac{d_u^2}{\sum_{i=1}^{N} n_i a_{(i)}^2} \tag{4.3}$$

To take conservative judgment on a ductile specimen, a specimen is considered as ductile when the discriminant constant $\widetilde{D}$ is larger than 1.1, not 1.0. Likewise, if the discriminant constant $\widetilde{D}$ is smaller than 1.1, the specimen is considered as brittle.

For a more intuitive expression, the above criterion can also be expressed in terms of the ultimate displacement d_u. By substituting the values for n_i and $a_{(i)}$ as shown in Table 4.1 and Figure 4.6, the denominator of Eq. (4.3) can be expressed in terms of the amplitude increment parameter Δ_a as follows:

$$\begin{aligned}\sum_{i=1}^{N} n_i\, a_{(i)}^2 = d_y^2 \cdot [&3 \cdot 1^2 + 3 \cdot (1+\Delta_a)^2 + 3 \cdot (1+2\Delta_a)^2 \\ &+3 \cdot (1+6\Delta_a)^2 + 3 \cdot (1+8\Delta_a)^2 + 3 \cdot (1+10\Delta_a)^2 \\ &+(1+8\Delta_a)^2 + (1+6\Delta_a)^2 + (1+4\Delta_a)^2 \\ &+2(1+2\Delta_a)^2 + 3 \cdot 1^2 + 4 \cdot \left(\tfrac{1}{2}\right)^2] \\ = (739\Delta_a^2 + 206\Delta_a + 27) \cdot d_y^2\end{aligned} \tag{4.4}$$

Finally, by introducing the default value 0.5 for the amplitude increment parameter Δ_a, the criterion describing whether a test specimen is ductile or brittle is defined in terms of the ultimate displacement d_u as follows:

$$\begin{cases} Ductile: d_u > 18d_y \\ Brittle: d_u < 18d_y \end{cases} \tag{4.5}$$

4.2.2.3. *Proposed cyclic loading history*

The configurations for the proposed cyclic loading history are presented in Figure 4.6. However, the amplitude increment parameter Δ_a needs to be specified to determine the amplitudes of the loading. The amplitude increment parameter Δ_a is proposed differently depending on whether the test specimen is ductile or brittle.

For ductile components, the maximum amplitude a_6 is taken as $6d_y$. As a result, the amplitude increment parameter Δ_a as follows:

$$\Delta_a = 0.5\ (for\ ductile\ specimen) \tag{4.6}$$

Note that the deformation of $6d_y$ is large enough to cover the range of general responses of structures in service under dynamic excitations, including earthquakes.

For brittle components that collapse during the cyclic loading test with the maximum amplitude of $6d_y$, the amplitude increment parameter Δ_a should be calibrated to ensure that the test specimen can withstand the cyclic loading history to the end. Using Eqs. (4.3) and (4.4), the amplitude increment parameter Δ_a is calculated such that the discriminant constant $\widetilde{D}$ is larger than 1.1, which is expressed as follows:

$$\widetilde{D} = \frac{1}{739\Delta_a^2 + 206\Delta_a + 27}\frac{d_u^2}{d_y^2} > 1.1 \tag{4.7}$$

which is equivalent to the following inequality:

$$739\Delta_a^2 + 206\Delta_a + 27 < 0.91\frac{d_u^2}{d_y^2} \tag{4.8}$$

Finally, the amplitude increment parameter Δ_a for brittle components is determined as a maximum value that satisfies the inequality in Eq. (4.7), which is expressed as follows:

$$\Delta_a = \max\left\{\Delta_a \middle| 739\Delta_a^2 + 206\Delta_a + 27 < 0.91\frac{d_u^2}{d_y^2}\right\} \quad (4.9)$$
$$(for\ brittle\ specimen)$$

Note that the ultimate displacement d_u and the yield displacement d_y are determined in advance from the pushover analysis.

Table 4.1 The amplitudes of the proposed cyclic loading history

Step $\boldsymbol{i}$	1	2	3	4	5	6
$\boldsymbol{a_i/d_y}$	1	$1+\Delta_a$	$1+2\Delta_a$	$1+6\Delta_a$	$1+8\Delta_a$	$1+10\Delta_a$

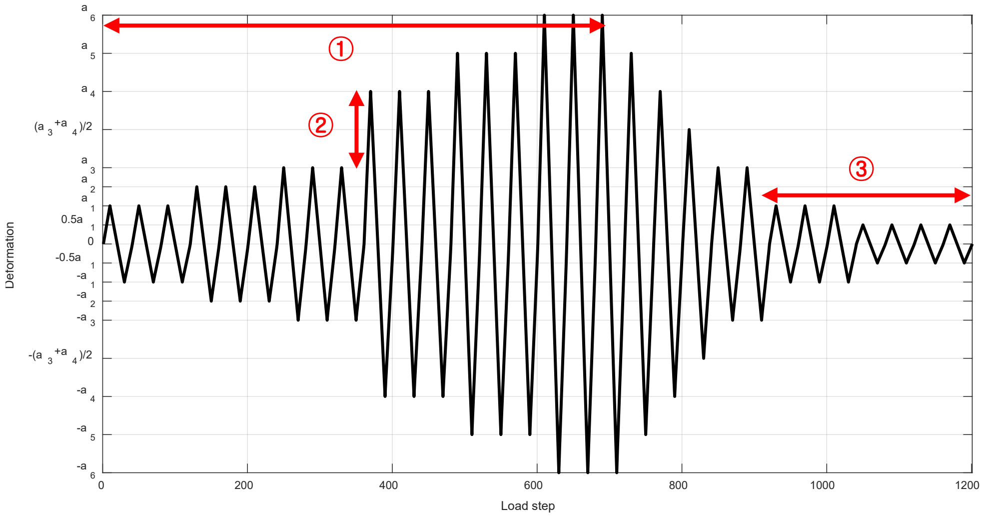

Figure 4.6 Proposed cyclic loading history that can induce the full modes of hysteretic behaviors of a component susceptible to cracks

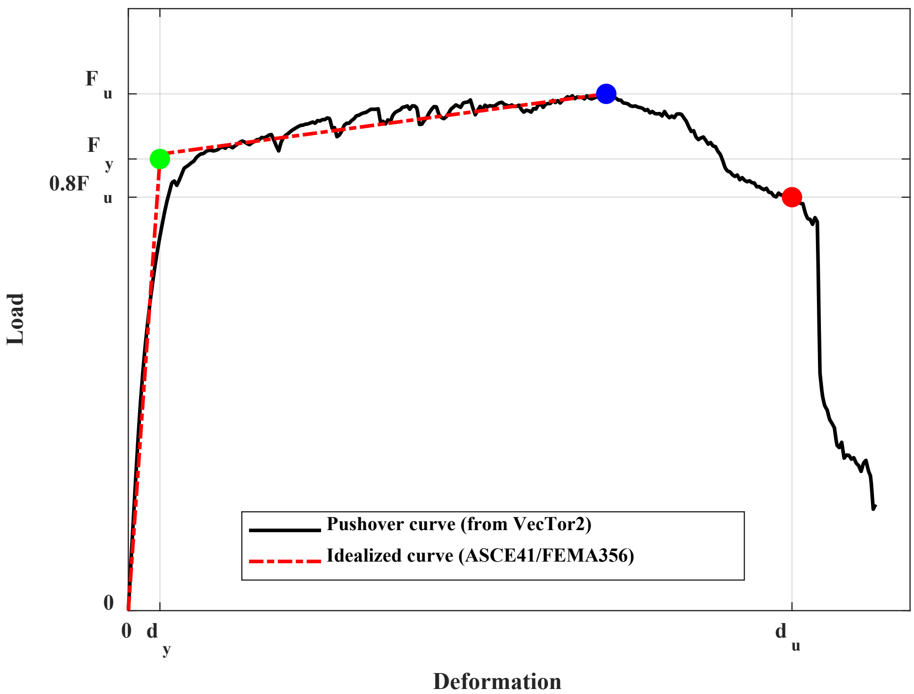

Figure 4.7 An illustrative description of the yield displacement d_y, the ultimate displacement d_u, the yield force F_y, and the ultimate force F_u

4.2.3. Step 3: Model fitting strategy

4.2.3.1. Genetic algorithm

In this thesis, model fitting refers to the parameter estimation, in other words, parameter identification, for Bouc-Wen class models. Identifying the Bouc-Wen hysteretic parameters is an important and nontrivial task in practical application due to the inherent nonlinearity and memory nature (Wang and Lu, 2017). For identifying the hysteretic parameters in Bouc-Wen class models, various methodologies have been proposed, including genetic algorithm-based identification, Kalman filter-based identification, constrained nonlinear optimization-based identification, and so on (Ismail et al., 2009). The hysteretic parameters are estimated by such methodologies using the load-deformation data obtained from the quasi-static cyclic loading test. Among the various state-of-the-art methods, the standard genetic algorithm is used to identify the parameters of the proposed Bouc-Wen model in this study.

Genetic algorithm, which was first suggested by Goldberg and Holland (1988), is one of the heuristic optimization algorithms widely employed for parameter estimation (Kim, 2021). The algorithm mimics the natural strategy that the population closer to an optimal design is more likely to survive for the next generation. The standard genetic algorithm incorporates the following four steps: (1) fitness evaluation, (2) selection, (3) crossover, and (4) mutation. The optimal population with the minimum value of the fitness, i.e., the objective function, is achieved after several iterations of the four steps. In this study, the mean squared error (MSE), i.e., the difference between the true restoring force and the estimated restoring force for the given displacement, is used for the objective function.

Genetic algorithm is a powerful optimization algorithm; however, it shows drawbacks in terms of the computational cost and the convergence issue in high-dimensional problems. The proposed Bouc-Wen model presented in Section 3.2 has a total of 15 parameters, and 12 parameters need to be estimated using the genetic algorithm while the other three parameters, i.e., initial stiffness k_0, yield force F_y, and post-yield stiffness ratio α, are determined from the pushover analysis. Since it is inefficient to estimate the other 12 parameters at once, a more detailed strategy for accurate and efficient parameter identification is required.

4.2.3.2. Sequential parameter identification

For efficient parameter identification, first, the proposed cyclic loading history is divided into three regions, i.e., elastic region, inelastic region, and re-elastic region. Figure 4.8 shows the three regions on the proposed cyclic loading history. First, the elastic region refers to the section with the small amplitudes close to the yield displacement at the beginning (denoted as number 1 in Figure 4.8). Second, the inelastic region indicates the section consisting of the large amplitudes that induce inelastic behaviors (denoted as number 2 in Figure 4.8). Last, the re-elastic region refers to the section with the small amplitudes that appear after the inelastic region (denoted as number 3 in Figure 4.8). The regions are designed to have overlapped each other to ensure the integrity of the parameter identification results. A total of 12 parameters that will be estimated by the genetic algorithm are assigned to a corresponding region in which the parameter has the most significant influence. The parameters with the corresponding region are shown in Table 4.2.

Next, the genetic algorithm is applied to estimate the parameters in each region sequentially. The sort of regions to which the genetic algorithm is applied is presented in decreasing order in terms of sensitivities of each region to hysteresis. It is obvious that the region with more parameters have a stronger influence on the overall hysteretic behaviors. Hence, the nine parameters belonging to the second region are first estimated. Subsequently, the two parameters of the first region and one parameter of the last region are sequentially estimated. While the nine parameters of the second region are estimated, the other three parameters, i.e., β, n, and c_h, are fixed as 0.5, 2.0, and 1.5, respectively. Likewise, during the parameter identification of the first region is in progress, the only remaining parameter c_h is fixed as 1.5.

4.2.3.3.Bounds on the parameters

The feasible domain for the parameters of the proposed Bouc-Wen model should be identified before processing the genetic algorithm. Moreover, one can facilitate the genetic algorithm in terms of convergence if the feasible domain can be narrowed. For the existing thirteen parameters that are also parameters for the m-BWBN model, the bounds specified in Kim (2021) are used. In Kim (2021), the bounds of parameters are obtained from the experimental dataset for the RC columns provided by the PEER Center, which contains 414 datasets. For the two newly introduced parameters for the proposed Bouc-Wen model, the bounds are also determined using 50 out of 414 experimental data for the RC columns. The bounds for each parameter are specified in Table 4.3.

Table 4.2 The corresponding region for each parameter
(Region 1 / 2 / 3: elastic region / inelastic region / re-elastic region, respectively)

Parameter	β	n	δ_ν	δ_η	ζ_0	p	q	ψ	δ_ψ	λ	c_ε	c_h
Region	1	1	2	2	2	2	2	2	2	2	2	3

Table 4.3 Bounds for the parameters of the proposed Bouc-Wen class model

Parameter	**Description**	**Bounds**
α	Post-yield stiffness ratio	$0 \le \alpha \le 0.5$
k_0	Initial stiffness	$0.05s \le T \le 5s$
F_y	Yield force	$0.05g \le F_y \le 1.5g$
β	Basic hysteretic shape control	$0.01 \le \beta \le 0.99$
n	Sharpness of yield	$1 \le n \le 5$
δ_ν	Strength degradation rate	$0 \le \delta_\nu \le 0.36$
δ_η	Stiffness degradation rate	$0 \le \delta_\eta \le 0.39$
ζ_0	Measure of total slip	$0 \le \zeta_0 \le 1$
p	Pinching slope	$0 \le p \le 1.38$
q	Pinching initiation	$0.01 \le q \le 0.43$
ψ	Pinching magnitude	$0.1 \le \psi \le 0.85$
δ_ψ	Pinching rate	$0 \le \delta_\psi \le 0.09$
λ	Pinching severity	$0.01 \le \lambda \le 0.8$
c_ε	Hysteretic energy amplification factor	$50 \le c_\varepsilon \le 500$
c_h	Crack closure coefficient	$0.01 \le c_h \le 1.5$

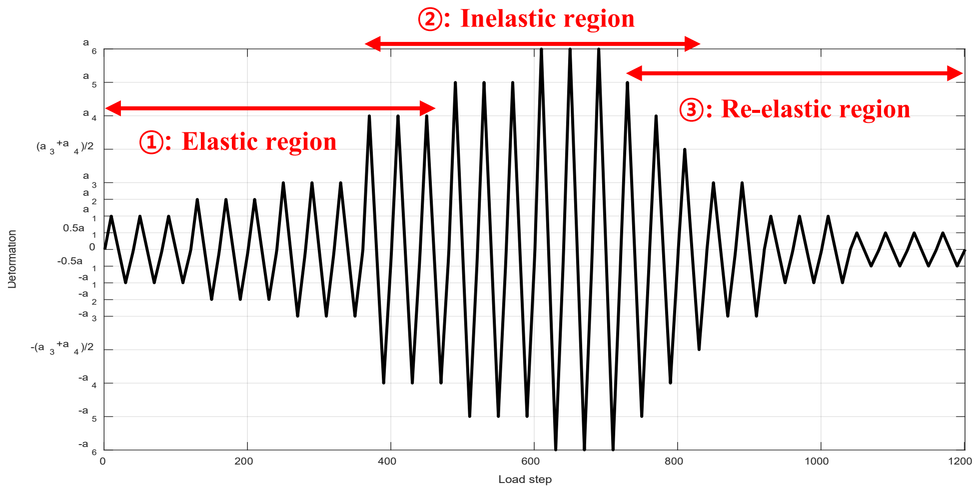

Figure 4.8 Three regions indicated on the proposed cyclic loading history

4.2.4. The overall procedure of the proposed loading protocol

The following three steps describe the overall procedures to identify 15 parameters of the proposed Bouc-Wen model.

Step 1: *Pushover analysis*. Three parameters are determined from the pushover curve, e.g., initial stiffness k_0, yield force F_y, and post-yield stiffness ratio α. The idealized pushover curve from which the three parameters are calculated follows the method suggested in De Luca et al. (2013).

Step 2: *Cyclic loading test*. For the cyclic loading test, a cyclic loading history that induces the full modes of hysteretic behaviors is proposed. The proposed cyclic loading history includes an elastic-region, inelastic region, and re-elastic region, in which the magnitudes of amplitudes depend on the ductile characteristic of the test specimen. The ductile characteristic of a speicmen is determined by the ultimate displacement and the yield displacement calculated from the pushover curve.

Step 3: *Parameter identification*. A genetic algorithm is applied to the load-deformation data obtained from the cyclic loading test. For an efficient estimation of the remaining twelve parameters, the load-deformation data are categorized into three groups, i.e., the groups corresponding to the elastic region, inelastic region, and the re-elastic region. The nine parameters belonging to the inelastic group are first estimated, and the two parameters of the elastic group and the one parameter of the re-elastic group are estimated sequentially.

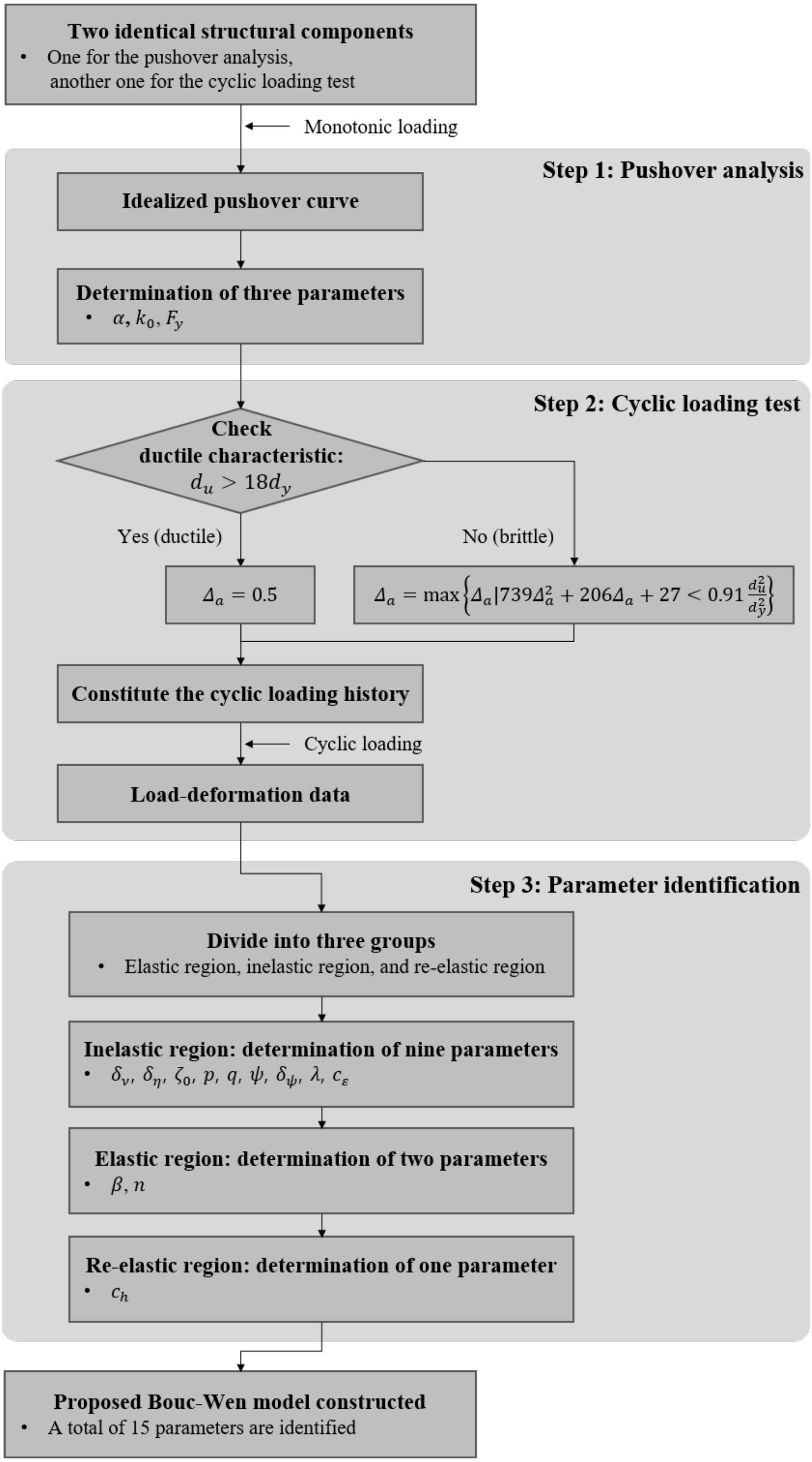

Figure 4.9 Flowchart of the proposed loading protocol for model fitting

Chapter 5. Numerical examination using nonlinear finite element analysis

The procedure for the numerical examination using nonlinear finite element analysis is as follows. First, construct finite element models for the actual structural components. Second, apply the proposed loading protocol on the finite element models. Third, identify the parameters of the proposed Bouc-Wen class model using the load-deformation data obtained from the finite element analysis. Fourth, apply various loads on the finite element models. Fifth, predict the response of the finite element models subjected to the various loads using the proposed Bouc-Wen class model. Last, compare the results from the finite element analysis and from the proposed Bouc-Wen class model.

This chapter describes the numerical examination procedures and results for the proposed hysteresis modeling framework. To this end, the details for the numerical examples for RC columns are provided. Moreover, various loads that are used to demonstrate the proposed framework are described. Lastly, the numerical examination results are illustrated.

5.1. Numerical examples for RC columns

To validate a modeling framework for structural components, real-world experiments on different components under various loads are often used. However, performing many experiments may entail unaffordable time and cost. Thus, the finite element method employing detailed structural properties and advanced constitutive laws is used as an alternative for actual experiments. To represent the behaviors of real-world structures using the finite element method, the structural properties for

RC columns are used in details, which are described in the first section. A nonlinear finite element analysis program used in this study is also explained. Subsequently, the validity of the finite element models constructed for each RC column is confirmed by comparing the load-deformation data obtained from the actual experiments and the finite element analysis.

5.1.1. Experimental data in PEER structural performance database

The structural performance database by the Pacific Earthquake Engineering Research (PEER) Center compiled by Berry et al. (2004) provides the experimental results for 253 rectangular-reinforced columns and 163 spiral-reinforced columns. The database provides not only the results for quasi-static cyclic loading tests, i.e., the measured forces and displacements, but also reinforcement layout, loading scenario, sectional properties, material properties, and failure type of the columns. Regardless of test configurations, all lateral force-displacement histories are documented in terms of an equivalent cantilever column.

In this study, among the available 416 test results in the PEER database, a total of 50 rectangular RC columns is used to demonstrate the proposed hysteresis modeling framework. The statistics of the RC columns used in this study in terms of depth, aspect ratio, axial load ratio, and longitudinal and transverse reinforcement ratios are summarized in Table 5.1. In the table, Std and CoV stand for standard deviation and coefficient of variation, respectively.

Table 5.1 Statistics of the 50 RC column specimens used for demonstration

Column property	Max	Min	Mean	Std	CoV
Depth (mm)	1784	160	1104.1	567.5	0.514
Aspect ratio	4	1	3.01	0.963	0.320
Axial load ratio	0.801	0.032	0.370	0.241	0.651
Longitudinal steel ratio, ρ_l (%)	3.8	0.680	2.005	0.849	0.423
Transverse steel ratio, ρ_s (%)	3.5	0.2	1.399	0.806	0.576
Failure type (%)	Flexure		Shear	Flexure-Shear	
	81.3		10.4	8.3	

5.1.2. Finite element modeling

To perform nonlinear finite element analysis, VecTor2 (Wong et al., 2013) is used in this study. VecTor2 is a nonlinear finite element analysis program to analyze two-dimensional RC structures subjected to quasi-static or dynamic load conditions. This specialized program uses a smeared rotating crack approach based on the modified compression-field theory (Vecchio and Collins, 1986) and the disturbed stress field model (Vecchio, 2000; Vecchio 2001), which are considered rational methods to model the shear behavior of RC structures over the years and have been successfully applied in accurately simulating the behavior of numerous RC structures (Saatci and Vecchio 2009). With this formulation, reinforcement is assigned as a property to the membrane element and then smeared with concrete properties. This element formulation is used to account for inelastic shear deformation and shear-flexure-axial interaction (Boivin and Paultre, 2012). A default constitutive laws in VecTor2 as summarized in Table 5.2 are chosen to model the material responses of concrete and reinforcement steel. The details of the selected constitutive laws are provided in Wong et al. (2013). Although the program provides a wide array of advanced constitutive models, VecTor2 employs simple techniques for finite element modeling, using low order four-node rectangular, four-node quadratic, or three-node triangular elements.

Using the constitutive laws in Table 5.2 and the structural properties including material properties, reinforcement layout, geometric properties, and the loading scenario, 50 FE models corresponding to 50 rectangular RC columns are constructed. In addition, P-delta effects are considered in the FE analysis in order to account for the real-world experiment having geometric nonlinearities. For the FE elements modeling, four-node quadratic elements are used to implement the P-delta effects.

The mesh size was determined according to the past experience within the range of 10 mm to 30 mm depending on the depth of the column, keeping the aspect ratio smaller than 1.5. For the boundary conditions, only the elements located at the bottom of the support plate are fixed in both x and y directions.

An example of the constructed FE model is shown in Figure 5.1. The longitudinal reinforcements are modeled explicitly as expressed in dark blue vertical lines in Figure 5.1, while the transverse reinforcements, i.e., stirrup steels, are smeared with the confined concrete which are illustrated as blue elements. The smeared approach for transverse reinforcement can be justified in that the stirrups are evenly distributed along the specimen. The steel loading plate and support plate are shown as grey elements in Figure 5.1. To represent out-of-plane confinement effects in the concrete near the support plane, out-of-plane reinforcement is added to the neighboring elements so that ductility of the FE models can reach that of the experimental data without shear failure near the support plate. This calibration technique often has been used to ensure the ductility of FE models, despite some strength enhancement (Vecchio and Shim, 2004). The dark green and light green elements denote the confined concrete with the additional out-of-plane reinforcement of 5% and 2.5%, respectively. The elements with light blue color represent unconfined concrete.

Table 5.2 Selected concrete and reinforcement steel constitutive laws for each response

Material	Modeled response	Constitutive law
Concrete	Compression pre-peak	Hognestad parabola
	Compression post-peak	Modified Park-Kent
	Compression softening	Vecchio (e1/e2-Form)
	Tension stiffening	Modified Bentz
	Tension softening	Nonlinear (Hordijk)
	FRC tension	Simplified diverse embedment model
	Confined strength	Kupfer-Richart
	Lateral expansion	Variable Poisson's ratio (Kupfer)
	Cracking criterion	Mohr-Coulomb (Stress)
	Crack stress calculation	Tensile: Modified compression field model Shear: Disturbed stress field model
	Crack slip calculation	Walraven
	Creep and relaxation	Not considered
	Hysteretic response	Nonlinear with plastic offsets
Steel	Stress-strain response	Trilinear
	Hysteretic response	Seckin model with Baushinger effect
	Dowel action	Tassios model
	Buckling	Refined Dhakal-Maekawa model
	Concrete bond	Eligehausen model

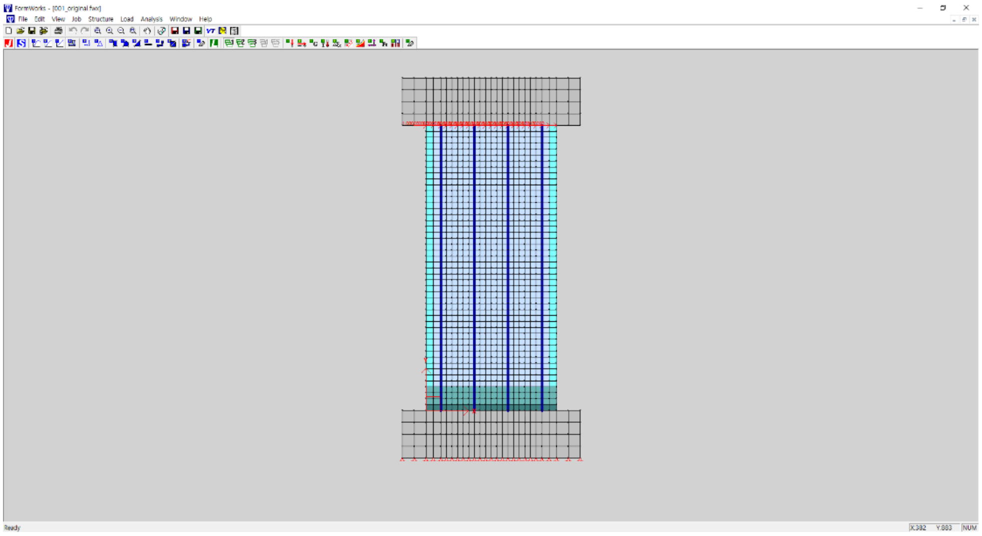

Figure 5.1 An example of the constructed FE model using the VecTor2

5.1.3. Validity of the finite element models

To check the validity of the FE models, three accuracy measures are selected from a previous study (Huang and Kwon, 2015): peak force ratio, initial stiffness ratio R_K, and energy dissipation capacity ratio R_E. Peak force ratio R_F is the ratio of predicted peak force using the FE analysis and experimentally measured peak force in both positive and negative directions. Initial stiffness ratio R_K is the ratio of the predicted initial stiffness and the measured initial stiffness. The secant stiffness at 0.1% drift, which is consistently used in all numerical results (Huang and Kwon, 2015), is used to represent the initial stiffness herein. Last, energy dissipation capacity ratio R_E is the ratio of dissipated energy from the FE analysis to the dissipated energy from the experimental data. The energy dissipation capacity ratio is considered an accuracy measure for hysteretic loop because the dissipated energy can indirectly quantify the differences in the hysteretic curves. The results of FE analysis for the 50 RC columns are presented in Figure 5.2 as box plots to provide the overall accuracy of the FE model construction results. Note that the closer the accuracy measures are to 1, the more accurately a FE model simulates the real RC column. The FE analysis results show reasonable accuracy with the experimental data, which implies the constructed FE models are valid. The difference in the initial stiffness may arise from the different loading configuration that may significantly affects the P-delta effects. In addition, the force-displacement loops for the first eight RC columns obtained from the FE analysis compared to the measured force-displacement loops are presented in Figure 5.3. The hysteresis loops from the FE analysis, denoted as red dotted lines in Figure 5.3, well match the experimental data given in black solid lines.

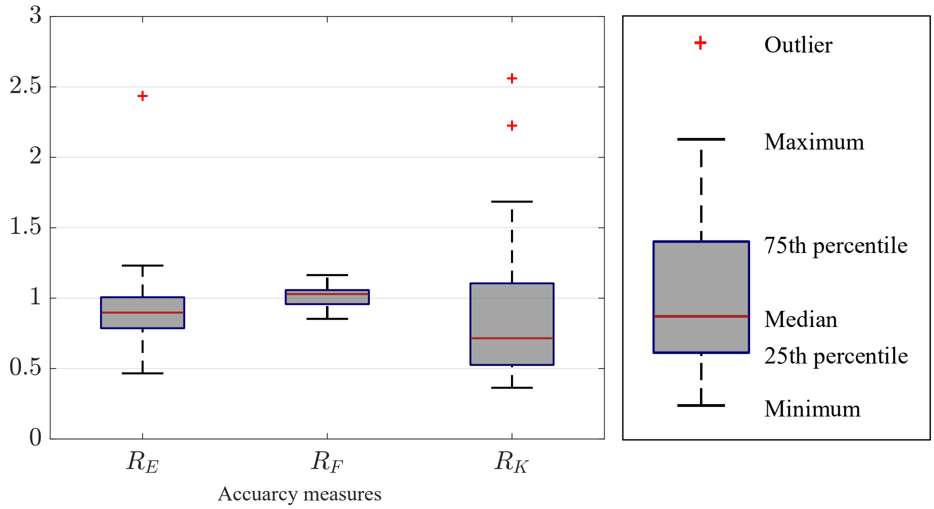

Figure 5.2 Box plots indicating the validity of the 50 FE models

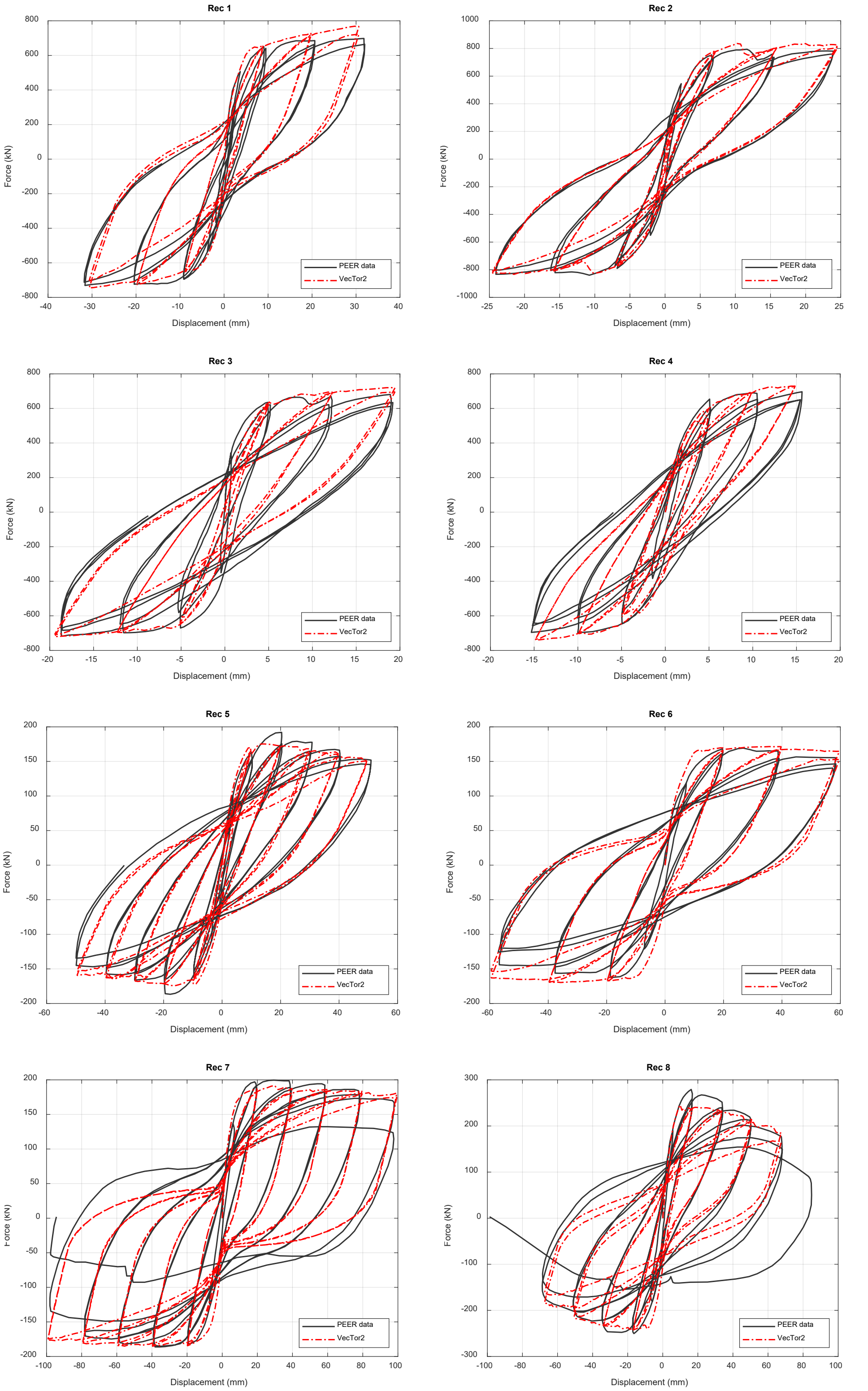

Figure 5.3 Force-displacement data for the first eight RC columns obtained from the FE analysis (red dotted line) compared to the experimental data (black solid line)

5.2. Loads used for numerical examination

As stated in Section 2.4, the lack of consistency issue has been consistently reported in the existing hysteresis modeling framework. In other words, even though a Bouc-Wen model properly describes the hysteresis loop with the identified parameters, the fitted model may not predict the responses under other loads. Additionally, because of the limitations of the existing hysteresis modeling framework, an equivalent SDOF system using a hysteretic model has struggled with a nonlinear dynamic analysis.

To demonstrate whether the proposed hysteresis modeling framework overcomes the issues in the existing approaches, two types of loads are introduced: quasi-static loads and dynamic loads. First, regarding quasi-static loads, three loading histories are suggested as loads for tests, which are illustrated in Figure 5.4. The first quasi-static loading history, a load in Figure 5.4(a), represents the existing loading history for RC structures provided by the ACI 374 protocol, and the second load shown in Figure 5.4(b) is suggested to clarify the performance for one-way cyclic loads. The last quasi-static loading history shown in Figure 5.4(c) consists of two parts: a section in which a difference between adjacent amplitudes is large and a section with a small amplitude following a large amplitude. The amplitudes of the three loading histories are expressed in terms of the yield displacement d_y. Using the last quasi-static loading history, the ability of Bouc-Wen models to describe the hysteretic behaviors associated with cracking effects can be identified.

Regarding a nonlinear time history analysis, a sufficient number of ground motions are arguably beneficial to verify the proposed approach since the inherent variability exists in earthquake ground motions. However, due to time constraints, two earthquake ground motions are used for validating the proposed hysteresis modeling framework in terms of a nonlinear time history analysis. The first ground motion is the zero-degree component of ground acceleration recorded at El Centro station during the earthquake in 1940 with a magnitude of 6.9. The duration of the El Centro ground motion is 53.76 s with a time step of 0.02 s. The second ground motion used for the nonlinear time history analysis is 270-degree component of ground acceleration recorded at Loma Prieta during the earthquake in 1989 with a magnitude of 6.9. The duration of the record is 39.98 s and the time step is 0.02 s. Figure 5.5 represents the two ground acceleration records used for a nonlinear time history analysis in this study.

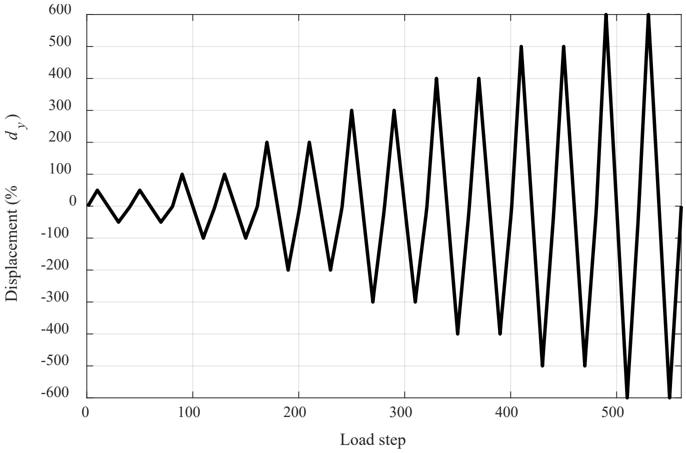

(a)

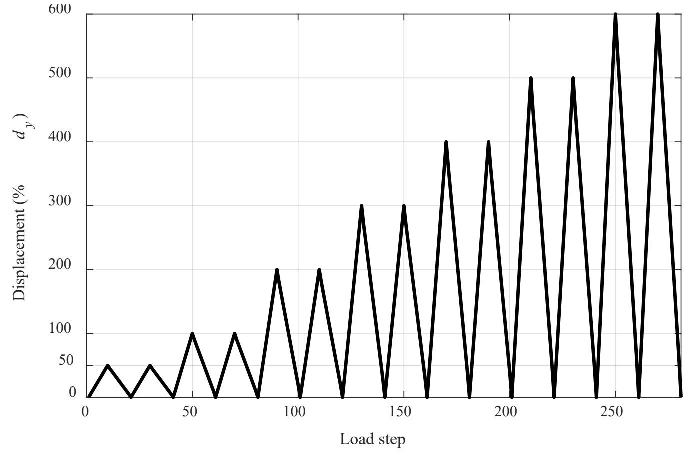

(b)

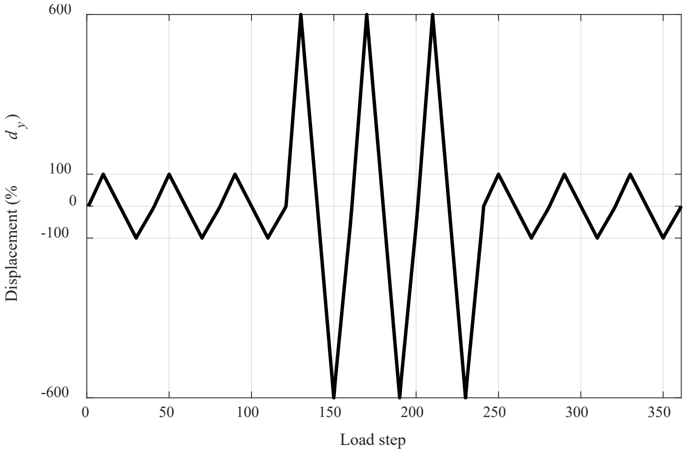

(c)

Figure 5.4 Three loading histories used for numerical examination under quasi-static load condition

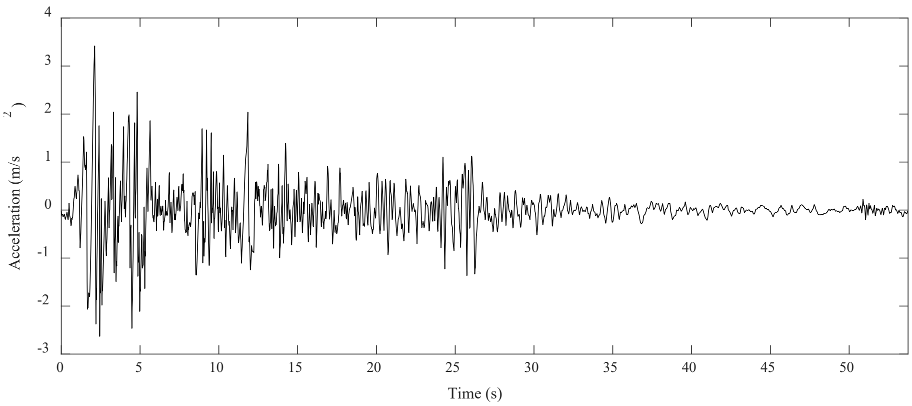

(a)

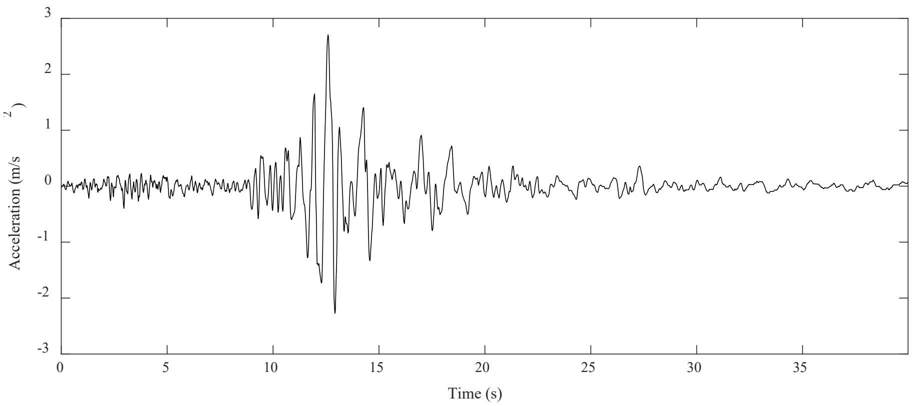

(b)

Figure 5.5 Two ground acceleration records used for numerical examination under dynamic condition (a: El Centro earthquake, b: Loma Prieta earthquake)

5.3. Numerical examination

The proposed hysteresis modeling framework is demonstrated using the FE models and the various loads described above. However, the hysteretic models need to be constructed before the demonstration. Thus, the hysteretic models for each FE model are fitted following the proposed loading protocol shown in Figure 4.9. For the hysteretic models, two models are used for comparison: the m-BWBN model and the Bouc-Wen class model proposed in this study. After the model fitting, validity of the proposed framework is confirmed by comparing the response prediction results from the FE analysis to those by the hysteretic models.

5.3.1. Hysteretic model fitting results

The Bouc-Wen class model proposed in this thesis and the reference model are fitted following the loading protocol proposed in Section 3.2. Figure 5.6 summarizes the fitting results of each model for 50 RC columns along with the failure modes, i.e., flexure or shear failure. The flexure-shear failure is considered as a shear failure for simplicity. A total of 41 and 9 RC columns failed in flexure and shear, respectively. Using the accuracy measures used for demonstrating the validity of FE models in Section 5.1.3, three quantitative measures, i.e., energy dissipation ratio, peak force ratio, and initial stiffness ratio, are calculated as summarized in Figure 5.6. Both red boxes and blue boxes representing the proposed model and the m-BWBN model, respectively, are located close to 1, indicating that both models are fitted well enough to simulate the FE analysis.

For example, Figure 5.7 represents the model fitting results of the proposed Bouc-Wen model for the four RC columns having flexure failure and the other four

RC columns having shear failure, compared to the FE analysis results. It is seen that the red dotted lines that indicate the proposed Bouc-Wen model show good match with the black solid lines that denote the hysteretic loops obtained from the FE analyses, which implies that the proposed Bouc-Wen model is well constructed. The model fitting results for the m-BWBN model is also presented in Figure 5.8. The blue dotted lines are the fitting results for the m-BWBN model and the FE analysis results are represented as black solid lines. The overall fitting results show a good matching with the FE analysis results as well.

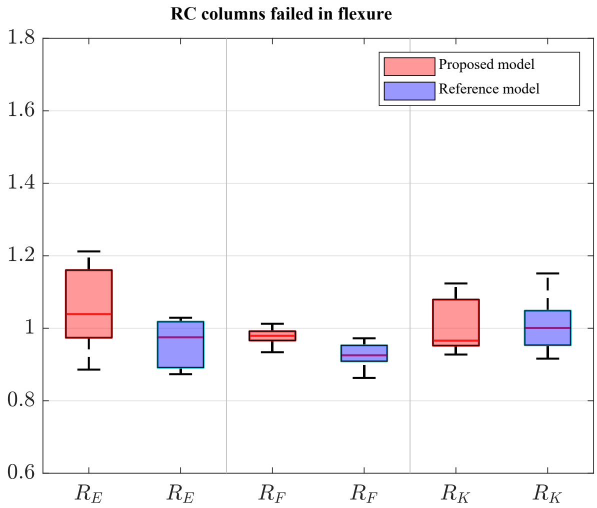

(a)

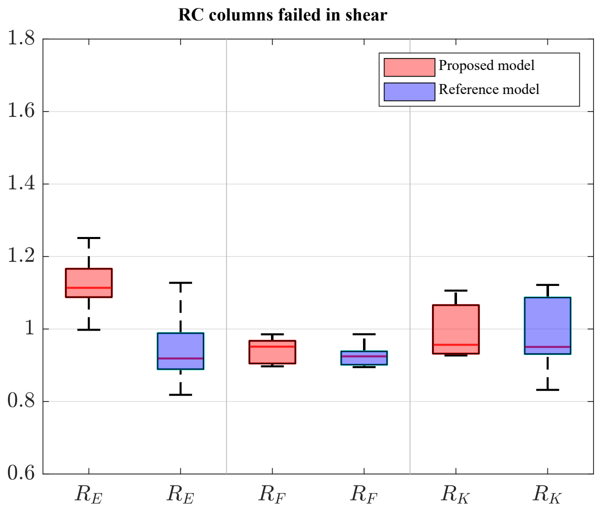

(b)

Figure 5.6 Box plots indicating the fitness of proposed and reference models for the 50 RC columns.

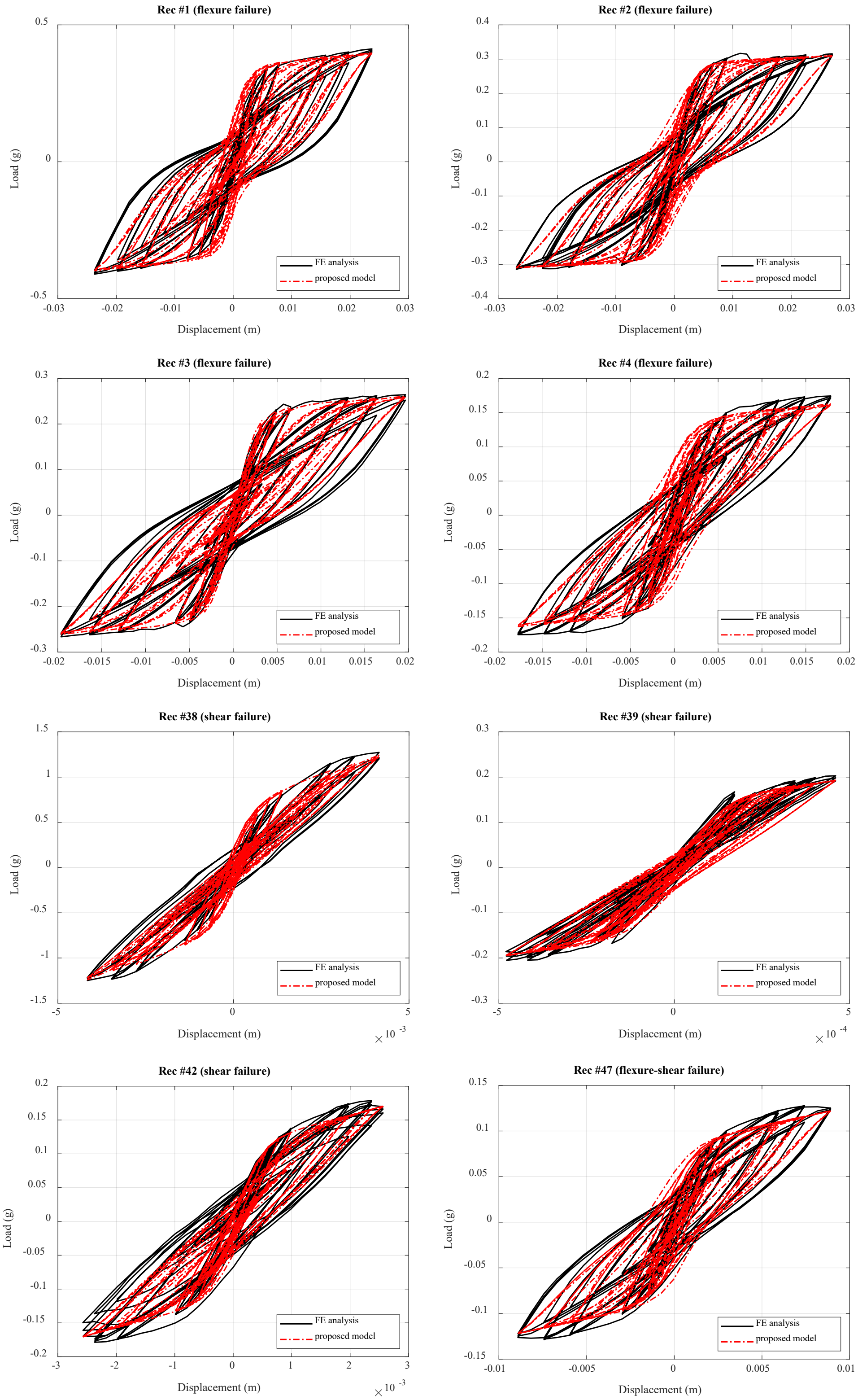

Figure 5.7 Model fitting results for the eight RC columns having various failure modes using the proposed Bouc-Wen model (red dotted line) and the FE analysis (black solid line)

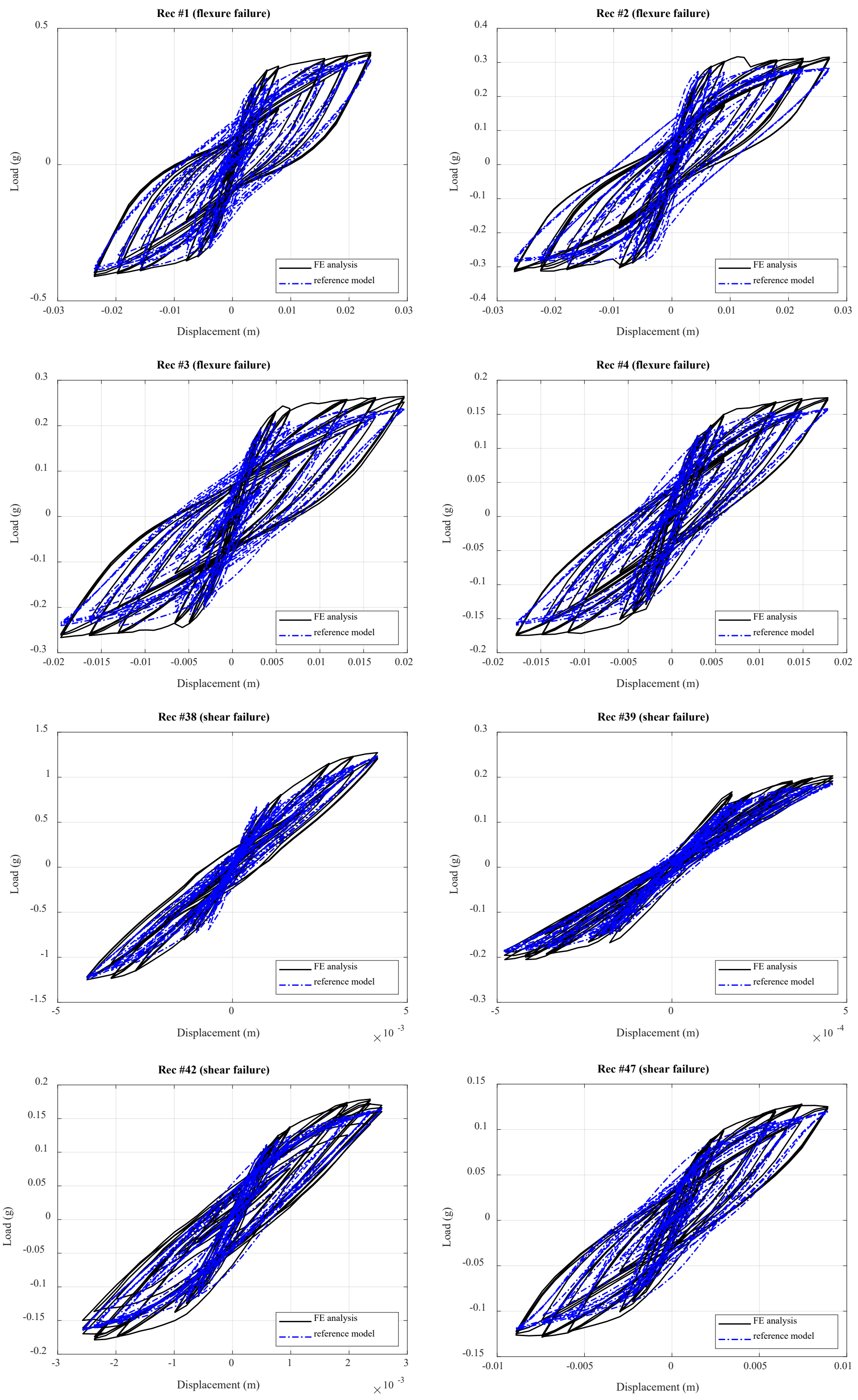

Figure 5.8 Model fitting results for the eight RC columns having various failure modes using the reference model (red dotted line) and the FE analysis (black solid line)

5.3.2. Response prediction: Quasi-static loads

As described in Section 2.4, one of the significant issues in the existing hysteresis modeling framework is that hysteretic model often shows poor performance in response prediction for a new loading other than the load used for fitting the model. Accordingly, the prediction performance for new loads was evaluated using the proposed model and the m-BWBN model which are fitted as Figures 5.7 and 5.8, respectively. The new loads used for the prediction performance evaluation are the quasi-static loading histories shown in Figure 5.4.

The box plots that depict the prediction performance of each model for the three quasi-static loads are provided in Figures 5.9, 5.10, and 5.11, respectively. In Figures 5.9 to 5.11, the red boxes indicate the results from the proposed model and the blue boxes stands for the results from the reference model. For the first quasi-static load in Figure 5.9, the accuracy measures for both the reference model and the proposed model are close to 1, except for the results from the reference model for the RC columns showing a shear failure. It means that although the reference model showed drawbacks in describing the behavior of RC columns failed in shear, both models showed satisfactory predictive performance for the first quasi-static load. Note that the first loading history is suggested by ACI 374.

On the other hand, in the case of the third load that involves a section with a large difference in amplitudes, the superior predictive accuracy of the proposed model to that of the reference model can be clearly confirmed. The red boxes are much closer to 1 than the blue boxes in Figure 5.11, which indicates that the proposed model predicted much closer responses to the FE analysis results than the reference model did. In addition, the difference in predictive performance becomes even larger for the RC columns having shear failure.

However, the proposed model has limitations in estimating the responses for the second quasi-static load, as shown in Figure 5.10. Except for the energy dissipation ratio, the proposed model showed better overall estimation performance for the other two criteria. For the energy dissipation ratio, the values obtained from the proposed model were far from 1, whereas the reference model showed close estimation to the FE analysis results. However, the fact that energy dissipation ratio calculated from the reference model is closer to 1 does not necessarily mean that the reference model can estimate the overall response more accurately than the proposed model. It can be confirmed by the examples shown in Figures 5.12 and 5.13.

The examples for the response prediction results are given in Figures 5.12 and 13. Two examples of RC columns for each failure mode are presented. The results for the response estimation performance presented in Figures 5.9 to 5.11 can be recognized more apparently through the examples shown in Figures 5.12 and 5.13. The numerical experimental data using FE analysis are denoted as black solid lines in Figures 5.12 and 5.13, while the red and blue dotted lines represent the force-displacement data predicted by the proposed and reference models, respectively. Each column (as an antonym for row) in Figures 5.12 and 5.13 represents an independent RC column, while the analysis results for each three load histories for each RC column are placed in each row.

In the case of RC columns having flexure failure, the proposed Bouc-Wen model returns a close force-displacement relationship to the FE analysis results, while the reference model failed to predict the hysteresis loops especially corresponding to the second and the third loads. Given that the energy dissipation ratio was accurately estimated in the reference model, the controversial results were accidental consequences from the lack of implementation of the pinching effect near the origin.

For the RC columns that are governed by shear behaviors shown in Figure 5.13, the superior response prediction performance of the proposed model is demonstrated more clearly. The force-displacement relationships obtained from the proposed model show good fitness to the FE analysis, but the reference model fails to simulate the hysteretic behaviors, showing divergence in several plots in Figure 5.13.

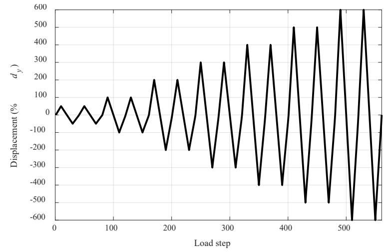

(a)

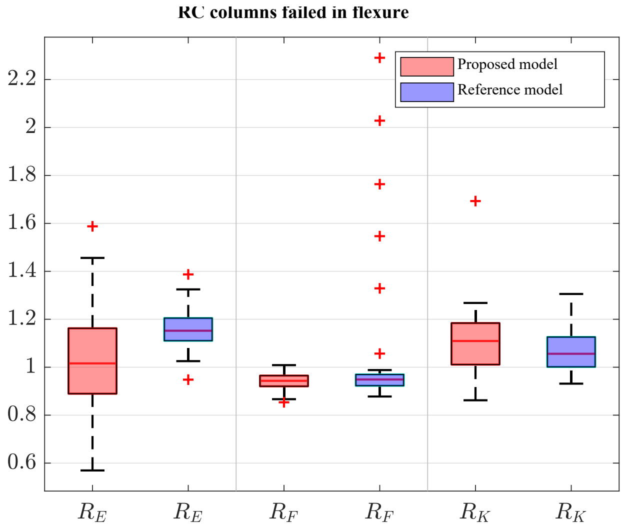

(b)

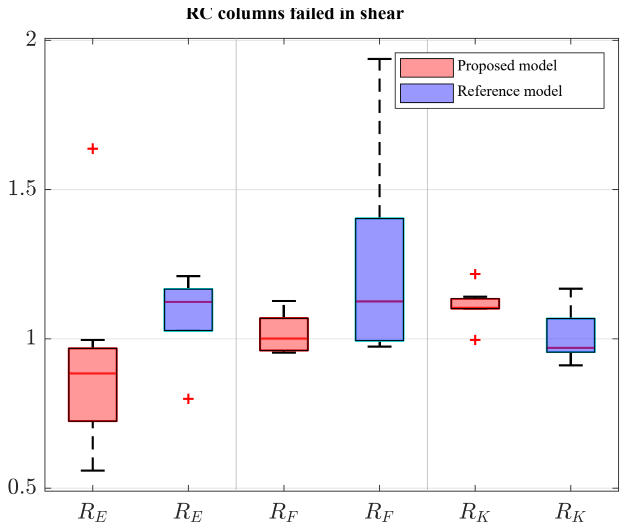

(c)

Figure 5.9 Response prediction results for the first quasi-static load ((a): the first quasi-static load, (b): box plots indicating the response prediction results for the RC columns failed in flexure, (c): box plots indicated the response prediction results for the RC columns failed in shear)

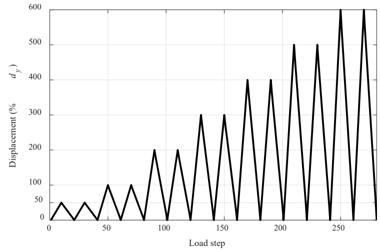

(a)

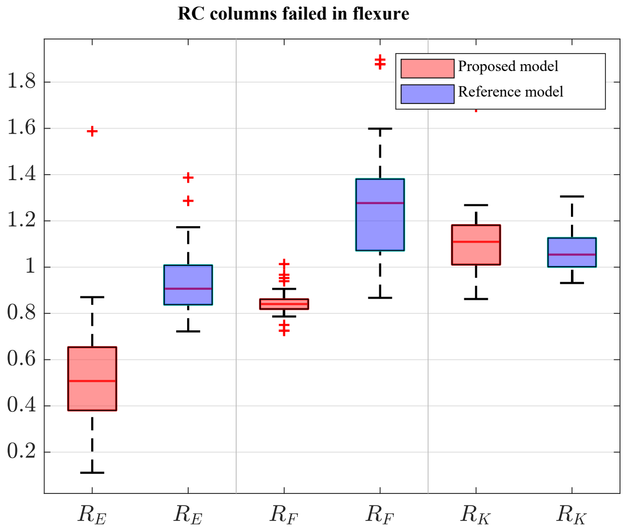

(b)

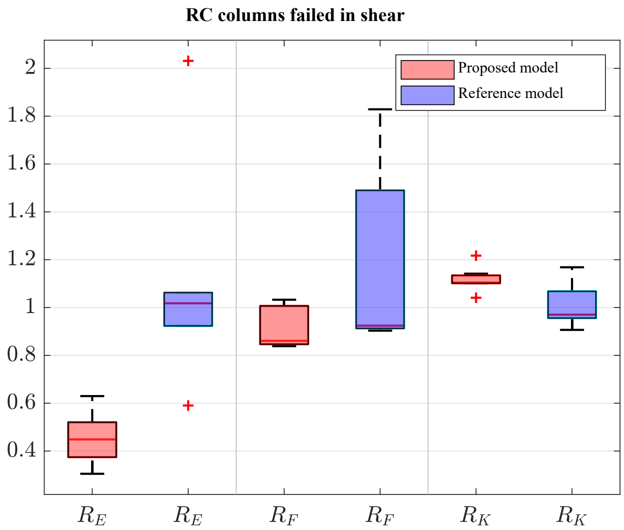

(c)

Figure 5.10 Response prediction results for the second quasi-static load ((a): the second quasi-static load, (b): box plots indicating the response prediction results for the RC columns failed in flexure, (c): box plots indicated the response prediction results for the RC columns failed in shear)

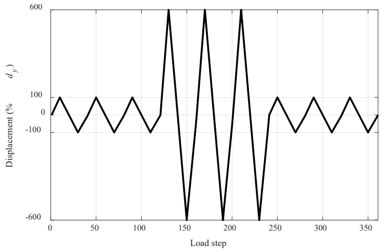

(a)

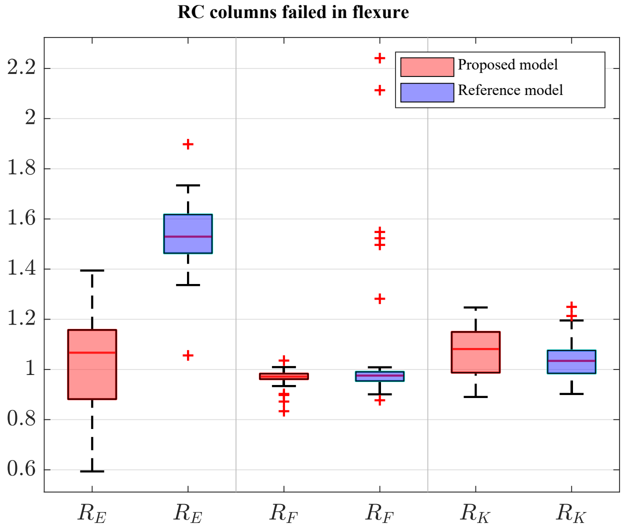

(b)

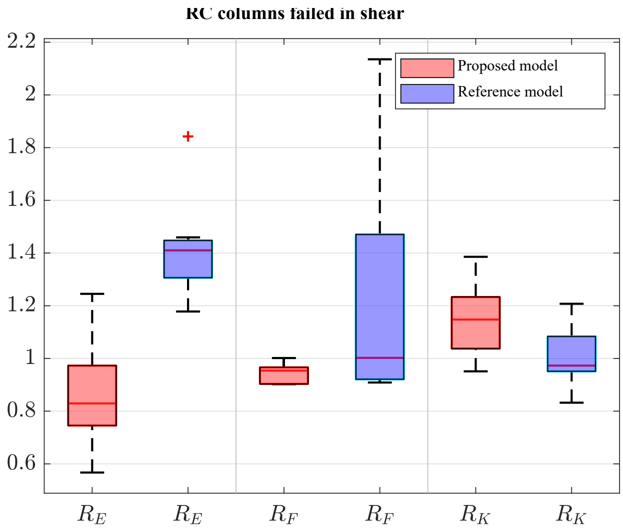

(c)

Figure 5.11 Response prediction results for the third quasi-static load ((a): the third quasi-static load, (b): box plots indicating the response prediction results for the RC columns failed in flexure, (c): box plots indicated the response prediction results for the RC columns failed in shear)

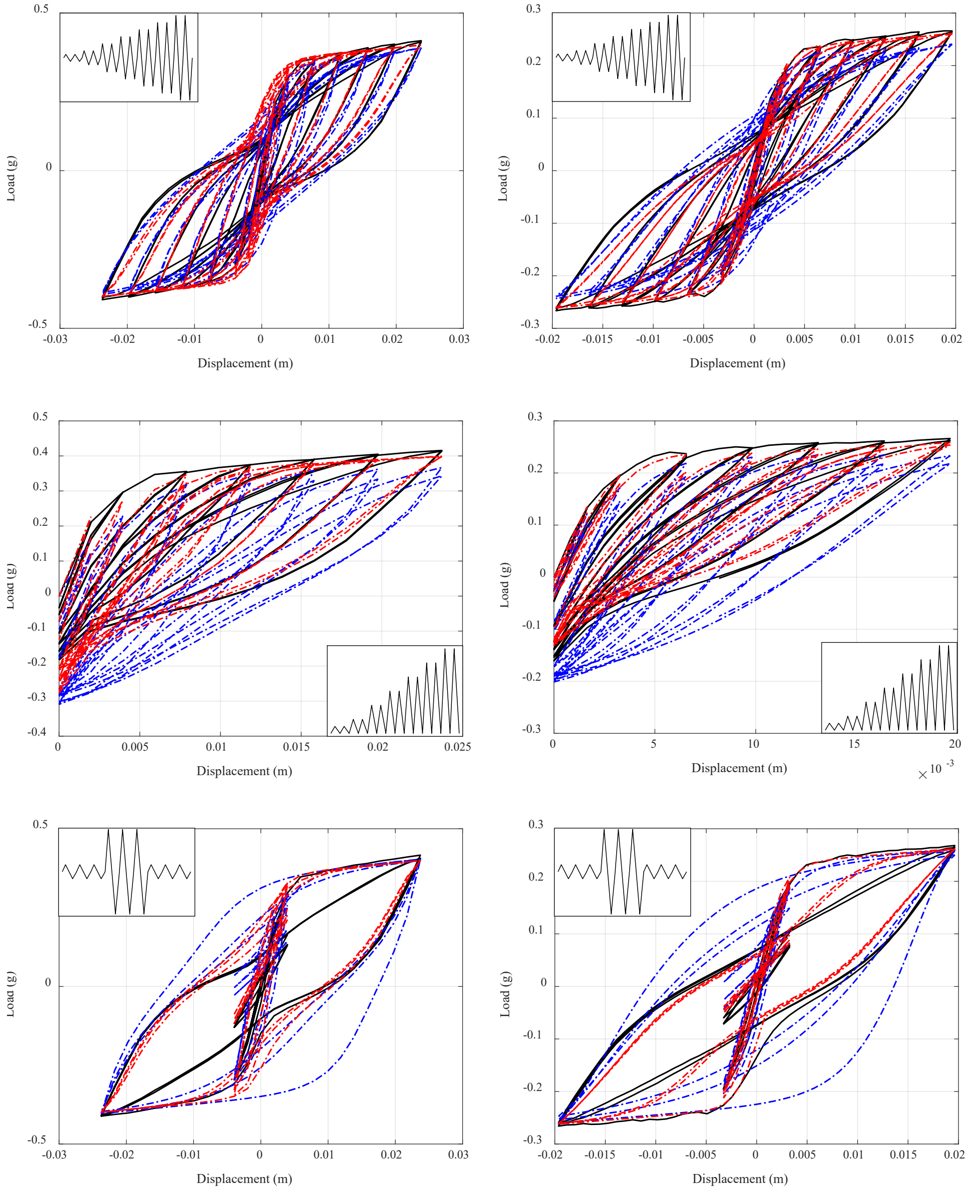

Figure 5.12 Response prediction results for RC columns failed in flexure using the reference model (blue dotted line), the proposed model (red dotted line), and the FE analysis (black solid line) (The corresponding loads are placed at the corner of each plot)

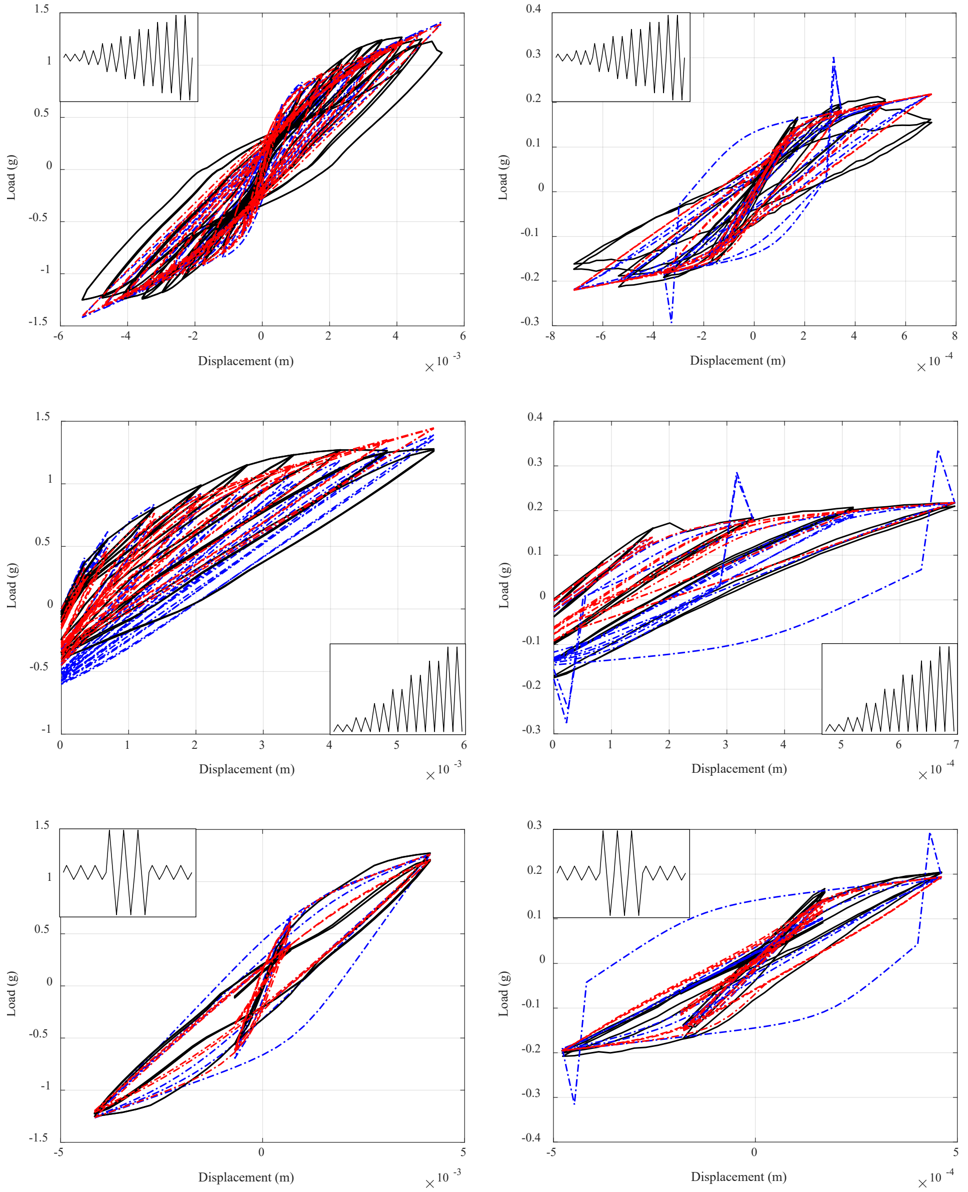

Figure 5.13 Response prediction results for RC columns failed in shear using the reference model (blue dotted line), the proposed model (red dotted line), and the FE analysis (black solid line) (The corresponding loads are placed at the corner of each plot)

5.3.3. Response prediction: Nonlinear time history analysis under seismic loads

Beyond the evaluation of the prediction accuracy for arbitrary quasi-static loads, applicability of the proposed hysteresis modeling framework is evaluated for dynamic analysis. In the numerical examination on the nonlinear time history analysis, the displacement response prediction results using the reference model and the proposed model are also compared with the dynamic finite element analysis results. To perform a dynamic analysis using the nonlinear finite element analysis program VecTor2, Newmark's implicit constant acceleration method was implemented for numerical integration of equation of motion. The details for the nonlinear finite element dynamic analysis equipped in the VecTor2 program can be found in Saatci and Vecchio (2009).

In the dynamic analysis procedure of VecTor2, the masses of elements are distributed equally to the top of a column as lumped masses. The reason for distributing the lumped masses along the top of a column is to equalize the total mass and stiffness with those used for the equivalent SDOF system. In addition, in order to prevent the local crushing at the top of a RC column, a thin steel plate was made upon the elements on the top and the total mass was uniformly distributed along the nodes on the steel plate. The total mass used for the dynamic analysis was determined such that the RC column experiences far beyond the elastic behavior. Accordingly, the total masses used for the dynamic analysis vary with the applied dynamic loads even in the same specimen.

Determining an equivalent damping ratio is also a significant issue during the dynamic analysis. However, determining the damping ratio from the physical state of the structure, such as the dimensions, member size, or materials used, is impractical (Saatci and Vecchio 2009; Chopra and McKenna, 2016). Therefore, damping is usually calculated from a mathematical perspective because a damping ratio can stabilize numerical solutions. For the dynamic analysis in VecTor2, the Rayleigh damping, which is pervasive in nonlinear response history analysis of structures, is introduced. Furthermore, to make the effects of higher modes enfeeble so that the results may represent the responses of a SDOF system, the damping ratio of 0.1% to 1% was assigned to the first mode while larger than 40% was taken in the modes higher than the second mode.

In case of an equivalent SDOF system with a hysteretic model, the nonlinear response history analysis can be conducted based on the equation of motion in Eq. (2.1) with the formulations regarding the restoring force for each hysteretic model. Owing to the mathematical tractability of Bouc-Wen class models, Eq. (2.1) can be solved using numerical analysis techniques. In this thesis, the Runge-Kutta-Fehlberg method, i.e., Runge-Kutta method of order four and five, which is widely known to have stable accuracy and convergence, is used. Additionally, it is also important to determine a suitable equivalent damping ratio when performing dynamic analysis using an equivalent SDOF system. Based on the value of damping ratio assigned to the first mode in VecTor2, the equivalent damping ratio was determined for the SDOF system after a slight calibration process. The calibration process can be justified in that VecTor2 is capable of modeling the majority of energy dissipating mechanisms that stems not only from hysteretic models for each material but also from cracks in concrete elements or buckling in reinforcement steel elements (Saatci, 2009). The values of damping ratio for an equivalent SDOF system determined through the processes above are within the range of 0.1% to 5%.

The examples for the nonlinear time history analysis results are presented in

Figures 5.14 and 5.15. Figure 5.14 is an example for a RC column having flexure failure while Figure 5.15 provides an example for a RC having shear failure. In Figures 5.14 and 5.15, the estimated response histories by the FE analysis, the proposed and the reference models are denoted as black solid lines, red dotted lines, and blue dotted lines, respectively. Each figure shows that the response history estimated using the proposed model is closer to the time history analysis result using FE analysis than the reference model.

The results for a total of 50 RC columns are summarized in Figure 5.16 summarized by the box plots in Figure 5.16. As quantitative criteria to assess the prediction accuracy in time history analysis, the errors in peak displacements in both directions predicted by each model in comparison to the results from FE analysis are used. The proposed model showed less error than the reference model in terms of peak displacement, one of the most important demand variables for structural seismic design.

Beyond the nonlinear time history analysis for the two earthquakes, i.e., El Centro and Loma Prieta, the responses to the following six earthquakes were estimated for a RC column governed by flexure behavior: earthquakes recorded at San Francisco in 1906, Helena in 1935, El Centro in 1940, Loma Prieta in 1989, Umbria-Marche in 1997, and Parkfield in 2004. The results for the six earthquakes are given in Figure 5.15. The responses predicted given the input dynamic excitations using the proposed Bouc-Wen model show notable matching to the results from VecTor2. It implies that an equivalent SDOF system with the proposed Bouc-Wen model can replace the FE analysis when the parameters of the model are suitably identified. Quantitative measures for the estimation performance in time history analysis are presented in Table 5.3. The proposed hysteresis modeling framework shows high accuracy in terms of peak response, while requiring much less computational cost than FE analyses.

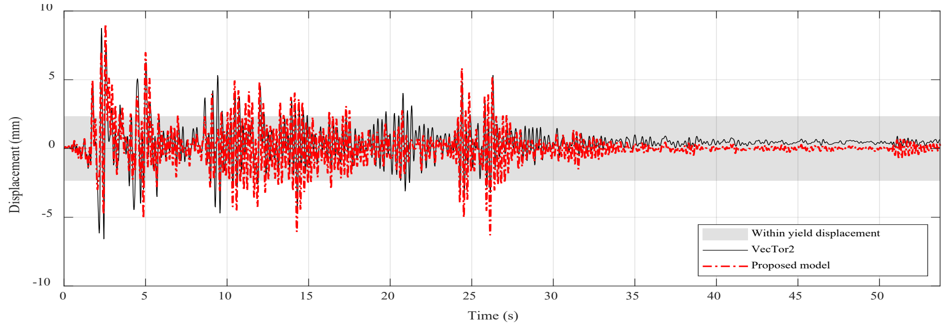

(a)

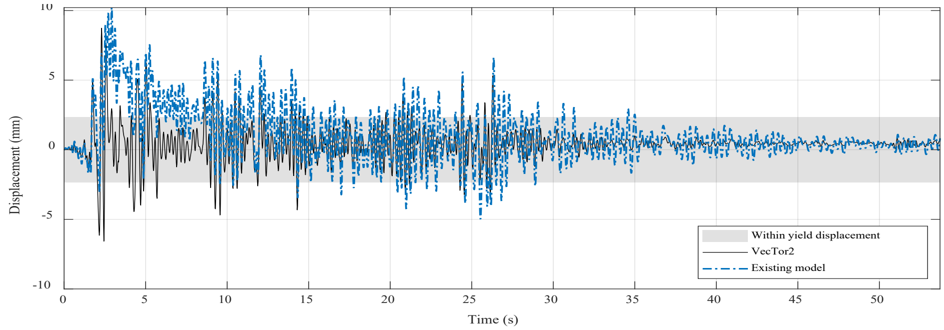

(b)

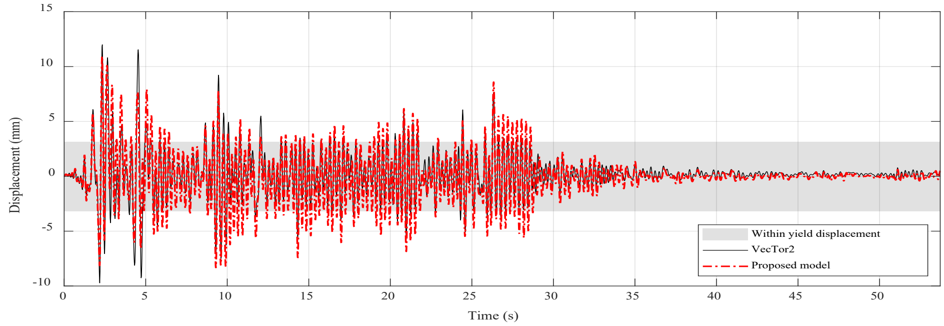

(c)

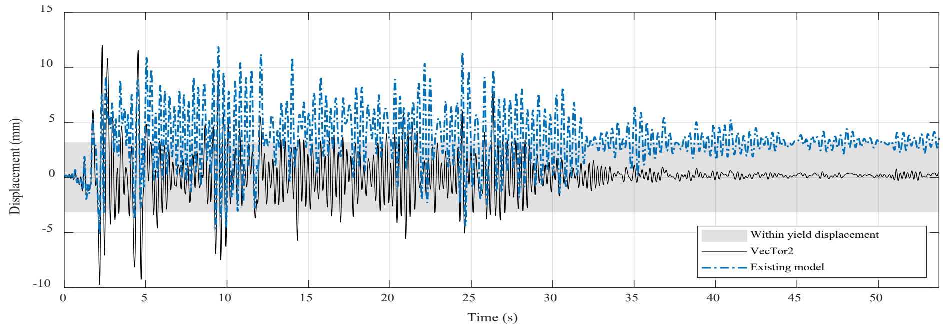

(d)

Figure 5.14 Nonlinear time history analysis for a RC column having flexure failure under two earthquakes using the equivalent SDOF model and the FE model ((a): proposed model for El Centro, (b): reference model for El Centro, (c) proposed model for Loma Prieta, (d): reference model for Loma Prieta)

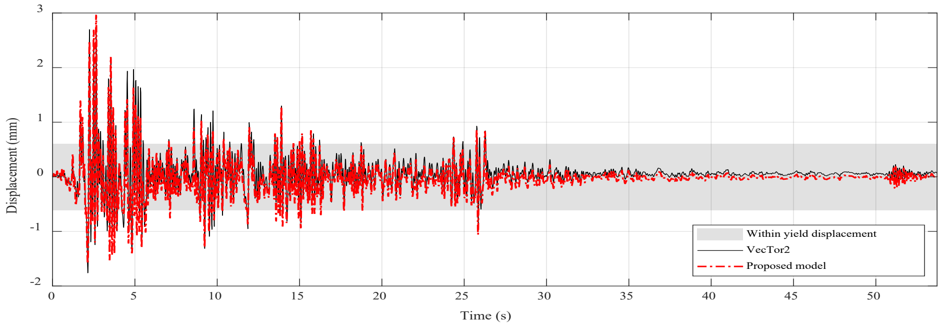

(a)

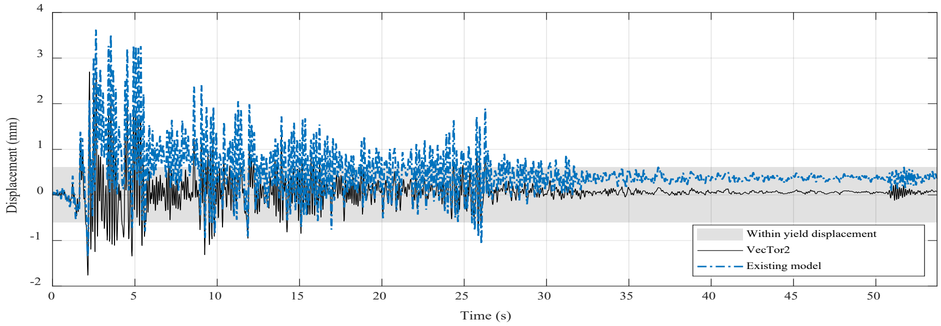

(b)

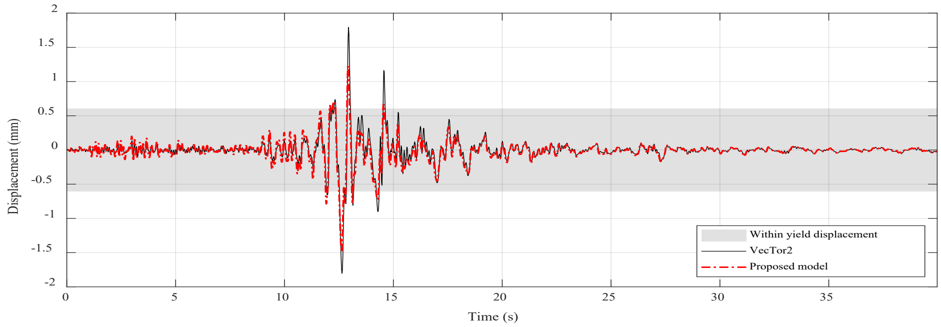

(c)

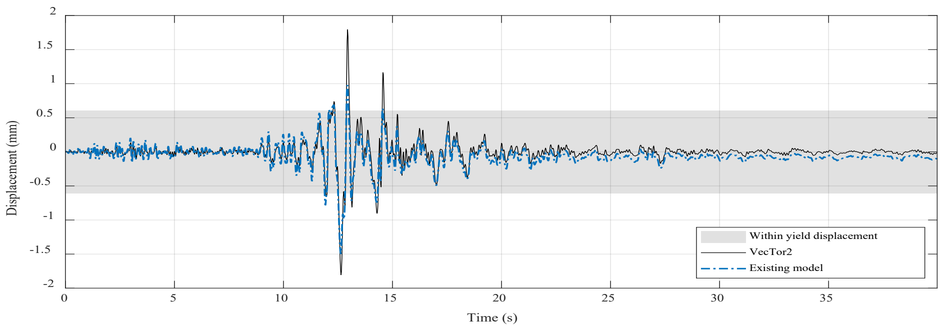

(d)

Figure 5.15 Nonlinear time history analysis for a RC column having shear failure under two earthquakes using the equivalent SDOF model and the FE model ((a): proposed model for El Centro, (b): reference model for El Centro, (c) proposed model for Loma Prieta, (d): reference model for Loma Prieta)

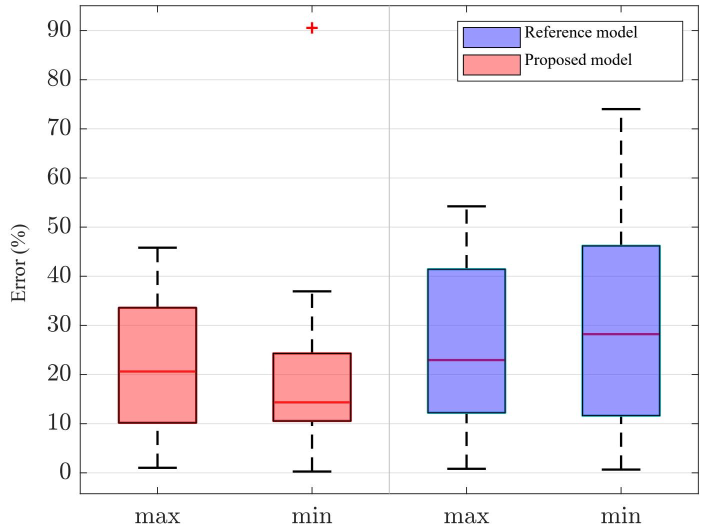

(a)

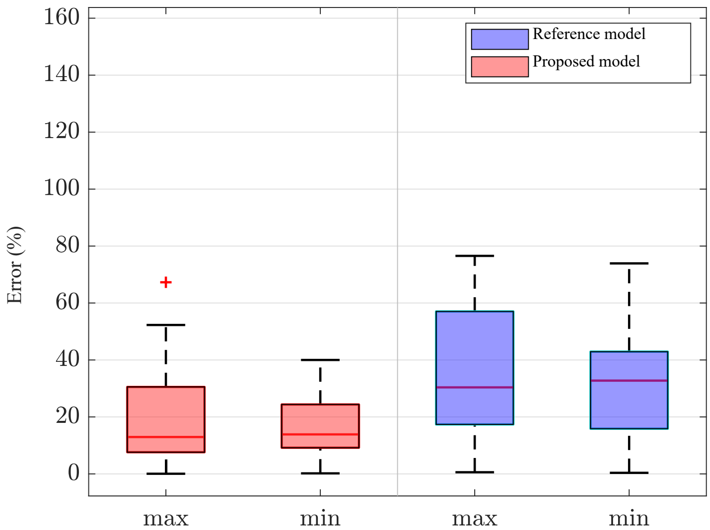

(b)

Figure 5.16 Box plots indicating the response prediction results for the 50 RC columns under seismic loads
((a): El Centro earthquake, (b): Loma Prieta earthquake)

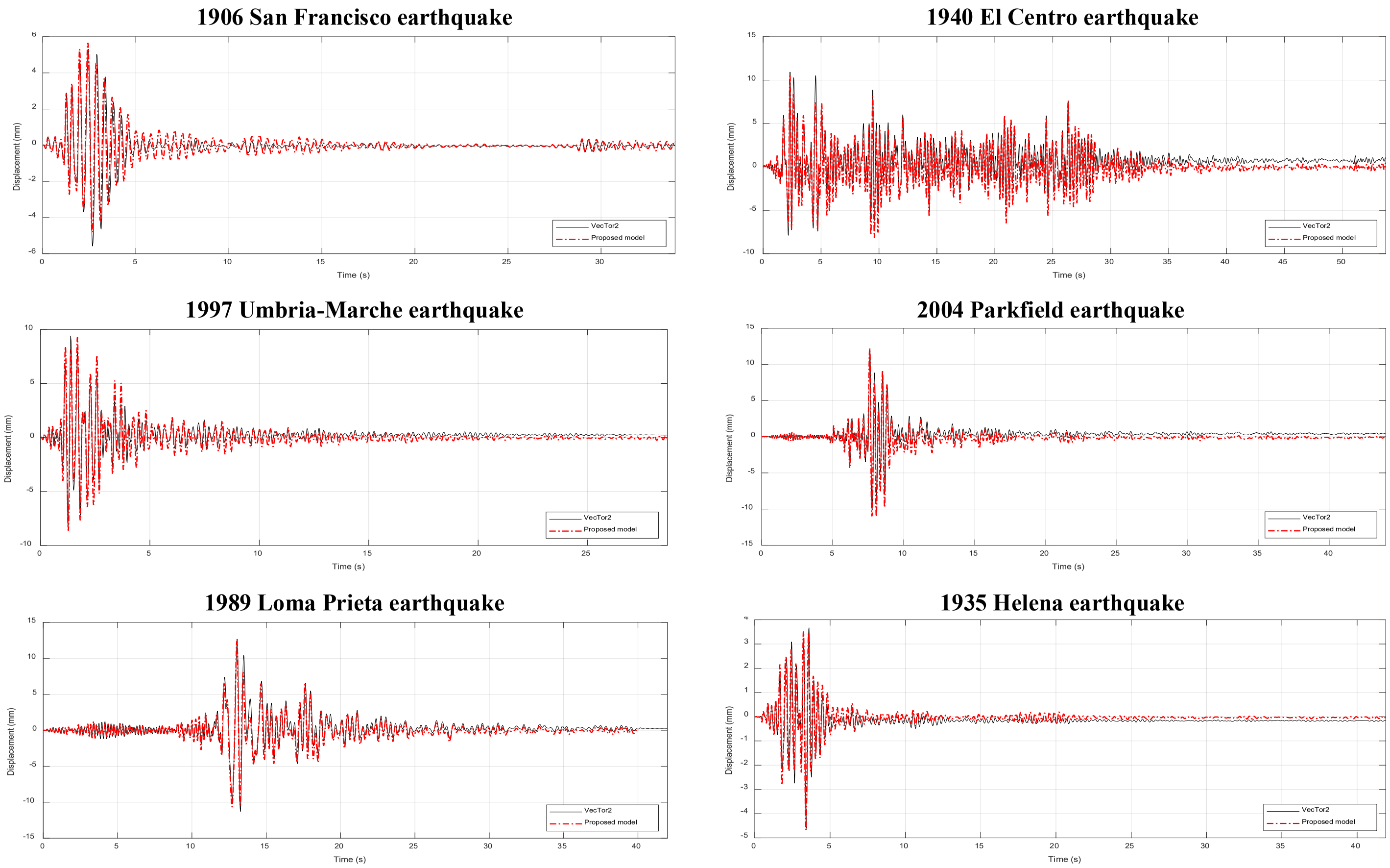

Figure 5.17 Nonlinear time history analysis results for six earthquakes of a RC column

Table 5.3 Comparison of the estimated peak displacement and the required computational cost using the proposed hysteresis modeling framework and the FE analysis

	Earthquakes	El Centro	Parkfield	Helena	San Francisco	Umbria-Marche	Loma Prieta
Peak displacement (+ / - , mm)	VecTor2	10.93 / -7.88	12.21 / -10.09	3.67 / -4.61	5.32 / -5.58	9.41 / -8.34	12.67 / -11.28
	Proposed framework	10.68 / -8.18	12.14 / -11.06	3.52 / -4.66	5.65 / -4.82	9.27 / -8.62	12.42 / -10.66
	Error	**2.33% / 3.88%**	**0.55% / 9.64%**	**4.16% / 1.19%**	**6.32% / 13.57%**	**1.55% / 3.33%**	**1.97% / 5.53%**
Computational cost	VecTor2	> 14h	> 15h	> 19 h	> 15 h	> 21 h	> 12 h
	Proposed framework	**7.16 s**	**3.96 s**	**4.18 s**	**3.10 s**	**5.44 s**	**4.29 s**

Chapter 6. Conclusions

Bouc-Wen class models have been widely used to predict the responses of structural elements and materials. Besides, because it can simulate a variety of hysteretic behaviors. However, the issue has been consistently raised as to whether a Bouc-Wen class model can be used to predict the response to a new arbitrary load other than the load used to fit the model. In order to predict the response of a structure subjected to an arbitrary load including dynamic loads, first, a Bouc-Wen model should be able to express all possible hysteretic behaviors from the elements, and secondly, such hysteresis should be sufficiently reflected in the force-displacement data that are used for model fitting. If there exists a mathematical model that can simulate all the hysteretic behaviors of the elements and the parameters of the model can be accurately estimated, the nonlinear time history analysis that requires significant computational costs from iterative calculates using finite element analysis can be replaced with an equivalent SDOF system, which results in much more efficient process for seismic evaluation.

With such motivation, this thesis aimed at developing a modeling framework to cover a wider range of load-deformation relationships, especially including a crack-induced hysteresis. To this end, first, a novel Bouc-Wen model considering cracking effects was developed. Two parameters, the hysteretic energy amplification factor c_ε and the crack closure coefficient c_h, were newly introduced. The hysteretic energy amplification factor is introduced to consider stepwise deterioration due to cracks, and the crack closure coefficient is added to consider the pinching relaxation caused by the crack closure effect.

Next, a loading protocol is developed for accurate and consistent model fitting.

A loading protocol incorporates a series of procedures to identify parameters of the proposed Bouc-Wen model. In order to identify 15 parameters in the proposed Bouc-Wen model efficiently, three steps are proposed. First, estimate the three main parameters, i.e., initial stiffness, yield force, and the post yield stiffness ratio, from a pushover curve. Second, conduct a quasi-static cyclic loading test with the developed cyclic loading history that induces all modes of hysteretic behaviors for elements susceptible to cracks, and obtain a force-displacement dataset that reflects the hysteresis of the specimen. Last, identify the other 12 parameters from the force-displacement dataset using the sequential parameter identification strategy.

Using the nonlinear finite element analysis program, VecTor2, with the experimental data for RC columns from the PEER database, the response prediction performance of the proposed hysteresis modeling framework to various loads was demonstrated. Three quasi-static loads and two seismic loads were used in this regard. For the response prediction to quasi-static loads, the proposed model showed a good agreement with the results from FE analysis in most cases regardless of the loading history or the failure mode of RC columns, while the existing Bouc-Wen model showed a good prediction accuracy only for columns with flexure failure and loads with monotonically increasing amplitudes. In addition, in the time history analysis, the proposed model predicted peak displacements in both directions more accurately than the existing model. To further investigate the performance of the proposed method, responses to a total of 6 earthquakes were estimated for one RC column showing flexure failure. As a result, the overall appearance of the time history, as well as the peak displacement, were accurately estimated in all cases. Compared to the time history analysis using the finite element method, it took much less computational time and costs without compromising the prediction performance.

For future research can be conducted by addressing several limitations of this thesis. First, a more accurate strategy for parameter estimation may extend the applicability of the framework proposed in this thesis. To be specific, a parameter estimation procedure based on systematic sensitivity analysis for each parameter would be advantageous to ensure robust predictive performance. Moreover, reducing the range of parameters by increasing the number of RC column examples would also be helpful. Such an advanced parameter estimation scheme would result in a reliable performance in response prediction. In addition to a future research for more reliable strategies, studies that develop a structured way to determine the equivalent damping ratio can make the framework consistent. Currently, the damping ratio for an equivalent SDOF system is determined partially by the author's subjective judgment. Based on the more robust and reliable strategies for parameter identification and determination of the damping ratio, the proposed hysteresis modeling framework shall be extended to structural systems. If the hysteretic behavior of structural systems can be successfully described using the proposed hysteresis modeling framework, a fast and convenient nonlinear time history analysis for structural systems would be achieved by replacing the finite element analysis with the equivalent SDOF system.

Appendix

Appendix A. Incremental algorithm for the proposed Bouc-Wen model

To define the inelastic restoring force of the proposed Bouc-Wen class model, the hysteretic displacement z should be solved first. Accordingly, an incremental form for the integrated mathematical formulation of the proposed model, Eqs. (3.8) to (3.20), is required to solve z with a numerical scheme. Using Eq. (3.8), the restoring force at time t_{i+1} becomes,

$$f(u,z)_{i+1} = \alpha k_0 u_{i+1} + (1-\alpha) F_y z_{\mathrm{i+1}} \tag{A.1}$$

Additionally, the rate equation of z, Eq. (3.9), is discretized using the Backward Euler method as follows:

$$\begin{aligned} z_{\mathrm{i+1}} &= z_i + \Delta t \frac{h_{i+1}}{\eta_{i+1}} \frac{(u_{i+1}-u_i)}{\Delta t} \\ &\qquad \times \left[1 - |z_{i+1}|^n \left\{\gamma + \beta \cdot sgn\left(\frac{(u_{i+1}-u_i)}{\Delta t} z_{i+1}\right)\right\} \nu_{i+1}\right] \frac{k_0}{F_y} \\ &= z_i + \frac{h_{i+1}}{\eta_{i+1}} (u_{i+1} - u_i) \\ &\qquad \times \left[1 - |z_{i+1}|^n \left\{\gamma + \beta \cdot sgn\left(\frac{(u_{i+1}-u_i)}{\Delta t} z_{i+1}\right)\right\} \nu_{i+1}\right] \frac{k_0}{F_y} \end{aligned} \tag{A.2}$$

where ε_{i+1} is found by discretizing Eqs. (3.16) to (3.18) with the Backward Euler method as follows:

$$\varepsilon_{i+1} = \left(\varepsilon_{+_{i+1}} \cdot H(u_{i+1}) + \varepsilon_{-_{i+1}} \cdot \left(1 - H(u_{i+1})\right)\right) \tag{A.3}$$

$$\varepsilon_{+_{i+1}} = \varepsilon_{+_i} + \{1 + c_\varepsilon \cdot H(u_{i+1} - u_{i+1}^{max})\}(1-\alpha) \frac{k_0}{F_y} z_{i+1}(u_{i+1} - u_i) \tag{A.4}$$

$$\varepsilon_{-_{i+1}} = \varepsilon_{-_i} + \{1 + c_\varepsilon \cdot H(u_{i+1}^{min} - u_{i+1})\}(1-\alpha)\frac{k_0}{F_y} z_{i+1}(u_{i+1} - u_i) \quad \text{(A.5)}$$

in which the definitions for $H(\cdot)$, u_i^{max}, and u_i^{min} are presented in Section 3.2. The values for z_{i+1}, u_{i+1}, and ε_{i+1} should be restored for the next step after each incremental step. The above incremental equations are solved by Newton-Raphson method for incremental displacement $(u_{i+1} - u_i)$. The details for the Newton-Raphson method-based incremental algorithm are summarized as the following steps:

Step 1. Calculate the evaluation function $\boldsymbol{\Gamma(z_{i+1})}$

The evaluation function $\Gamma(z_{i+1})$ for the Newton-Raphson method is defined as

$$\Gamma(z_{i+1}) = z_{i+1} - z_i - h_{i+1} a_2 (u_{i+1} - u_i)\frac{k_0}{F_y} \quad \text{(A.6)}$$

where h_{i+1} and a_2 are given as

$$h_{i+1} = 1 - \zeta_{1_{i+1}} \exp\left(-\left(z_{i+1} \cdot sgn\left(\frac{(u_{i+1} - u_i)}{\Delta t}\right) - qZ_{u_{i+1}}\right)^2 / \zeta_{2_{i+1}}^2\right) \times \left(1 - \exp\left(-c_h \frac{|\tilde{u}_{i+1}|}{d_y}\right)\right) \quad \text{(A.7)}$$

$$a_2 = \frac{1 - |z_{i+1}|^n a_1 \nu_{i+1}}{\eta_{i+1}} \quad \text{(A.8)}$$

where $\zeta_{1_{i+1}}$, $Z_{u_{i+1}}$, $\zeta_{2_{i+1}}$, a_1, ν_{i+1}, and η_{i+1} are defined as

$$\zeta_{1_{i+1}} = \zeta_0(1 - \exp(-p\varepsilon_{i+1})) \quad \text{(A.9)}$$

$$Z_{u_{i+1}} = \left(\frac{1}{\nu_{i+1}(\beta+\gamma)}\right)^{\frac{1}{n}} \quad \text{(A.10)}$$

$$\zeta_{2_{i+1}} = (\psi + \delta_\psi \varepsilon_{i+1})(\lambda + \zeta_{1_{i+1}}) \quad \text{(A.11)}$$

$$a_1 = \gamma + \beta \cdot sgn\left(\frac{(u_{i+1}-u_i)}{\Delta t} z_{i+1}\right) \tag{A.12}$$

$$\nu_{i+1} = 1 + \delta_\nu \varepsilon_{i+1} \tag{A.13}$$

$$\eta_{i+1} = 1 + \delta_\eta \varepsilon_{i+1} \tag{A.14}$$

The definition for $\tilde{u}_{i+1}$ can be found in Eq. (3.22), and ε_{i+1} is obtained from Eqs. (A.3) to (A.5).

Step 2. Evaluate the derivative of $\Gamma(z_{i+1})$ *with respect to* z_{i+1}

The derivative of the evaluation function $\Gamma(z_{i+1})$ is expressed as

$$\Gamma'(z_{i+1}) = 1 - (h'_{i+1} a_2 + h_{i+1} a'_2)(u_{i+1} - u_i)\frac{k_0}{F_y} \tag{A.15}$$

where the derivatives of h_{i+1} and a_2 are written as

$$h'_{i+1} = a_3\left(\zeta'_{1_{i+1}} - a_4 + \zeta'_{2_{i+1}} a_5\right) \tag{A.16}$$

$$a'_2 = \frac{1}{\eta^2_{i+1}} \cdot [\eta'_{i+1}(1 - |z_{i+1}|^n a_1 \nu_{i+1})$$

$$-\eta_{i+1}(n|z_{i+1}|^{n-1} a_1 \nu_{i+1} \cdot sgn(z_{i+1}) + |z_{i+1}|^n a_1 \nu'_{i+1})] \tag{A.17}$$

where a_3, $\zeta'_{1_{i+1}}$, a_4, $\zeta'_{2_{i+1}}$, a_5, η'_{i+1}, and ν'_{i+1} are given as

$$a_3 = -\exp\left(-\left(z_{i+1} \cdot \mathrm{sgn}\left(\frac{(u_{i+1}-u_i)}{\Delta t}\right) - qZ_{u_{i+1}}\right)^2 / \zeta^2_{1_{i+1}}\right)$$

$$\times \left(1 - \exp\left(-c_h \frac{|\tilde{u}_{i+1}|}{d_y}\right)\right) \tag{A.18}$$

$$\zeta'_{1_{i+1}} = p\zeta_0 \exp(-p\varepsilon_{i+1})\, \varepsilon'_{i+1} \tag{A.19}$$

$$a_4 = \frac{2\zeta_{1_{i+1}}}{\zeta_{2_{i+1}}^2}\left(z_{i+1} \cdot \mathrm{sgn}\left(\frac{(u_{i+1}-u_i)}{\Delta t}\right) - qZ_{u_{i+1}}\right)$$

$$\times\left(\mathrm{sgn}\left(\frac{(u_{i+1}-u_i)}{\Delta t}\right) - qZ'_{u_{i+1}}\right) \quad \text{(A.20)}$$

$$\zeta'_{2_{i+1}} = \psi\zeta'_{1_{i+1}} + \lambda\delta_\psi\varepsilon'_{i+1} + \delta_\psi\varepsilon'_{i+1}\zeta_{i+1} + \delta_\psi\varepsilon_{i+1}\zeta'_{1_{i+1}} \quad \text{(A.21)}$$

$$a_5 = \frac{2\zeta_{1_{i+1}}}{\zeta_{2_{i+1}}^3}\left(z_{i+1} \cdot \mathrm{sgn}\left(\frac{(u_{i+1}-u_i)}{\Delta t}\right) - qZ_{u_{i+1}}\right)^2 \quad \text{(A.22)}$$

$$\eta'_{i+1} = \delta_\eta\varepsilon'_{i+1} \quad \text{(A.23)}$$

$$\nu'_{i+1} = \delta_\nu\varepsilon'_{i+1} \quad \text{(A.24)}$$

where ε'_{i+1} and $Z'_{u_{i+1}}$ are written as

$$\varepsilon'_{i+1} = \varepsilon'_{+_{i+1}} \cdot H(u_{i+1}) + \varepsilon'_{-_{i+1}} \cdot \left(1 - H(u_{i+1})\right) \quad \text{(A.25)}$$

$$Z'_{u_{i+1}} = -\frac{\nu'_{i+1}(\beta+\gamma)}{n}\left(\frac{1}{\nu_{i+1}(\beta+\gamma)}\right)^{1+\frac{1}{n}} \quad \text{(A.26)}$$

Where $\varepsilon'_{+_{i+1}}$ and $\varepsilon'_{-_{i+1}}$ are given as

$$\varepsilon'_{+_{i+1}} = \{1 + c_\varepsilon \cdot H(u_{i+1} - u_{i+1}^{max})\}(1-\alpha)\frac{k_0}{F_y}(u_{i+1} - u_i) \quad \text{(A.27)}$$

$$\varepsilon'_{-_{i+1}} = \left\{1 + c_\varepsilon \cdot H\left(u_{i+1}^{min} - u_{i+1}\right)\right\}(1-\alpha)\frac{k_0}{F_y}(u_{i+1} - u_i) \quad \text{(A.28)}$$

Step 3. Obtain the trial value $\boldsymbol{z_{i+1}^{new}}$

The trial value in the Newton-Raphson method is calculated as

$$z_{i+1}^{new} = z_{i+1} - \frac{\Gamma(z_{i+1})}{\Gamma'(z_{i+1})} \quad \text{(A.29)}$$

Step 4. Update the trial value

Using the trial value obtained as Eq. (A.29), the value for z_{i+1} is updated as

$$z_{i+1}^{old} = z_{i+1}, \;\; z_{i+1} = z_{i+1}^{new} \tag{A.30}$$

Step 5. Iterate until convergence

Iterate from Step 1 to 4 until the following convergence condition is achieved:

$$\left|z_{i+1}^{new} - z_{i+1}^{old}\right| < \varepsilon_0 \tag{A.31}$$

where ε_0 represents the prescribed tolerance for the convergence check.

References

ACI. (2013). Guide for Testing Reinforced Concrete Structural Elements under Slowly Applied Simulated Seismic Loads. Report No. ACI 374.2R-13, American Concrete Institute, Farmington Hills, MI.

ASCE. (2013). Seismic Evaluation and Rehabilitation of Existing Buildinds, Report No. ASCE/SEI 41-13 (Public Comment Draft), American Society of Civil Engineers, Reston, VA.

ATC. (1992). Guidelines for Cyclic Seismic Testing of Components of Steel Structures. Report No. ATC-24, Applied Technology Council, Redwood City, CA.

ATC. (1997). Seismic evaluation and retrofit of concrete buildings. Report No. ATC-40, Applied Technology Council, Redwood City, CA.

ATC. (2010). Modeling and Acceptance Criteria for Seismic Design and Analysis of Tall Buildins. Report No. PEER/ATC-72-1, Applied Technology Council, Redwood City, CA.

Baber, T. T., & Noori, M. N. (1985). Random vibration of degrading, pinching systems. *Journal of Engineering Mechanics*, 111(8), 1010-1026.

Blasi, G., De Luca, F., & Aiello, M. A. (2018). Hybrid micro-modeling approach for the analysis of the cyclic behavior of RC frames. *Frontiers in Built Environment*, 4, 75.

Boivin, Y., & Paultre, P. (2012). Seismic force demand on ductile reinforced concrete shear walls subjected to western North American ground motions: Part 1—parametric study. *Canadian Journal of Civil Engineering*, 39(7), 723-737.

Bouc, R. (1967). Forced vibrations of mechanical systems with hysteresis. In *Proc. of the Fourth Conference on Nonlinear Oscillations, Prague*, 1967.

Charalampakis, A. E., & Koumousis, V. K. (2009). A Bouc–Wen model compatible with plasticity postulates. *Journal of Sound and Vibration*, 322(4-5), 954-968.

Chopra, A. K., & McKenna, F. (2016). Modeling viscous damping in nonlinear response history analysis of buildings for earthquake excitation. *Earthquake Engineering & Structural Dynamics*, 45(2), 193-211.

Krawinkler, H., Parisi, F., Ibarra, L., Ayoub, A., & Medina, R. (2001). *Development of a testing protocol for woodframe structures* (Vol. 102). Richmond, CA: CUREe.

Gatto, K., & Uang, C. M. (2002). *Cyclic response of woodframe shearwalls: Loading protocol and rate of loading effects*. Washington, DC: Consortium of Universities for Research in Earthquake Engineering.

De Luca, F., Vamvatsikos, D., & Iervolino, I. (2013). Near-optimal piecewise linear fits of static pushover capacity curves for equivalent SDOF analysis. *Earthquake engineering & structural dynamics*, 42(4), 523-543.

Elwood, K. J. (2004). Modelling failures in existing reinforced concrete columns. *Canadian Journal of Civil Engineering*, 31(5), 846-859.

European Committee for Standardization. (2003). Eurocode8: design of structures for earthquake resistance – Part 1: general rules, seismic actions and rules for buildings. Brussels, Belgium.

FEMA. (2000). Predstandard and commentary for the seismic rehabilitation of buildings. Report No. FEMA 356, Washington, D.C.

FEMA. (2005). Improvement of nonlinear static seismic analysis procedures. Report No. FEMA 440, Washington, D.C.

FEMA. (2007). Interim Testing Protocols for Determining the Seismic Performance Characteristics of Structural and Nonstructural Components. Report No. FEMA 461, Washington, D.C.

FEMA. (2009). Quantification of Building Seismic Performance Factors. Report No. FEMA P695, Washington, D.C.

Hamburger, R., Deierlein, G., Lehman, D., Lowes, L., Shing, B., Van de Lindt, J., ... & Hortacsu, A. (2016). ATC-114 next-generation hysteretic relationships for performance-based modeling and analysis. In *Proceedings of the SEAOC Convention* (No. CONF). Structural Engineers Association of California.

Haselton, C., Deierleien, G., Bono, S., Ghannoum, W., Hachem, M., Malley, J., ... & Cedillos, V. (2016). Guidelines on nonlinear dynamic analysis for performance-based seismic design of steel and concrete moment frames. In *2016 SEAOC Convention* (No. CONF).

Hossain, M. R., Ashraf, M., & Padgett, J. E. (2013). Risk-based seismic performance assessment of Yielding Shear Panel Device. Engineering Structures, 56, 1570-1579.

Huang, X., & Kwon, O. S. (2015). Numerical models of RC elements and their impacts on seismic performance assessment. *Earthquake Engineering & Structural Dynamics*, 44(2), 283-298.

Ibarra, L. F., Medina, R. A., & Krawinkler, H. (2005). Hysteretic models that incorporate strength and stiffness deterioration. *Earthquake engineering & structural dynamics*, 34(12), 1489-1511.

Ikhouane, F., Mañosa, V., & Rodellar, J. (2007). Dynamic properties of the hysteretic Bouc-Wen model. *Systems & control letters*, 56(3), 197-205.

Ismail, M., Ikhouane, F., & Rodellar, J. (2009). The hysteresis Bouc-Wen model, a survey. *Archives of computational methods in engineering*, 16(2), 161-188.

Kang, J. D., Furukawa, T., & Mori, Y. (2017). Equivalent sdof system model for estimating the seismic response of building structures with displacement-dependent passive dampers. In *16th World Conference on Earthquake Engineering*.

Kim, T., Kwon, O. S., & Song, J. (2019). Response prediction of nonlinear hysteretic systems by deep neural networks. *Neural Networks*, 111, 1-10.

Krawinkler, H. (2009, October). Loading histories for cyclic tests in support of performance assessment of structural components. In *The 3rd international conference on advances in experimental structural engineering*, San Francisco.

Lee, C. S., & Han, S. W. (2021). An Accurate Numerical Model Simulating Hysteretic Behavior of Reinforced Concrete Columns Irrespective of Types of Loading Protocols. *International Journal of Concrete Structures and Materials*, 15(1), 1-16.

Ma, F., Zhang, H., Bockstedte, A., Foliente, G. C., & Paevere, P. (2004). Parameter analysis of the differential model of hysteresis. *Journal of Applied Mechanics*, 71(3), 342-349.

Ma, F., Ng, C. H., & Ajavakom, N. (2006). On system identification and response prediction of degrading structures. Structural Control and Health Monitoring: The Official Journal of the International Association for Structural Control and Monitoring and of the European Association for the Control of Structures, 13(1), 347-364.

Marder, K. J., Motter, C. J., Elwood, K. J., & Clifton, G. C. (2018). Effects of variation in loading protocol on the strength and deformation capacity of ductile reinforced concrete beams. *Earthquake Engineering & Structural Dynamics*, 47(11), 2195-2213.

Minakawa, K., Newman Jr, J. C., & McEvily, A. J. (1983). A critical study of the crack closure effect on near-threshold fatigue crack growth. *Fatigue & Fracture of Engineering Materials & Structures*, 6(4), 359-365.

Ning, C. L., Cheng, Y., & Yu, X. H. (2021). A simplified approach to investigate the seismic ductility demand of shear-critical reinforced concrete columns based on experimental calibration. *Journal of Earthquake Engineering*, 25(10), 1958-1980.

Pacific Earthquake Engineering Research Center. (2021). [Untitled illustration of a reinforced concrete column for a quasi-static cyclic test]. 2021 Reinforced Concrete Column Blind Prediction Contest. https://peer.berkeley.edu/news-and-events/2021-reinforced-concrete-column-blind-prediction-contest

Pelliciari, M., Marano, G. C., Cuoghi, T., Briseghella, B., Lavorato, D., & Tarantino, A. M. (2018). Parameter identification of degrading and pinched hysteretic systems using a modified Bouc–Wen model. Structure and Infrastructure Engineering, 14(12), 1573-1585.

Pippan, R., & Hohenwarter, A. (2017). Fatigue crack closure: a review of the physical phenomena. *Fatigue & fracture of engineering materials &*

structures, 40(4), 471-495.

Ritchie, R. O. (1999). Mechanisms of fatigue-crack propagation in ductile and brittle solids. *International journal of Fracture*, 100(1), 55-83.

Saatci, S., & Vecchio, F. J. (2009). Nonlinear finite element modeling of reinforced concrete structures under impact loads. *ACI Structural Journal*.

Sengupta, P., & Li, B. (2013). Modified Bouc–Wen model for hysteresis behavior of RC beam–column joints with limited transverse reinforcement. Engineering Structures, 46, 392-406.

Sengupta, P., & Li, B. (2017). Hysteresis Modeling of Reinforced Concrete Structures: State of the Art. *ACI Structural Journal*, 114(1).

Song, J., & Der Kiureghian, A. (2006). Generalized Bouc–Wen model for highly asymmetric hysteresis. *Journal of engineering mechanics*, 132(6), 610-618.

Suresh, S. G. F. R. O., Zamiski, G. F., & Ritchie, D. R. (1981). Oxide-induced crack closure: an explanation for near-threshold corrosion fatigue crack growth behavior. *Metallurgical and Materials Transactions A*, 12(8), 1435-1443.

Vecchio, F. J., & Collins, M. P. (1986). The modified compression-field theory for reinforced concrete elements subjected to shear. ACI Journal, 83(2), 219-231.

Vecchio, F. J. (2000). Disturbed stress field model for reinforced concrete: formulation. *Journal of structural engineering*, 126(9), 1070-1077.

Vecchio, F. J. (2001). Disturbed stress field model for reinforced concrete: implementation. *Journal of Structural Engineering*, 127(1), 12-20.

Vecchio, F. J., & Shim, W. (2004). Experimental and analytical reexamination of classic concrete beam tests. *Journal of Structural Engineering*, 130(3), 460-469.

Wang, L., & Lu, Z. R. (2017, May). Identification of Bouc-Wen hysteretic parameters based on enhanced response sensitivity approach. In *Journal of physics: conference series* (Vol. 842, No. 1, p. 012021). IOP Publishing.

Wen, Y. K. (1976). Method for random vibration of hysteretic systems. Journal of the engineering mechanics division, 102(2), 249-263.

Wolf, E. (1970). Fatigue crack closure under cyclic tension. *Engineering fracture mechanics*, 2(1), 37-45.

Yu, B., Ning, C. L., & Li, B. (2016). Hysteretic model for shear-critical reinforced concrete columns. *Journal of Structural Engineering*, 142(9), 04016056.

Zhong, J., Gardoni, P., & Rosowsky, D. (2010). Stiffness degradation and time to cracking of cover concrete in reinforced concrete structures subject to corrosion. *Journal of engineering mechanics*, 136(2), 209-219.

초 록

Bouc-Wen 모델을 기반으로 하는 Bouc-Wen계 이력 거동 모델들은 다양한 공학 분야에서 시스템의 힘-변위 관계를 묘사하기 위한 수학적 모델로 널리 활용되어 왔다. 그러나 Bouc-Wen계 모델들은 모델의 매개변수 산정에 사용한 하중 이력이 아닌, 새로운 임의 하중에 대한 응답 예측 성능을 보장할 수 없다는 문제점이 꾸준히 제기되어 왔다. 이에 구조물의 지진 성능 평가 시 Bouc-Wen계 모델을 이용한 단자유도 시스템은 주로 비선형 정적 해석에 활용되었으며, 정밀하고 정확한 모델을 요구하는 비선형 시간이력해석에는 활용이 힘들다.

본 연구에서는 지진 하중을 포함한 다양한 하중에 대한 예측 성능을 확보할 수 있는 Bouc-Wen계 모델을 이용한 이력 거동 모델링 프레임워크를 제안한다. 이를 위해 먼저, 균열에 취약한 구조 요소의 이력 거동도 포함할 수 있도록 기존 Bouc-Wen계 모델의 적용 범위를 확장한 새로운 Bouc-Wen계 모델을 개발하였다. 균열이 이력 현상에 미치는 영향을 고려하기 위해 두 가지 새로운 매개변수가 제안되었다.

다음으로, 개발한 Bouc-Wen 모델의 매개변수를 효과적으로 추정할 수 있는 하중 프로토콜을 제시한다. 본 연구의 하중 프로토콜은 매개변수를 추정할 데이터를 얻기 위한 주기 하중 이력 뿐만 아니라 효율적인 매개변수 추정 전략을 통합한 일련의 모델 피팅 과정이다. 준정적 주기 하중 실험에서 사용될 주기 하중 이력은 실험 시편에서 보이는 다양한 특징의 이력 거동을 모두 발현할 수 있도록 고안되었다.

비선형 유한요소 해석과 철근 콘크리트 기둥에 대한 총 50세트의 실제 실험 데이터를 이용하여 제안한 이력 거동 모델링 프레임워크를 검증하였다. 검증 결과, 본 연구에서 개발한 이력 모델은 기존 모델보다 다양한 준정적 하중에 대한 응답 예측을 더욱 정확하고 안정적으로 수행하고 있음을 확인하였다. 또한 El Centro 지진과 Loma Prieta 지진에 대한 비선형 시간이력해석에서도 본 연구에서 개발한 모델이 최대 변위 응답에 대해 유한요소 해석 결과에 더욱 가까운 결과를 보여주었다. 나아가 하나의 철근 콘크리트에 대해서는 6개 지진에 대한 비선형 시간이력해석을 수행하였고, 제안한 Bouc-Wen 모델을 이용한 단자유도 시스템으로 구조물의 응답 이력을 추정한 결과, 모든 지진에 대해 유한요소 해석 결과와 상당히 유사한 양상을 보였다. 이는 본 연구에서 제안한 이력 거동 모델링 프레임워크가, 다루기 힘들고 많은 시간을 소요하는 유한요소 해석을 대체할 수 있음을 의미한다. 나아가 현재 구조 요소로 한정되어 있는 검증 예제를 복잡 구조시스템으로 확장한다면, 다양한 구조시스템에 대한 비선형 시간이력해석을 보다 간편하게 수행함으로써 효율적인 성능 기반 설계에 기여할 수 있을 것이다.

주요어: 이력 거동, Bouc-Wen 모델, 하중 프로토콜, 비선형 유한요소법, 비선형 시간이력해석, 균열 효과

학번: 2020-27136

Acknowledgements

Foremost, I would like to acknowledge and give my warmest thanks to my advisor Professor Junho Song for his sincere support, endless patience, and thoughtful guidance. His guidance on both my future career as well as research has been invaluable. Although it was a short period of two years, it has been my thorough gratitude to be his student. I could not have imagined having a better advisor and mentor for my Master's study. Professor Song was a great role model and indeed a perfect mentor for me.

I would also like to express my special appreciation to my research co-advisor, Dr. Taeyong Kim for his insightful comments and enthusiastic guidance. His sincere support helped me in all the time of research and writing of this thesis. From his serious passion for research, I was able to learn about a desirable attitude as a researcher.

I am grateful to all of the members in Structural System Reliability Group with whom I have had the pleasure to work: Jihwan, Chulyoung, Jungho, Minkyu, Seoungmin, Changuk, Dongkyu, Seonghyun, Youngjun, Woojun, Jaehwan, Sumin, Yujin, and Uichan. It was my great fortune to have active interactions and discussions with such resourceful members.

Last, but not least, I dedicate this thesis to my beloved Hee-kyung, who supports and encourages my dreams with unchanging faith, and to my beloved family, father, mother, and older brother, who have always been my strong support. I promise to become a researcher who can beneficially contribute to the world in the future.